Title

Prediction of Flow and Drawdown for the Site Characterization and Validation Site in the Stripa Mine

Authors

Long, J.C.S.
Mauldon, A.D.
Nelson, K.
et al.

Publication Date

1992

LBL-31761
UC-802

Lawrence Berkeley Laboratory
UNIVERSITY OF CALIFORNIA

EARTH SCIENCES DIVISION

Prediction of Flow and Drawdown for the Site Characterization and Validation Site in the Stripa Mine

J.C.S. Long, A.D. Mauldon, K. Nelson, S. Martel, P. Fuller,
and K. Karasaki

January 1992

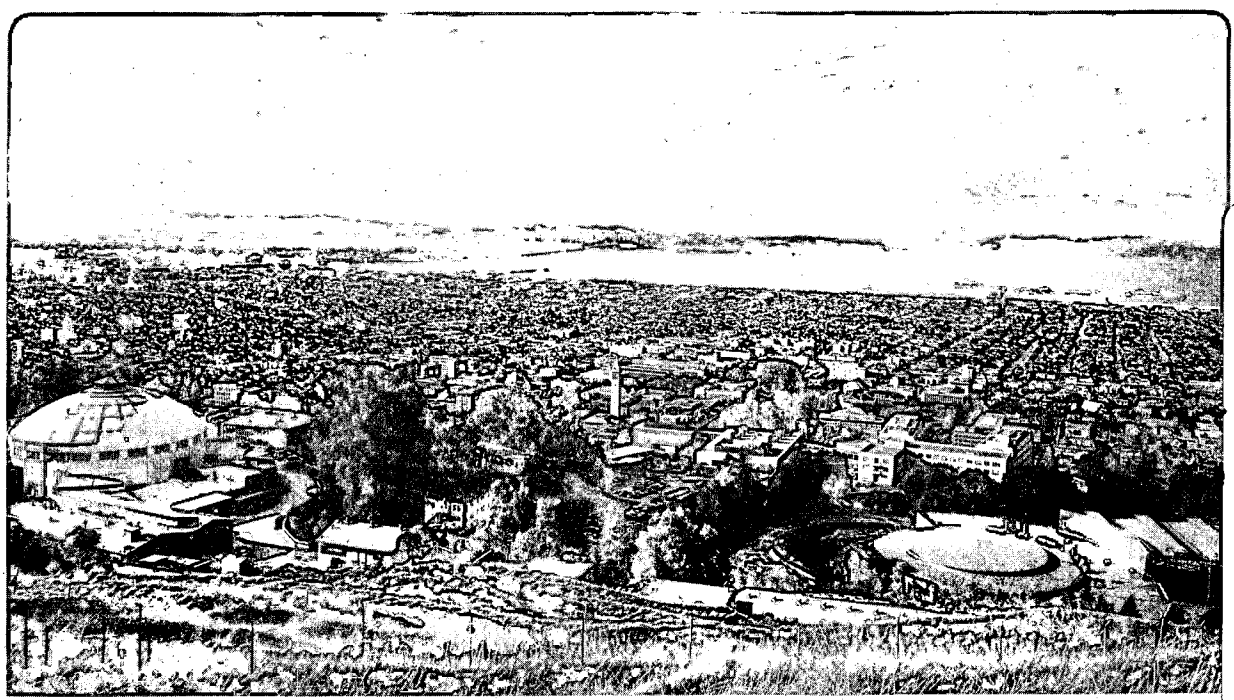

Prepared for the U.S. Department of Energy under Contract Number DE-AC03-76SF00098

DISCLAIMER

LBL-31761

Prediction of Flow and Drawdown for the Site Characterization and Validation Site in the Stripa Mine

Jane C. S. Long, Amy Davey Mauldon, Kent Nelson, Stephen Martel, Peter Fuller, and Kenzi Karasaki

Earth Sciences Division
Lawrence Berkeley Laboratory
University of California
Berkeley, California 94720

January 1992

This work was supported by the Office of Civilian Radioactive Waste Management, Office of Strategic Planning and Internal Programs, of the U.S. Department of Energy under Contract No. DE-AC03-76SF00098.

Table of Contents

List of Figures

List of Tables

Abstract

Geophysical and hydrologic data from a location in the Stripa Mine in Sweden, called the Site Characterization and Validation (SCV) block, has been used to create a series of models for flow through the fracture network. The models can be characterized as "equivalent discontinuum" models. Equivalent discontinuum models are derived starting from a specified lattice or "template". An inverse analysis called "Simulated Annealing" is used to make a random search through the elements of the lattice to find a configuration that can reproduce the measured responses. Evidence at Stripa points to hydrology which is dominated by fracture zones. These have been identified and located through extensive characterization efforts (Olsson et al., 1990, and Black et al., 1991). Lattice templates were arranged to lie on the fracture zones identified by Black and Olsson.

The fundamental goal of this project was to build a fracture flow model based on an initial data set, and use this model to make predictions of the flow behavior during a new test. Then given data from the new test, predict a second test, etc. The first data set was an interference test called C1-2. Both a two-dimensional and a three-dimensional model were annealed to the C1-2 data and use this model to predict the behavior of the Simulated Drift Experiment (SDE). The SDE measured the flow into, and drawdown due to reducing the pressure in a group of 6 parallel boreholes. Then both the C1-2 and SDE data were used to predict the flow into and drawdown due to an excavation, the Validation Drift (VD), made through the boreholes. Finally, all the data was used to predict the hydrologic response to opening another hole, T1.

Annealing to the C1-2 test gave an excellent prediction of the SDE. The Validation Drift effects were dominated by near-field physics that were not predictable. However, the calculations and measurements could be used to postulate that a dramatic decrease in hydraulic conductivity near the drift was due to degassing of nitrogen as the inflowing water was depressurized.

Acknowledgements

This work was supported by the Office of Strategic Planning and Internal Programs within the Office of Civilian Radioactive Waste Management of the U. S. Department of Energy under Contract DE-ACO3-76SF00098. We are grateful for their support. We also wish to thank the Stripa Project for accommodating and supporting our efforts. We are also grateful to Yvonne Tsang and George Moridis for their thoughtful review.

1.0. INTRODUCTION

1.1. Background

Investigations related to the geologic storage of nuclear waste have been ongoing at the Stripa Mine in Sweden for more than ten years. The latest of these investigations is called Phase III, and is sponsored by the OECD Nuclear Energy Association (NEA) as an international cooperative effort managed by the Swedish Nuclear Fuel and Waste Management Company (SKB).

The Stripa Phase III project includes the Site Characterization and Validation (SCV) experiment, which is designed to test current abilities to characterize fractured rock before it is used for nuclear waste storage. The effort is centered on a block of rock 230 m long × 200 m wide × 190 m deep centered at a depth of about 330m. The block lies between previous experimental sites, the Macropermeability/Buffer Mass Test site and the 3-D Migration site (Figures 1.1 and 1.2. The SCV work is divided into two cycles of three stages each: data-gathering, prediction, and validation. The first cycle of work included drilling of 6 boreholes (N2, N3, N4, W1, W2, and V3) and measurements of geology, fracture characteristics, in-situ stress, single borehole geophysical logging, radar, seismics, and hydrogeology (Olsson et al., 1988a). Olsson et al. give background information describing the site and the results of the first cycle of data-gathering and prediction. The second cycle included drilling 11 new wells (the C- and D-holes), the Simulated Drift Experiment (SDE), a series of large scale cross-hole tests (LSC), further geophysical measurements, the excavation of a drift through the D-holes (SCV drift), and radar tomography before and after saline injection. These are described in Black et al. (1991).

Lawrence Berkeley Laboratory (LBL) is contracted by the U.S. Department of Energy to participate in the hydrologic modeling of the SCV site. This is the second report of LBL efforts in fracture network modeling. The first is Long et al. (1991). The calculations presented here are

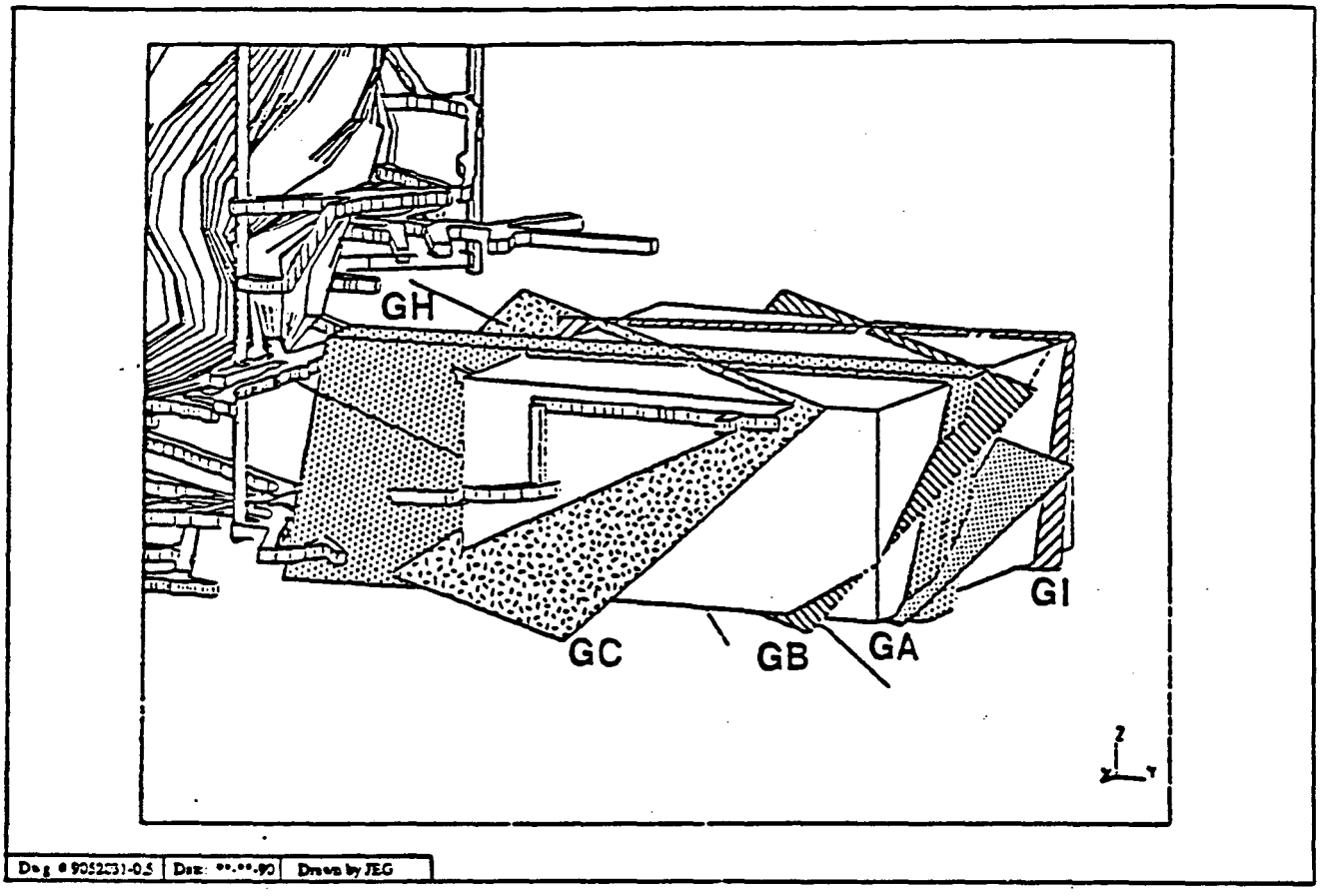

XBL 921-5529

Figure 1.1. Perspective view of the SCV block. Dotted area in the upper left is the mined out stopes (after J. Gale). GA, GB, GC, GH and GI are fracture zones.

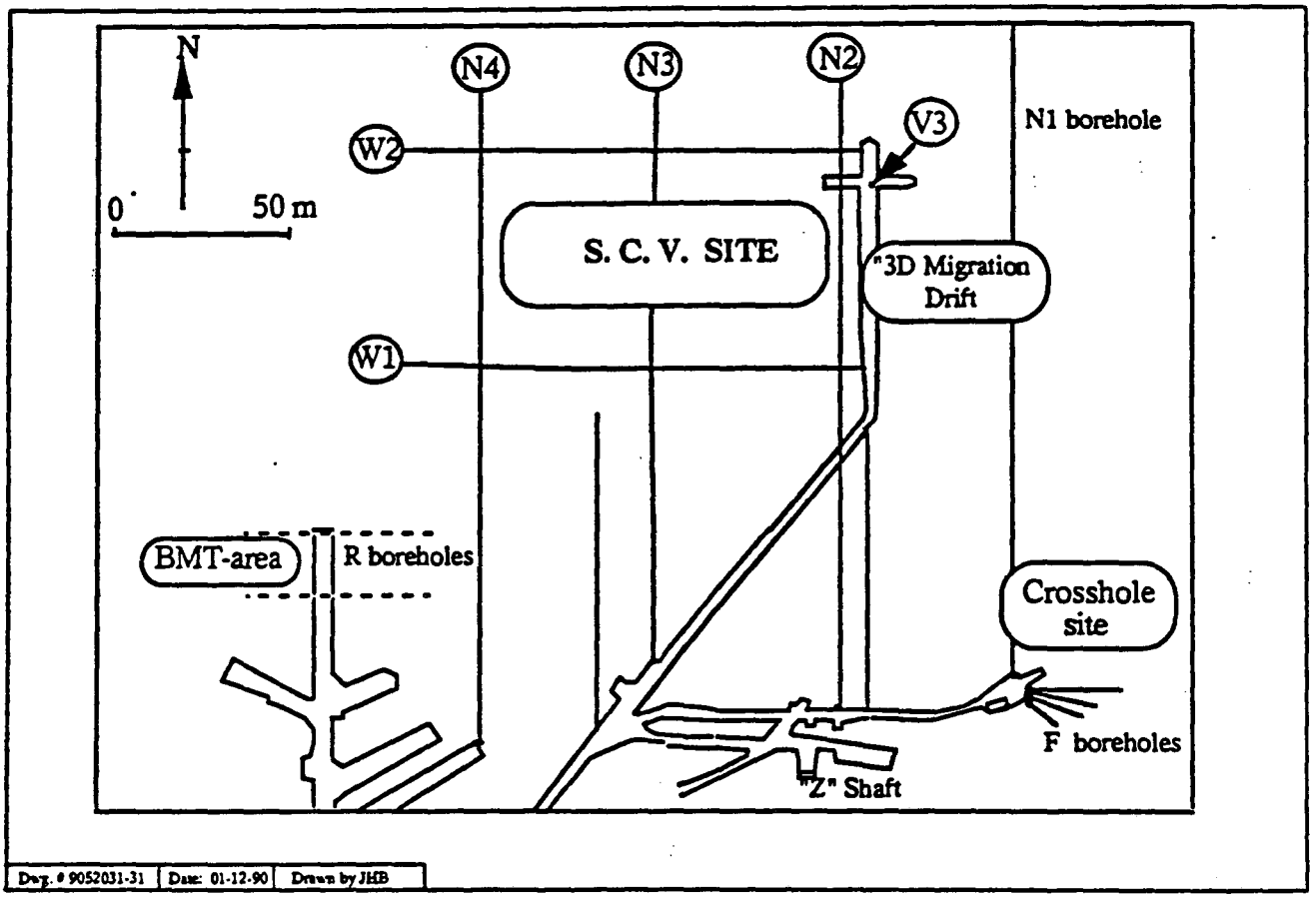

XBL 921-5530

Figure 1.2. Plan view of the SCV site.

based almost entirely on the information summarized in Olsson et al. (1989) and Black et al. (1991). Other information came from limited data collection efforts by LBL (documented in LBL reports) and through personal communication with the SCV principal investigators (documented herein where appropriate).

1.2. Modeling Approach

The Stripa Project was designed to test the ability to predict flow and transport in a fractured rock. Geophysical and hydrologic data have been collected in stages and used to develop models for fluid flow and transport. Calculations made with these models are then compared with measurements of flow and tracer concentrations.

This report describes models Lawrence Berkeley Laboratory is preparing for the Stripa Project. These models can be characterized as "equivalent discontinuum" models. An equivalent discontinuum model is a model which uses a partially filled lattice of one-dimensional conductors to represent equivalent fracture flow paths. The model is designed to represent the discontinuous nature of fracture flow in a simplest manner under two principles: 1) That all partially connected systems have universal properties described by percolation theory, and therefore, 2) It is reasonable to represent the real, complex system by a simpler lattice. In other words, fractures or fracture clusters can be represented by some average equivalent conductor and the flow of fluid through the rock can be modeled on a partially filled lattice of such conductors.

Equivalent discontinuum models are derived starting from a specified lattice or "template." An inverse analysis is performed on the template to find a pattern of lattice elements (a configuration) which can reproduce hydrologic data as observed in the field. There are three components to this process: 1) Choosing the lattice template on which to base the equivalent discontinuum model, 2) Identifying an inversion method, and 3) Choosing the data on which to base the inversion. After the inversion process, the model can be used to predict behavior in the fracture system under different flow conditions.

The lattice template is in effect a conceptual model for the fracture system. The lattice tem-

plate should be chosen based on as much a priori data as is available. In a case where nothing is known about the site, a three-dimensional grid could be constructed as a neutral template. However, in many rocks, the fracture hydrology is concentrated along fracture zones. These zones are usually highly heterogeneous, with parts of the fracture zones highly impermeable and unconnected to the rest of the system. In these cases it may make sense to construct the template only along the planes of the fracture zones because such a template is clearly a more efficient method for representing flow in the rock. Evidence at Stripa points to hydrology which is dominated by such fracture zones. These have been identified and located through extensive characterization efforts (Olsson et al., 1990 and Black et al., 1991).

Once the template is decided on, a method for finding the configuration of the lattice is needed. One method that has been developed at LBL is called "Simulated Annealing" (Davey et al., 1989). In this method, a random search is conducted through the elements of the lattice. At each iteration, the configuration is used to calculate the response to an in situ test, such as an interference test. The calculated response is compared to the real response and the "energy," a term expressing the difference between the measured responses and the calculated responses, is computed. Then a lattice element is chosen. If the element is present, or "on," then it is turned "off" or visa versa. The new energy is computed and compared to the old energy. If the energy is decreased, the change in the configuration is kept. If the energy is increased by the change, the choice of whether or not to keep the new configuration is based on a probability proportional to the amount of energy increase modified by a factor, T, called the temperature. This allows the algorithm to "wiggle" out of local minima and find a more global solution. Alternate forms of annealing change whole clusters of elements at one iteration (Cluster Annealing) or randomly choose the magnitude for the conductance rather than choosing simply on or off (Variable Aperture Annealing). However, these forms of annealing are still in the development phase. Use of the annealing algorithm is more completely documented in Davey et al. (1989) and Long et al. (1991), and is not repeated here.

It remains to choose a data set to try to match with the model results. In principle, any phy-

sical phenomena which can be numerically modeled and also monitored in the field can be used in the inverse method. In practice, it can be quite difficult to pick a good data set for analysis.

The simplest approach has been to use the steady-state head distribution resulting from a pumping test. The energy function is constructed as a function of the differences between modeled and measured heads or drawdowns. Drawdowns induced by such a test are conceptually simple to measure and steady flow is easy and quick to model, allowing many annealing iterations to be practical. However, for steady flow, the pattern of drawdowns is independent of the conductance of the medium. So, annealing using a single steady flow test will only give a pattern of conductors which matches the head distribution. The conductance of the elements is simply scaled up or down until the observed (or applied) flow conditions are matched. This means that the models obtained in this manner tend to be more sensitive predictors of head than they are of flow. For the Stripa Project, most of the predictions are centered around the prediction of flow.

Greater sensitivity to flow prediction could be gained by combining a series of steady flow tests. In this case, each of the separate tests would be modeled at each iteration and the element conductance would be chosen to best fit all the flow data. If constant head boundary conditions are used at the pumping well, the energy function can be constructed as an appropriately scaled combination of squared head differences and squared flow differences. If constant flow is applied at the pumping well, the energy function can include the head at the pumping well treated as any other observed head. Using multiple steady tests may actually be the most ideal of all for the annealing method because there is no dependence on storage coefficient and the time required for steady flow calculations is very small. However, in the field each steady-state test is very time consuming, and, consequently, few are available. In the case of the SCV site, multiple steady tests are not available.

Alternatively, one can use the transient interference data from a constant flow test. For example, the flow rate used in the field can be specified in the model in order to predict the transient drawdown response. At each iteration of annealing, the model will predict curves of drawdown versus time. These curves can be shifted in both the x- and y- directions (x-shift, y-shift) in

log-log space until a best match is obtained to the real curves. This process is similar to matching data to a Theis curve but in this case the shift corresponds to picking the best-fit conductance and storage coefficient for the lattice elements in the model. With several observation points, it becomes necessary to find the best shift on average. Although this process is conceptually simple, the difficulties of numerical calculation combined with the vagaries of real data can make curve matching extremely difficult to do automatically for thousands of iterations. The energy at each iteration is the sum of the differences in log of head for each observation point at selected times. The advantage of using this type of data in annealing is that the transients are reflecting the distribution of heterogeneities in space. A steady test is more likely to reflect the biggest bottle-neck, irrespective of where it is. The disadvantage of this data is that an assumption must be made about the relationship between storage and conductance; in other words there is more information, but another parameter to specify.

A slightly different procedure must be used if the transient test is a constant head test because in this case both the transient drawdown data at the observation wells and the transient flow rate at the pumping well should be used. Thus the energy will be a combination of log of flow differences and log of drawdown differences and a decision must be made about how to weight these. Another nuance is that the y-shift is not correct for the drawdown data but is correct for the flow data. This is because head is pegged by the constant head boundary condition. Consequently, constant head tests are somewhat more sensitive to the initial estimate of the element conductances and in practice more difficult to use in annealing than constant flow. At the SCV site, the main interference test is the Simulated Drift Experiment (as described in Section 3) which is a constant head test.

If several different tests are available, these can be combined. In principle any combination of steady, constant flow transients or constant heads transient can be combined. The main drawback for combining a large number of transients is the possibility of needing an enormous amount of cpu time. The number of calculations needed is the number of tests times the number of time steps times the number of iterations. It is not difficult to conceive of a problem with, for example,

5 tests × 50 time steps × 10,000 iterations, or $2.5 \cdot 10^5$ calculations. If it takes 2 minutes of cpu time per calculation, a month could be needed to anneal a big problem.

For multiple constant flow transients, the procedure is relatively straightforward. At each iteration, each test is simulated and the the curves are all shifted in both x- and y- directions to get the best fit. Theoretically, a steady flow case is a subset of a constant flow test, and the steady drawdowns predicted by the model can be matched to the data by a shift in the y-direction. The x-shift is irrelevant for steady-state conditions. However, once a constant head test has been included, a y-shift cannot be used to match the drawdown data from the constant head test. One approach might be to not to use the y-shift on any of the drawdown curves. In this case, a good a priori estimate of channel conductance is needed. Again, flow data should be included in the energy function for the constant head case. If the Large Scale Cross-hole (LSC) tests (described in Section 3) is combined with the SDE test then constant flow and constant head tests are being combined.

Given a cluster of wells, the utility of combining test data in co-annealing is optimized if the tests are conducted from wells at different parts of the cluster. Tests conducted from wells that are relatively close together will cause essentially the same responses in the observation wells. Therefore the combination of tests from wells in close proximity will not give much more information than a single test. This can be referred to this as "parallax" between tests.

Although annealing is simple in concept, application requires a thorough understanding of well test analysis and a great deal of attention to efficiency in calculation. In addition, the application to Stripa data precedes a complete theoretical understanding of annealing. In many cases presented here decisions are made based on judgement and these judgements have not yet been tested in controlled synthetic examples. Practical problems with real data have received the most attention.

1.3. Goals

The fundamental goal of this part of the program is to develop a fracture flow model based

on an initial data set and use this model to predict the flow and transport behavior during a new test. Then, given data from the new test, predict a second test, etc. The first prediction is inflow into a clustered group of boreholes (the D-holes). The measurement of flow into the D-holes is called the "Simulated Drift Experiment" (SDE). Then the Validation Drift is excavated and both inflow into the drift and head perturbation due to the drift is predicted. Finally, the hole, T-1 is opened in the H-zone and drawdown and inflow into the hole measured. In all cases, predictions are compared to the following measurements:

(1) The total rate of ground-water inflow into the D-holes.

In order to evaluate this modeling approach, the inflow into the D-holes using the Large Scale Cross-hole data and neglecting all information from the D-holes was predicted. The calculated flow can then be compared to the measurement of inflow from the SDE.

(2) The total rate of ground-water inflow into the Validation Drift.

The amount of inflow from the major fracture zone that intersects the drift (the H-zone) was predicted. The modeling approach for Stripa is based on the assumption that flow through these zones carries nearly all the flow. Therefore, calculation of flow into the drift through the major fracture zones is presented as an approximation of total flow into the drift.

The fracture flow models used to make this prediction were made by changing the permeability of the fracture elements near the drift to reflect changes in stress and two-phase flow conditions after excavation of the Validation Drift. This change is based on judgement and analogy with other sites. Consequently, comparison of these calculations with the actual measured drift inflow is not relevant to validation of the modeling approach. It is simply a measure of engineering judgement.

(3) The response of the ground-water head to the existence of the Validation Drift, including the magnitude and spatial distribution of the head changes.

The changes in head distribution in the block caused by the presence of the Drift are

predicted. The same qualifications raised in the drift inflow prediction apply.

(4) The inflow into the remaining D-holes after the excavation of the the Validation Drift. The same qualifications raised in the drift inflow prediction apply.

(5) The magnitude and spatial distribution of the ground-water head changes in the SCV site caused by opening a borehole (T-1) and allowing it to drain water.

These calculations were carried out using a series of models. The first models were simple two-dimensional models of the H-zone. Then a three-dimensional model of the seven fracture zones was used. The remaining report is organized according to the model type rather than the prediction.

1.4. Caveats Concerning These Predictions

Data. The predictions cannot be better than the available data. The Stripa project has collected a unique and impressive data set which is a tremendous resource. However, perturbations in the mine have taken place due to other activities such as the sealing experiments. During certain tests, it was found that wells were open and flowing when they were thought to be closed. The hydraulic system was never at rest during the entire span of the SCV project. Transients from the tests were superimposed on previous, unquantified transients. Pumps or packers failed in the middle of tests. The act of making measurements changed the system being measured. For example, flow was redistributed from one hole to another during the last stage of the SDE for no apparent reason. These types of problems are inherent in field studies, and are hard to quantify.

A second problem was insufficient or inappropriate data. Although Stripa represents a remarkably rich data base, the project is finite and was subject to limitations of time, budget and imagination. For example, cross-hole tests are the primary source of information for the inverse approach presented here. These tests were limited in number and extent. Only one of these could be used in annealing. More serious is the fact that there was little data that could be used to relate the tracer behavior to the flow behavior. However, the determination of how best to predict transport in a fractured media is a research project in itself. The major contribution of this work is

simply to try an approach with what was available and see how good the answers are.

Physics. The effects of excavation on the near-field hydrology are not well understood. Due to limitations of time and budget, the Stripa Project did not conduct any experiments designed to quantify these effects. Stress - permeability relationships were measured in the lab but may have little to do with in-situ behavior. There is some evidence that two-phase flow may exist due to de-gassing, drying or gas being blasted back into the rock. However, the effect of stress on flow is not separable from the two-phase flow effects. Even if the model does well predicting fluid flow elsewhere in the block, the effect of drift skin on inflow was so significant that it swamps any other effects. Any prediction of behavior as measured in the drift is not at this point a good measure of the applicability of a modeling approach.

Boundary Conditions. Flow into the numerous mine drifts and other drains surrounding the SCV block are largely unquantified. It is incorrect to simply model these as sinks at atmospheric pressure because many or all of them are surrounded by a low permeability skin which decreases the inflow. Likewise, when the excavation of the Validation Drift took place, there was a dramatic decrease in the inflow as compared to the flow to the D-holes (SDE). Consequently, the drift ceased to be as dominant a sink for the block. In this case, nearby drains outside the block may dominate flow gradients which will in turn dominate the tracer behavior. These effects are not well understood. This is a common problem for hydrologic models and should not be considered fatal. Due to time constraints the effect of the boundary conditions on the annealing solution was not examined.

Computation. Due to time constraints, only a few realizations of the equivalent discontinuum fracture network were constructed. It is not clear that a single realization is an appropriate indication of the power of the inverse approach. However, a single realization is a good way to evaluate the merits of this approach.

Another limit of computation is the size of the problem that can be handled. In a number of cases, it might have been useful to include more detail or more possible channels in the models, but this was simply impractical.

Conclusion. Although there are some serious caveats concerning the comparison of these model results with the measurements, such comparisons will be most important for what they tell us about what we do not know. For example, it was the prediction of inflow to the drift that made it obvious that we do not understand excavation effects. These calculations highlight processes that warrant careful investigation and areas where accurate measurements are particularly important.

1.5. Structure of this Report

Section 2 of this report summarizes the conceptual model defined in Black et al. (1991) and provides a geologic framework for the base model or template that used for annealing. Section 3 summarizes all the hydrologic data available for analysis. Section 4 describes the numerical scheme used to make the above predictions. Section 5 gives the results for all the two-dimensional models of flow and Section 6 gives the results for the three-dimensional cases. A substantial amount of additional cases were run for this project but are not included here because the data used to construct these models had not been corrected to account for superimposed transients. In fact, all of the cases run before June, 1991 used incorrect data and are excluded from this report. Finally, Section 7 presents conclusions and an analysis of what was learned from this exercise.

2.0. GEOLOGY OF FRACTURE ZONES AT STRIPA

Geophysical measurements and structural geologic studies were conducted to aid in the hydrologic examination of the SCV block. This section identifies the thin tabular features (fracture zones) inferred from the geophysical measurements. It then describes and interprets the fracture system geology of the SCV block as revealed in drift exposures, checks the interpretive model against borehole records, and discusses the hydrologic implications of the model.

Geophysical techniques were heavily relied upon heavily to identify and locate fracture zones within the SCV block. The fracture structure within the SCV block was difficult to define using geologic data alone because of the depth of the SCV block, the location of the block in a remote area of the mine, and the scarcity of bedrock exposures at the surface. For a discussion of the geophysical techniques, one should consult the report by Black et al. (1991).

Seven major fracture zones (A, B, H, Hb, I, M, and K) were inferred within the SCV block (Figures 2.1 and 2.2) based on the geophysical tests (Black et al., 1991). The orientations of the zones and the coordinates of a point in each zone are shown in Table 2.1. The projected intersections of the zones (as defined in Table 2.1) with the different boreholes at the SCV site are listed in Table 2.2. The actual intersections of the zones with the boreholes are listed in Table 2.3. The match between Tables 2.2 and 2.3 is good. All of the zones thus have been interpreted to be planar features, but as Olsson et al. (1989) note, these zones all have irregular appearances on geophysical tomograms and probably vary considerably in thickness and in their bulk material properties.

These zones can be grouped into three sets based on their orientation (Figures 2.1 and 2.2). Zones A and B dip moderately to the southeast. Zones H and Hb, which together form the feature with the most prominent geophysical fingerprint, steeply to the east, as does zone I. Zones M and K dip steeply to the northeast. Zones A, B, and H were considered to be extensive and continue

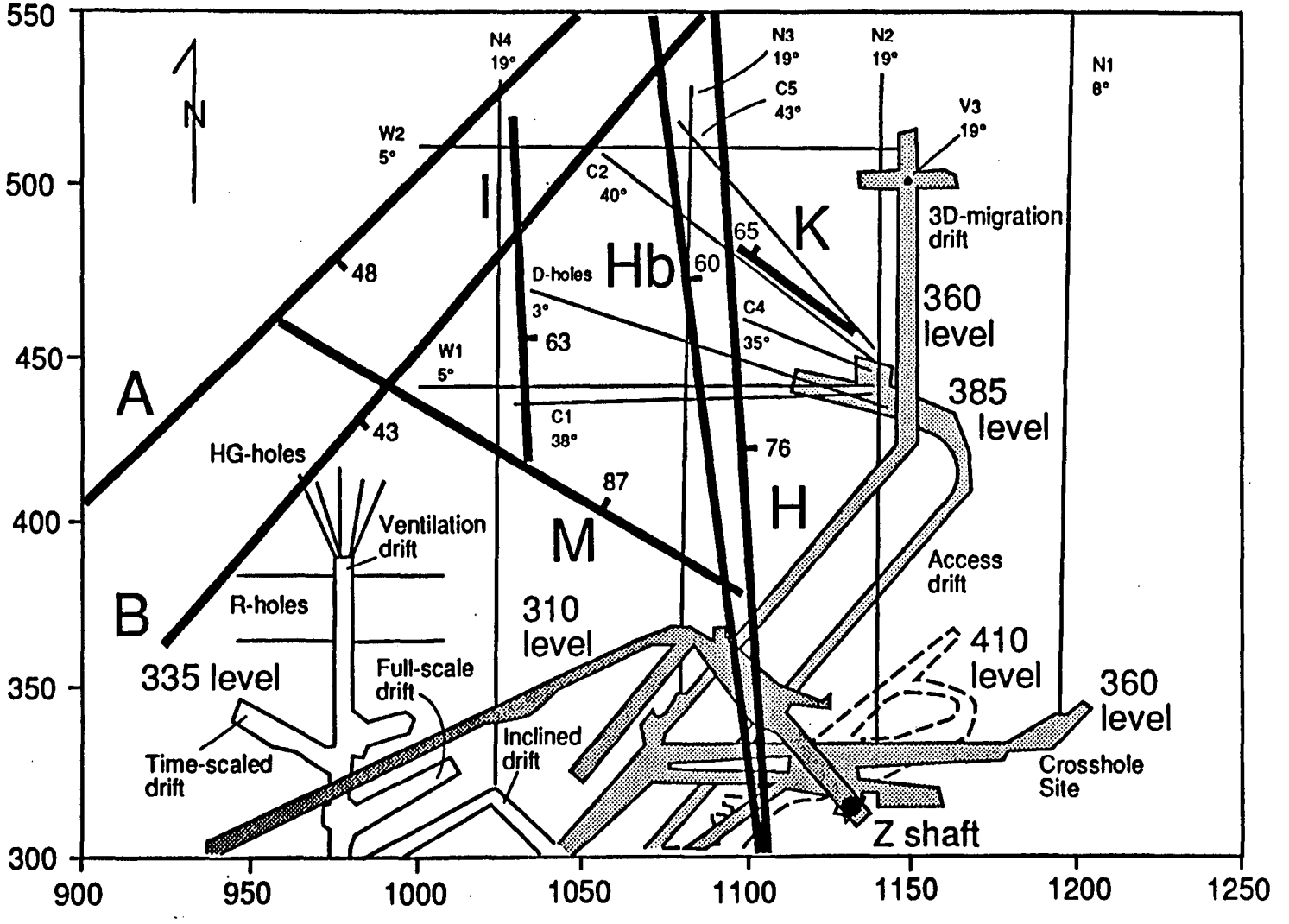

Figure 2.1. Conceptual model of the major SCV fracture zones (modified from Black et al., 1990).

Table 2.1. Inferred position and orientation of SCV fracture zones

Zone	Strike	Dip	Thickness	Coordinates of Zone Center		
				x	y	z
A	47°	48°	1-10 m	598	1100	360
B	40°	43°	1-10 m	567	1100	360
H	355°	76°	≈20 m	450	1097	360
Hb	353°	60°	≈ 5??m	450	1085	360
I	356°	63°	1-10 m	450	1033	360
M	300°	87°	1-10 m	450	967	360
K	305°	65°	1-10 m	479	1100	360

Table 2.2. Depths in meters of intersection of SCV fracture zones (as defined in Table 2.1) with SCV boreholes.

Zone	W1	W2	N2	N3	N4	C1	C2	C3	C5	D1
A	-	125.52	-	179.49	168.74	141.14	112.10	-	110.51	-
B	141.74	87.39	196.31	139.12	122.81	98.02	82.55	-	82.2	79.71
H	49.11	56.57	-	-	-	53.01	67.96	52.44	81.71	25.76
Hb	60.27	70.71	-	-	-	54.73	67.38	61.11	77.11	29.65
I	110.93	118.08	-	-	-	104.40	125.86	-	-	85.88
M	-	-	18.22	39.88	102.05	-	-	-	-	-
K	-	-	149.01	-	-	-	-	-	-	-

Table 2.3. Recorded depths of intersection of SCV fracture zones with SCV boreholes.

Zone	W1	W2	N2	N3	N4	C1	C2	C3	C5	D1
A	-	124-145	-	162-170	153-155	138-148	109-112	-	119	-
B	130-138	78-91	188-190	133-145	122-126	96-100	76-82	-	90	81-89
H	46-50	50-57	-	-	-	45-54	63-69	59-61	84-85	23-28
Hb	59-60	67-71	-	-	-	45-54	63-69	59-61	84-85	23-28
I	108-112	116-121	-	-	-	105 109	122 124	-	-	83
M	-	-	29-31	39	111					
K	-	-	151-153	-	-	-	-	-	-	-

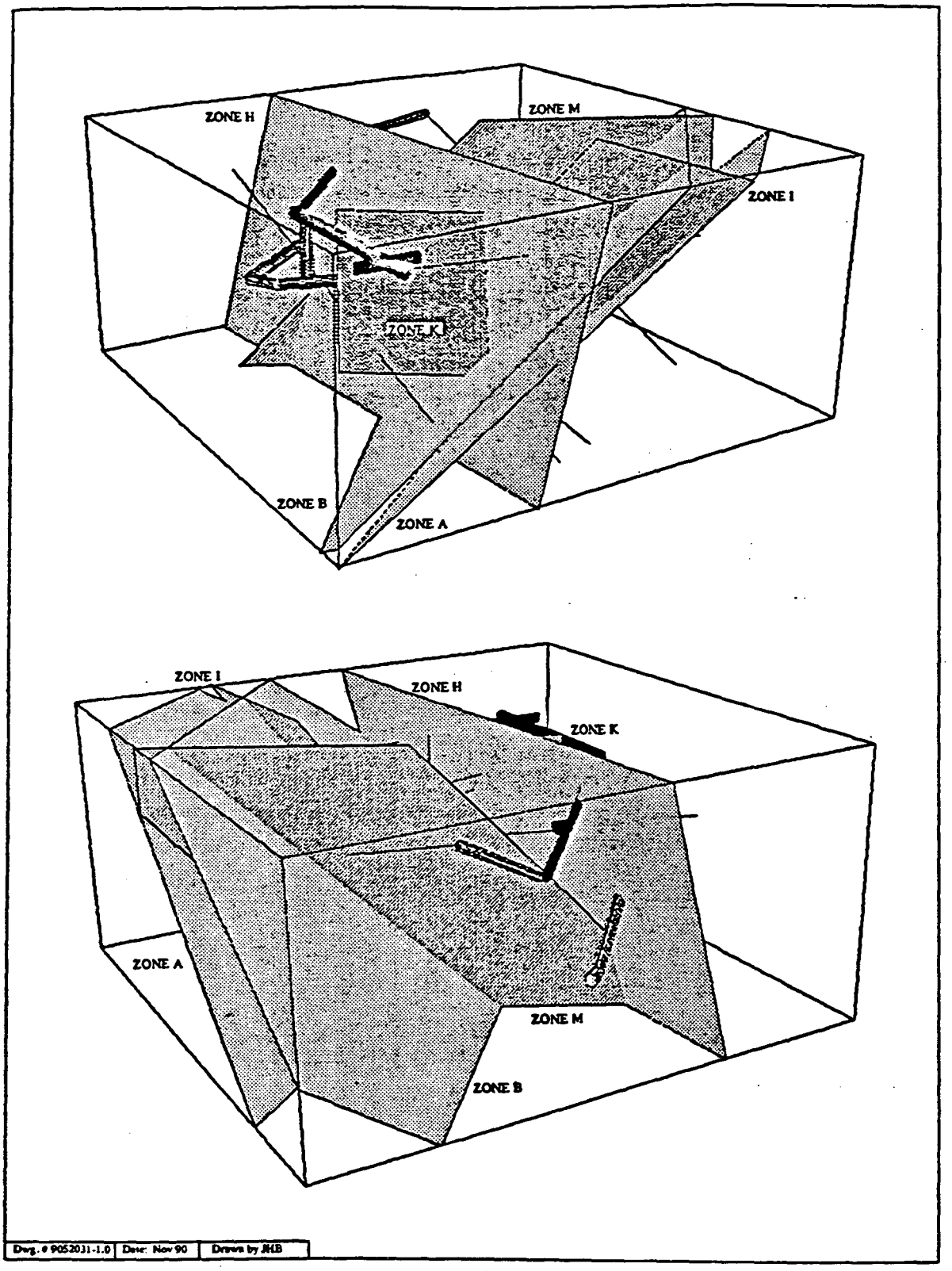

XBL 921-5532

Figure 2.2. The location of all the features of the conceptual model in 3D space.

well outside the SCV test volume (Black et al., 1991). Zones I, M, and K were inferred to have in-plane dimensions roughly equivalent to the length of the SCV block (approximately 100 meters).

Only zone H (together with Hb) appears to intersect accessible portions of the mine tunnels in or near the SCV block. The plane that passes through the center of H-zone exposures at the 310-, 360-, and 410-meter depth levels in the mine strikes north-south and dips ~64° to the east. Given the uncertainty in the estimate, this orientation cannot be distinguished from the average orientation of zones H and Hb based on geophysical, hydrologic and borehole data (Table 2.1).

The structure of the H-zone was examined in some detail to aid in the hydrologic modeling. Some of the particularly pertinent aspects of the H-zone are described below. For a more complete account the reader should refer to a forthcoming report by Martel (1991). The conclusions in that report differ substantially from those in a previous report by Long et al. (1991).

The H-zone (Figure 2.3) exposures are characterized by a red granite that contrast sharply with the grey granite typical of the mine. The thickness of the red granite across the H-zone appears to vary from ~5 m to ~40 m. The color of the H-zone is its most distinguishing feature; its edges are not sharply defined based on either the intensity or orientation of its fractures. Sealed fractures of numerous orientations occur at the H-zone exposures. Most individual fractures are difficult to trace more than a few meters. However, most of the longest fractures in the H-zone exposures strike approximately to the north and dip steeply to the east, subparallel to the zone as a whole. At the 360 level, the longest fractures west of the zone generally strike 20° or somewhat more to the west, and east of the zone they strike 20° or more to the east.

Many of the fractures in the H-zone are faults and they reveal a complex deformational history. The steeply dipping faults with a northerly strike apparently have accommodated a variety of different senses of displacement. Evidence for normal dip-slip displacement on these faults is most pronounced, and is evidenced by (a) fault surfaces with slickenlines that plunge down dip, (b) faults being linked by steeply inclined fractures or cavities, and (c) displaced subhorizontal veins. Evidence for reverse slip across some faults comes from subhorizontal fractures that splay

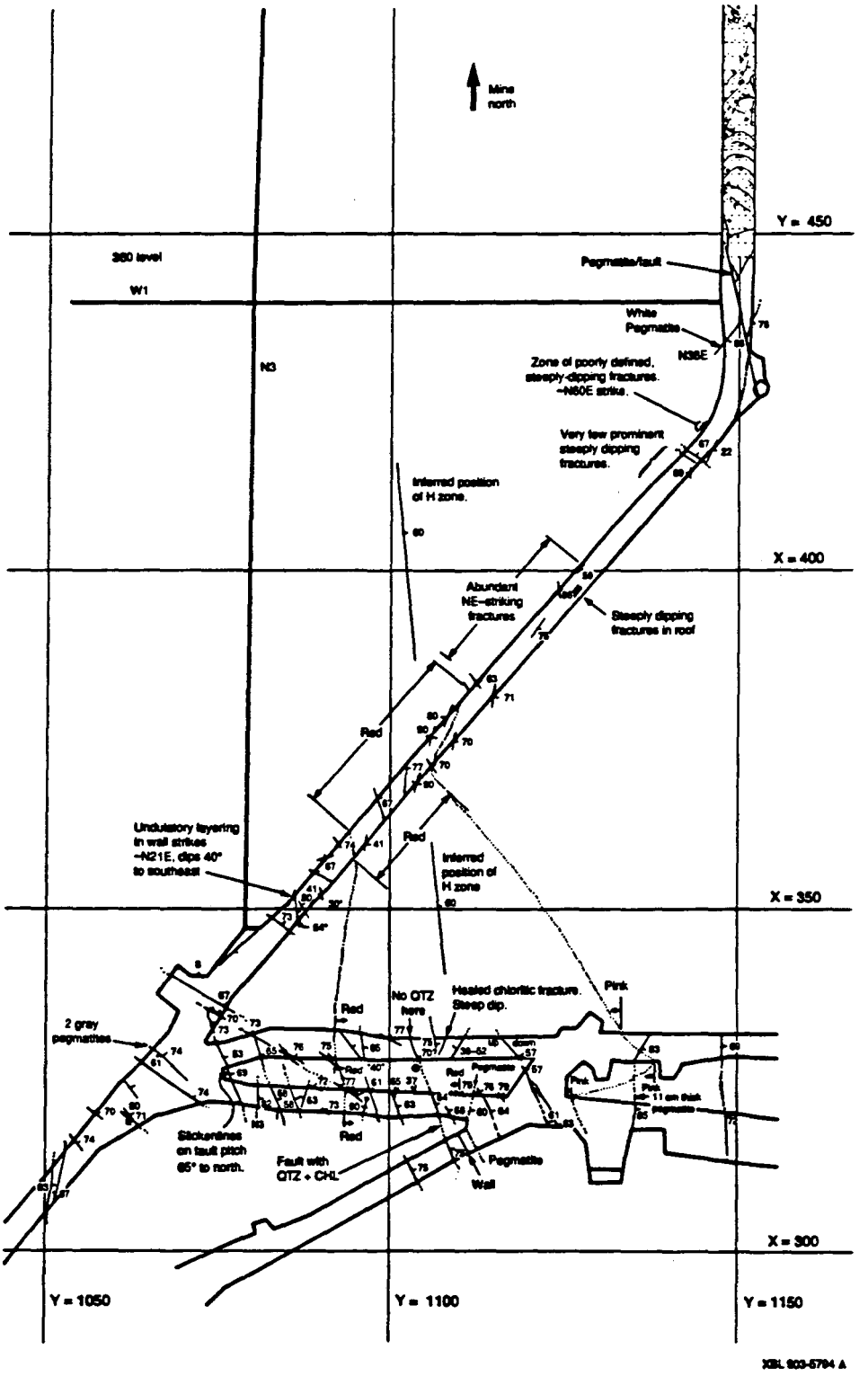

Figure 2.3. Map of prominent fractures in H-zone exposures at the 360m level.

from faults that dip steeply to the east. Finally, steeply-dipping fractures that splay to the northeast from some north-striking faults indicate that some H-zone faults have accommodated right-lateral strike-slip displacements. The rather chaotic arrangement of fractures in the H zone, the structural evidence for at least three episodes of slip on zone-parallel faults, and the previously published evidence (Wollenberg et al. 1980) for at least two episodes of mineralization along fractures at Stripa are consistent with the Stripa fracture zones being old reactivated fault zones.

Although most of the permeability and much of the porosity in the Stripa granite is due to the fractures, some cores show porosity in the form of pitting. The pitting has been interpreted to reflect dissolution of quartz from the granite (Carlsten (1985). This kind of high porosity has been located at one spot in the SCV block through geophysical techniques. Pitting in the granite can be observed in drift exposures along an H-zone fault at the 410 level. At this location, flourite has been precipitated in the granite and calcite has been precipitated in large cavities along the fault. These observations suggest that enhanced porosity in the SCV block may be due to the concentrated flow of reactive fluids along fractures.

Direct information on the fractures within the SCV site comes from four sets of boreholes (Figure 2.1). Although these holes trend in a variety of directions, most are shallowly inclined, so they are best-oriented to detect steeply-dipping fractures. Most of the fractures that are open in recovered drill cores are along pre-existing mineralized (or otherwise sealed) fractures. Independent of the location and orientation of a borehole, boreholes will tend to intersect the fractures nearly perpendicular to the borehole. This reflects either a (1) heterogeneous distribution of ordered SCV fractures together with a fortuitous siting of the holes or (2) borehole sampling bias. To test which is the case, the actual fracture orientation distribution encountered in each borehole was compared with the synthetic distribution expected if the borehole had sampled a uniform random distribution of fractures. The observed and synthetic cases match well. This indicates (1) there probably is a strong uniform random component to the actual distribution of in situ fracture orientations, and (2) the observed distribution is strongly affected by the orientation of the

borehole. The holes through the H-zone do show a higher density of steeply-dipping fractures that strike subparallel to the zone than uniform distributions would predict. Zone-parallel fractures are therefore either larger or more abundant than fractures of other orientations. The conclusion that the H-zone contains fractures of numerous orientations, but with fractures subparallel to the zone being largest or most common, squares with the drift wall observations.

2.1. Conceptual Model

The hydrologic model used is patterned directly after the seven-zone structural model of 1991 by Black et al. (Figure 2.1). The orientations of the zones in Table 2.1 are the same as those cited in a 1990 communique of Olsson's that updates the model of Black et al. (1991). The center point coordinates cited in Table 2.1 in some cases differ from the "fix points" in the Olsson communique; these shifts were made primarily for computational reasons, and in no cases cause the fracture zones to be translated more than three meters from the positions defined in the Olsson communique. Square meshes were imposed on the zones to define the possible locations of conducting elements. Square meshes were chosen because none of the available data indicated that the flow within the zones would be anisotropic because of structural anisotropy in the zones. The density of the zone meshes differ in accord with the amount of resolution needed; meshes are most dense for the H-zone.

3.0. DATA

Although a large amount of data was collected in the Stripa Project, a only small percentage of these data were useful for the modeling approach described here. The entire data set is described in Olsson et al (1989) and Black et al. (1991). A description of the subset of the hydrologic data that was used and in some cases, explanations for why certain data was not used is given here. Fundamentally, flow data and drawdown data were used to make predictions of flow and drawdown. It is important to recognize that much of the potentially useful flow and drawdown data cannot be used because insufficient time was available to collect high quality data. In addition, some potentially useful data was never reduced to a useable form, also due to time constraints.

There are essentially three hydraulic data sets that were useful. The first is the background head conditions with no open sinks in the block. The second is the Simulated Drift Experiment (SDE), and the third is the Large Scale Crosshole (LSC) tests. These are described below. All the data is related to monitoring intervals established in each of the wells. The exact geometry of these wells can be found in Black et al. (1991). The intervals are numbered within each well, so for example, C1-2 is the second interval from the bottom of the hole in well C1. In all, there were 40 intervals within the SCV block, and, of these intervals, 27 intersect fracture zones identified in the conceptual model. Because only fracture zones were modeled, only the data from the 27 intervals that intersect fracture zones was used.

3.1. Background Heads

The background heads are the values of hydraulic head measured when all the holes are closed, before the drift is excavated and most importantly, when all the heads have recovered to equilibrium values. Values of drawdown due to any perturbation were derived with respect to these equilibrium values. There was never a time in the history of the SCV Project that such

conditions were met (J. Black, personal comm.). Consequently, the period of time following the SDE was chosen to estimate what the heads would have been if they were allowed to fully recover. This time was chosen because it was not until after the SDE that the C-holes were instrumented with packers. Unfortunately, the data in the C-holes from this period after the SDE were either lost or rendered useless due to interference. Equilibrium head values in the SCV block are therefore only available in the W- and N-holes. The N-holes do not penetrate the H-zone, so there were only two values of equilibrium head in the H-zone (W1 and W2).

3.2. Simulated Drift Experiment

The Simulated Drift Experiment (SDE) was designed to mimic the hydraulic conditions imposed by an excavation with a series of boreholes (the D-holes) (Black et al. 1991). The six sub-horizontal D-holes were 100 m long and drilled in a ring of five with one in the center (Figure 3.1). The outer five boreholes lie on the periphery of the simulated tunnel. The pressure in the D-holes was lowered in three steps, each step lasting a few weeks. The last step lowered the pressure in the D-holes to 17 m above atmospheric. During each step, inflows to the D-holes were measured and pressures in the surrounding rock were monitored. Inflows were measured with a packer system that allowed the location of inflow to be estimated. After the SDE, the Validation Drift was excavated through the first 50 m of the D-holes, leaving the remaining 50 m of D-holes undisturbed. The 50 m of the D-holes that remain after excavation are called "the remaining D-holes."

The heads in the SCV block were not in equilibrium at the start of the SDE. These heads were still recovering from previous perturbations and the drawdown data presented in Black et al. (1991) were not corrected for this recovery. The reported drawdowns are simply the at the start of the SDE heads minus the measured heads at any point in time. Because the prior recovery is superimposed on the signal from the SDE, all of these reported drawdowns in Black et al. are too low. This problem was recently recognized and Black and Parry (pers. comm., 1991) were made an attempt to correct the drawdown data. Unfortunately, they were only able to correct the estimated steady state drawdown at the end of the last step of the SDE. None of the transient data

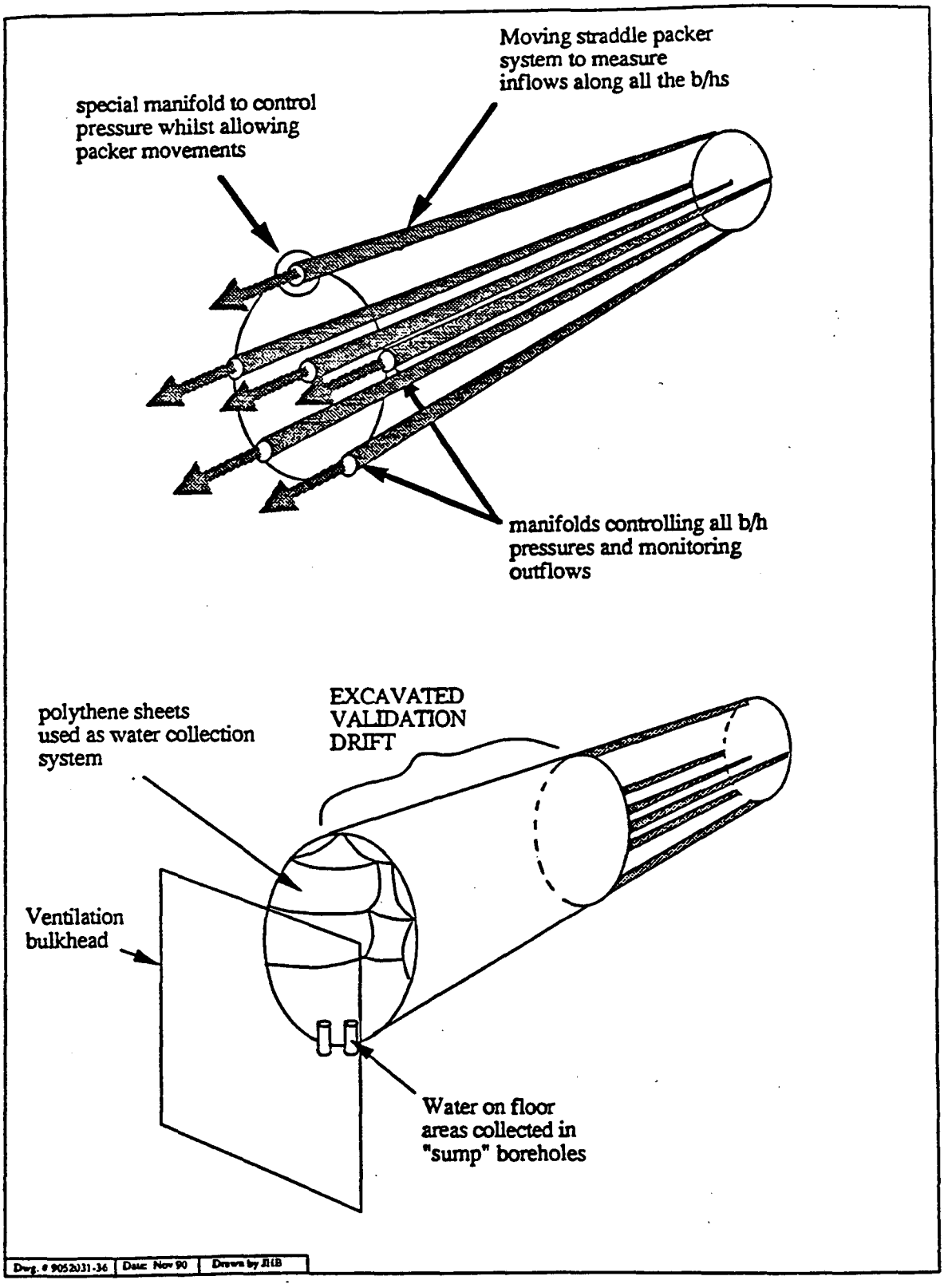

XBL 921-5533

Figure 3.1. The concept of the Simulated Drift Experiment (after Black et al., 1991)

was corrected. Furthermore, an equilibrium head value for the D-H and D-B zones is hard to estimate. The lack of this data is particularly unfortunate because this means that the imposed drawdown during the SDE is poorly known.

Table 3.1 gives the corrected steady state head and drawdown data for the SCV block for those borehole intervals that intersect fracture zones (after Black and Parry, 1991, pers. comm.). The recovered long term heads are estimates of the head that would have been measured in the block before excavation and with all the boreholes closed. Similarly, the extrapolated steady state heads for the third step of the SDE are estimates of the head that would have been measured in the block if the SDE had been allowed to reach steady state. In some cases, no estimate could be made and the table gives the minimum recorded head at the end of the SDE. In these cases, the head values in the table are expected to be too high. The error for these cases is unquantifiable but it is expected to be comparably larger than cases where an estimate could be made even though the value in the table is smaller. The drawdown due to the SDE is just the difference between the estimated equilibrium head and the estimated steady state head at the end of SDE, but in the cases where no estimate of the steady state head could be made, the table gives the instantaneous drawdown at the end of the SDE. Although an error for these cases is listed in the table, it also is actually unquantified and expected to be relatively large. Even in the cases where estimates can be made, the error associated with the drawdown estimates is rather large; any where from 12 to 42 m. Similarly the table gives the estimates of steady-state head and drawdown for the time after excavation of the Validation Drift and with the D-holes left open.

Because the only usable drawdown data for the SDE are the estimated steady state drawdown, the transient flow data cannot be used. Further, the choice of steady flow rates to use for the SDE inflow is problematic. Although the purpose of the SDE is to simulate the drift, the D-holes were never actually brought to atmospheric pressure as the drift would be. At the last step of the SDE, the head in the D-holes was held at 17 m above atmospheric (i.e. a total head equal to -8 m using a datum of 360 m below ground surface and the average drift elevation is 385 m). All the steps of the SDE are used to get an estimate of the flow when the head in the D-holes is

Table 3.1. Head and drawdown data (in meters above 360 m)

B/H Interval Name	B/H Interval Interval	Conceptual Zone in Interval	Recovered Long Term Head After SDE	Extrapolated Steady State Head for the 3rd Step SDE	Extrapolated Drawdown Due to SDE 3rd Step	Long Term Measured Head with Drift D-holes Open	Drawdown Due to Drift & D-holes
N2-1	161-207	B(188-190)	216±5	182.2[1]	45.4±5[2]	192.6±.6	23.4±5.6
N2-2	111-160	K(151-153)	210.4±4	134.7±18.5	75.7±22.5	185.6±.2	24.8±4.2
N2-4	2-75.0	M (29-31)	68.0±3	61.4[1]	9.2±3[2]	65.5±.1	2.5±3.1
N3-1	101-189	A (162-170), B (133-4)	212.7±7	121.8±15	90.9±22	171.0±.5	41.7±7.5
N3-2	2-100	M (38-39)	193.7±6	159.3[1]	39.3±6[2]	150.5±.5	43.2±6.5
N4-1	142-219	A (153-156)	208.4±6	130.2±21	78.2±27	180.0±.5	28.4±6.5
N4-2	109-141	B (122-126)	209.2±8	135.0±16	74.2±24	180.0±.5	29.2±8.5
N4-3	77-108	M (102)	253.8±10	160.6[1]	72.1±10[2]	182.4±1.5	71.4±11.5
W1-1	92-147	B (130-138), I (108-12)	210.1±5.0	146.7±13	63.4±18	No Data	No Data
W1-3	55-75	Hb (59-60)	216.9±4	155.8±16	61.1±20	157.9±2	59.0±6
W1-5	2-31.0	H (46-50)	212.5±2.5	117.1±19	95.4±21.5	152.5±3.5	60.0±6
W2-1	110-147	A (124-145), I (116-21)	212.2±6.0	141.6±12	70.6±18	192.0±1	20.2±7
W2-2	76-109	B (83-91)	225.1±4.0	179.2[1]	53.7±4[2]	194.0±1	31.1±5.0
W2-3	66-75	Hb (67-71)	218.1±7.0	181.3±35	36.8±42	194.0±1	24.1±8
W2-4	48-65	H (50-57)	226.0±13	155.2±25	70.8±38	194.0±.5	32.0±13.5
C1-2	40-70	H (45-54)					
C1-3	71-105	B (96-100)					
C1-4	106-150	A (138-148), I (105-9)					
C2-1	1-70.0	H (63-69)					
C2-2	71-86	B (76-82)					
C2-3	87-124	A (109-113), I (122-4)			No Data		
C3-1	1-70.0	H (59-61)					
C4	1-60.0	H (55-59)					
C5-1	83-140	A (118-9)					
C5-2	4-82.0	B (90), H (84-85)					
D2-H[3]	24-27	H (24-26)	212±5	-8±.5	220±5.5[4]	no data	no data
D5-B[3]	28-100	B (90-2), I (94-6)	212±5	-8±.5	220±5.5[4]		

[1]using SDE minimum

[2]using instantaneous drawdown (error associated with using this as an estimate of equilibrium drawdown is higher than indicated)

[3]D holes were connected to each other during SDE

[4]alternative estimate is 230 m ± 10.5 m which indicates the error in the drawdown estimate is closer to 16 m

atmospheric in order to estimate the flow into the Validation Drift. Flow rate into the D-holes should be a linear function of the drawdown. However, as Figure 3.2. shows, the relationship was not perfectly linear. According to Black et al. (1991) there was some error in the flow measurements due to flow redistribution caused by air bubbles coming out of solution at the third step and

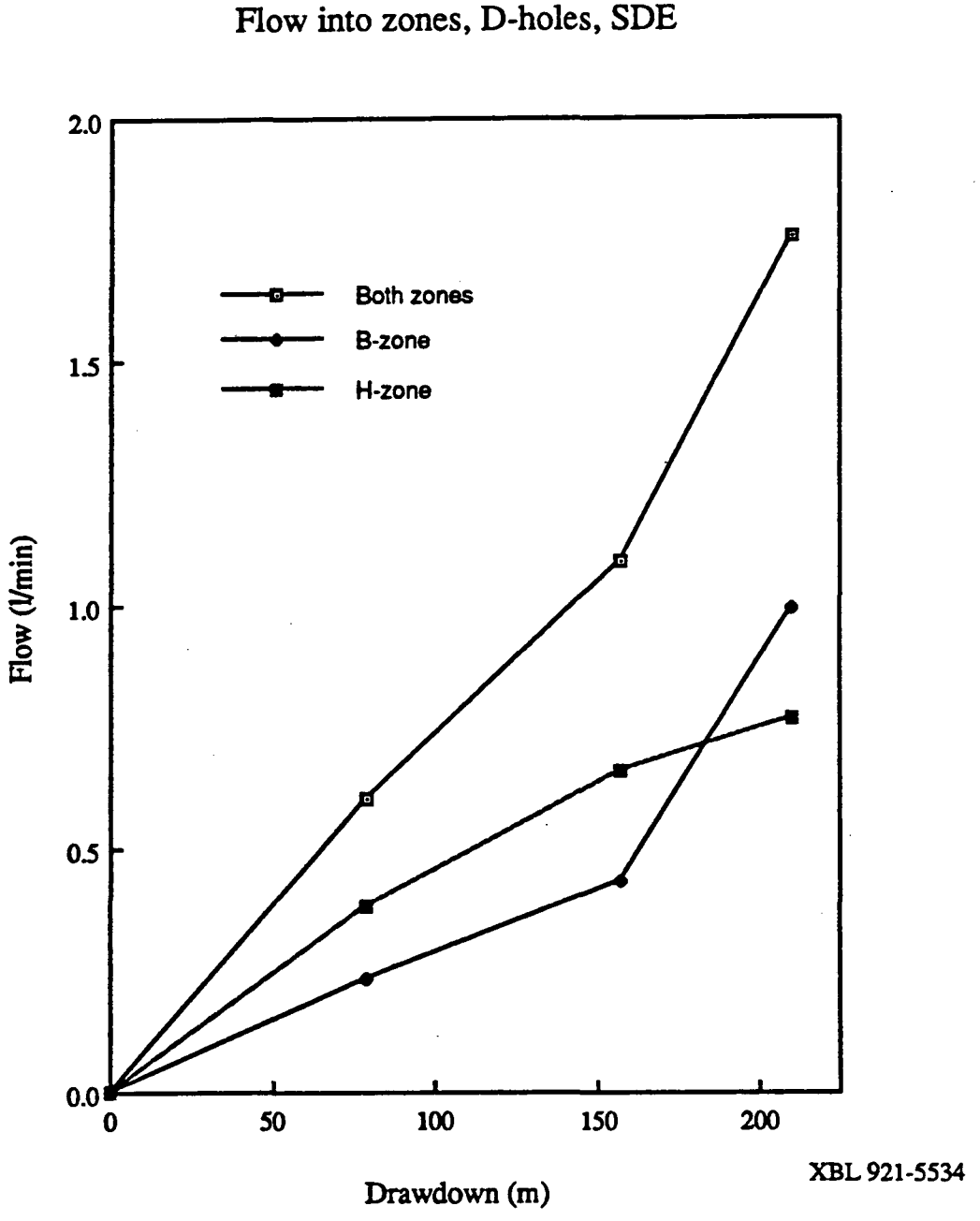

Figure 3.2. Flow measurements at the end of each of the three steps of the SDE.

due to a double counting of flow rate. The total flow on Figure 3.2. is more or less linear. However, only the separate flows into the H- and B-zones were required, and these plots are not linear. To add further ambiguity, it was possible to assign 80% of the measured inflow to either zone H or zone B, but it was not possible to assign a location for the inflow for the remaining 20%. Ten percent was arbitrarily assigned to each of the intervals (0–50 m and 50–100 m) and, it was assumed that all of the flow into the first interval is due to flow from zone H which intersects that interval, and likewise all of the flow into the second interval is due to flow from zone B.

Based on the measurements, Olsson (pers. comm., 1991) has made an estimate of the flow rate at the end of step 3. Knowing that the drawdown for step 3 was 220 m and that a drawdown of 237 would be required to bring the holes to atmospheric pressure, a linear extrapolation of the flow values gave an estimate of the flow rate which might have been measured at atmospheric. These are given in Table 3.2. In addition, Table 3.2 gives the actual measured values of inflow after excavation. Flow into the second interval (50–100 m) is flow into the remaining D-holes. The values for flow during the SDE are overestimates for these purposes because drawdown data which has been extrapolated to steady state was used, but the flow values are simply taken from the end of the SDE step 3. To be consistent, the flow values should also be corrected. However, as Figure 3.3 shows, such an extrapolation would be difficult.

Table 3.2. Flow data from the simulated drift experiment and Validation Drift.

Interval (zone)	Flow at the end of Step 3 (l/min)	Estimated flow at atmos. pres. (l/min)	Measured flow after excavation (l/min)
0 - 50 m (H - zone)	0.768 ± .2	0.827 ± ?	0.1 ± .?
50 - 100 m (B- zone)	0.942 ± .2	1.01 ± .2± ?	.563 ± .?

3.3. Large Scale Cross-hole Data

Five constant head or constant flow interference tests were performed in the SCV block. Each test is identified by the borehole interval used as the source for the test. The tests were

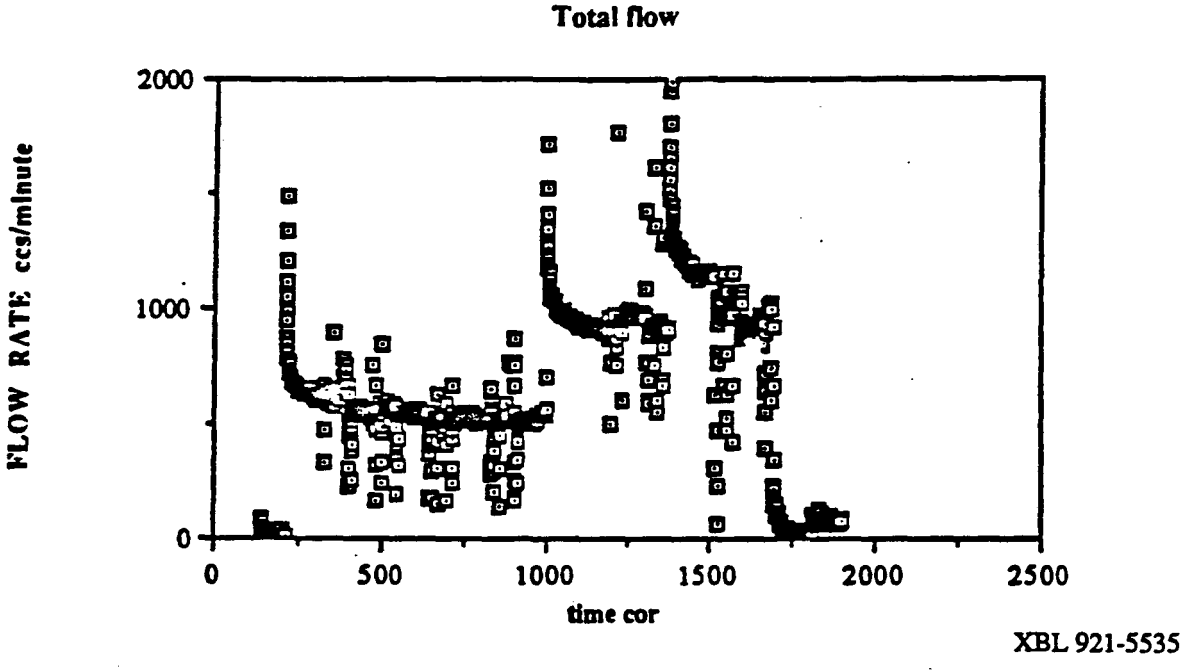

Figure 3.3. Total flow into the D-holes during the Simulated Drift Experiment.

designed to diagnose the hydrologic nature of the fracture zones that were identified with geophysics. In addition, the interval N4-3 was used as a source because injectivity is very high in this interval, even though no geophysical zone was found to intersect the borehole in this vicinity. Only the W2-3 test was a constant-head test. During each of the tests, the hydraulic head responses were monitored in all well intervals in the block.

Responses to the Large Scale Cross-hole (LSC) tests at intervals which intersect fracture zones are shown on Table 3.3. Significant responses primarily occur in these intervals which intersect fracture zones. Table 3.3 is based on data given in Black et al. (1991).

The N4-3 test was a short test (72 hrs) and very few (three) responses were observed in the block even though the N4-3 interval has a relatively high injectivity. The tentative conclusion is that N4-3 is not well connected to other fracture zones in the SCV block. However, responses observed nearby in the B-, I-, Hb- and A-zones may indicate that the test was just too short or too weak to be seen elsewhere. Consequently, this test probably does not contain much useful information for this approach.

The C1-2 test provides a very good test of the H-zone, with weak responses observed in other fracture zones throughout the block. This test was reasonably long (216 hrs.), and apparently well controlled. Of all the LSC tests, the C1-2 is the most important for this approach.

The W2-1 test was marred by having the N2-2 interval accidentally left open during the test. In the middle of the test, this zone was closed, so the remaining response is a superposition of N2-2 recovery and pumping from W2-1. The best way to use these data would be to leave N2-2 open to the atmosphere in the model and only use the first part of the data. However the flow from N2-2 was not measured because it was not supposed to be open. Therefore, there is no check on the strength of the source induced at N2-2 during this test. Also, the first part of the test is very short, about 50 hrs. Thus, the W2-1 test is of marginal utility.

The source in the W2-3 test was not well controlled (Black et al., 1991), and the duration of the test was only 72 hrs. In general, this test did create the broadest response of all the tests. However, for the intervals confined to the SCV block itself, the response to W2-3 was less than the

C1-2 test. The lack of a controlled source limits the reliability of the responses. This test is also judged to be of marginal utility.

Table 3.3. Large scale crosshole test responses as a percent of maximum drawdown in the source borehole at the end of the test.

B/H Interval		Source zones -> Type of test sup *->[1] Flow rate (ml/s)->[1] zone in source ->	N4-3 flow 2.3 M	C1-2 flow 2.9 H	W2-1 flow 5.3 A,I	W2-3 head ~16.2 Hb	N2-2 flow 1.9
name	interval	Conceptual zone in interval	%	%	%	%	%
N2-1	161-207	B(188-190)		1			
N2-2	111-160	K(151-153)		15		3	source
N2-4	2-75.0	M (29-31)					
N3-1	101-189	A (162-170), B (133-4)		3	10	4	0.4
N3-2	2-100	M (38-39)					
N4-1	142-219	A (153-156)		3	27		
N4-2	109-141	B (122-126)			17	5	
N4-3	77-108	M	source	3	10	5	
W1-1	92-147	B (130-138), I (108-12)	20	1	13	6	
W1-3	55-75	Hb (59-60)	8	[ ]	8	7	
W1-5†	2-31.0	H (46-50)		29		3	
W2-1	110-147	A (124-145), I (116-21)	3	1	source	5	
W2-2	76-109	B (83-91)		3	7	guard	
W2-3	66-75	Hb (67-71)		4	7	source	
W2-4	48-65	H (50-57)		5	6	guard	
C1-2	40-70	H (45-54)		source		5	0.6
C1-3	71-105	B (96-100)			8		
C1-4	106-150	A (138-148), I (105-9)			[ ]		
C2-1	1-70.0	H (63-69)		59		[ ]	
C2-2	71-86	B (76-82)		7		3	1.7
C2-3	87-124	A (109-113), I (122-4)		1	10	3	
C3-1	1-70.0	H (59-61)		39		6	0.6
C4	1-60.0	H (55-59)		61		5	0.8
C5-1	83-140	A (118-9)‡		5	[ ]	3	
C5-2	4-82.0	B (90), H (84-85)		24		4	
D2-H	24-27	H (24-26)		82		5	
D5-B	28-100	B (90-2), I (94-6)			16	5	

[1] "head" and "flow" tests are "constant flow" and "constant head"

[ ] = an expected response

† W1-4 actually intersects the H-zone, but W1-5 is used because it responds much more vigorously than W1-4.

‡ B and H on the boundary between C5-1, C5-2

The N2-2 test was also short (72 hrs). Response to this test was confined to five intervals in the block and all of these responses were extremely weak. N2-2 probably shows that the minor fracture zone, K is not an important hydrologic feature, but not much information is contained in this test either.

In summary C1-2 test was probably the best data of all the LSC tests. It is the longest, best controlled test and has the widest response. Thus C1-2 contains the most information for annealing. Ideally, all of the LSC tests would be used simultaneously. However, this would be a very substantial computational undertaking. Furthermore, if a test does not generate a response, then all that is known is that the source is not connected to the monitoring zones. Annealing will try to disconnect the source and the monitoring zone, but it may do this in a completely random way. One cannot infer how fractures are hydraulically connected from this kind of data.

Unfortunately, there is no cross-hole test providing information about the B-zone, which is the second most important zone in the block because it is the primary zone intersecting the remaining D-holes. Weak responses are seen from the C1-2 test in some B-zone intervals. If the pressure transients are confined to the fracture zones, the B-intervals are hydraulically distant from the C1-2 source in the H-zone. This is because the signal must travel through the H-zone, to the intersection between the H- and B-zones, and then through the B- zone. If the C1-2 test had been longer, or a stronger source, the pressure signal may have reached the B-zone. Transient data from the C1-2 test are shown in Figure 3.4.

3.4. Inter-Compatibility of the Data Set

Beyond the problems that arise within each of the three data sets, there are some compatibility problems with using the three data sets together. The primary problem is that there are some intervals which responded to the SDE test and did not respond to the C1-2 test. The SDE was a much longer test, so this lack of compatibility may simply be a limitation of the data. In a fully three-dimensional model, this limitation would not cause any problem. In a three-dimensional lattice of one dimensional conductors where a well interval could be connected to more than one "layer" of lattice elements, it would be possible to have interval A connected to

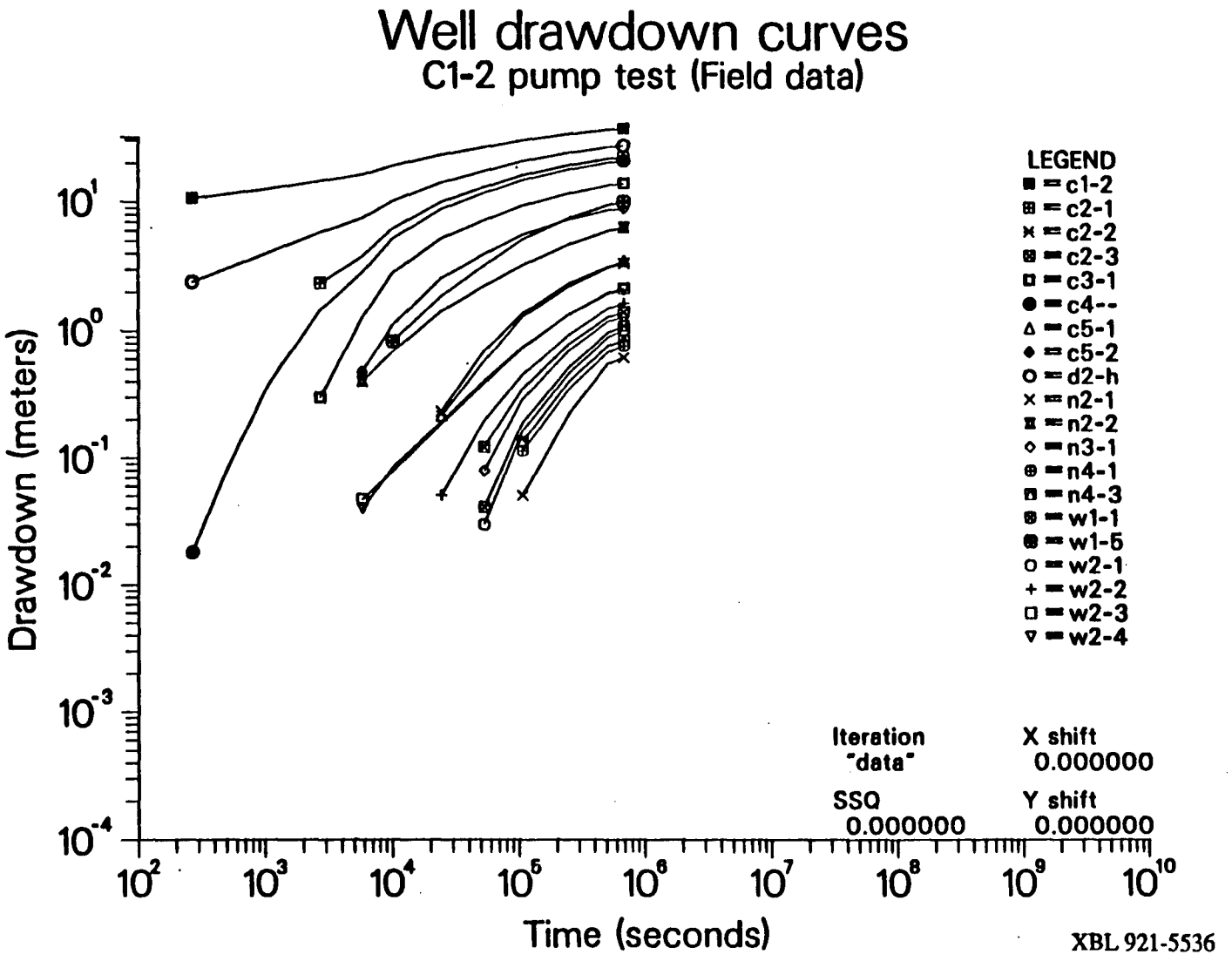

Figure 3.4. Transient data from the C1-2 test.

intervals B and C, but interval B not connected to interval C. However, the models used here are all two-dimensional (the H-zone model) or quasi-two dimensional (the zone model). In these models, if A is connected to B and C then B must be connected to C. This means there is no possible configuration of the model which responds to the SDE but does not respond to the C1-2. Thus, when these two data sets are used together, there are very few reliable and compatible data points. These are summarized in Table 3.4. If the compatibility and reliability ranking is 1, then the data point can be used to combine C1-2 and SDE data. If the ranking is 2, then either the data from the SDE was available and extrapolated to steady state, or the interval response to C1-2 was greater than the measurement limit (1%), but not both. If the ranking is 3, then the interval did not respond to C1-2 and did not respond to SDE or there was no SDE data for this interval. Only the data with rank 1 can be used to see if a given model behaves both like the C1-2 test and the SDE.

3.5. Summary

The reliable data available from the SCV applicable to this approach were much less than what was expected. The lack of good equilibrium head data and all the transients from the SDE were major problems for this analysis. Essentially, what is left is one transient test, C1-2, and one steady state test (SDE). Further, the errors for the steady state SDE drawdowns are very large, in some cases over 100%. No error estimates were available for the transient data. To some extent, this situation exists because the SCV project was not designed to collect the type of hydraulic data used here. The LSC tests which are an integral part of this analysis, were added essentially as an after-thought squeezed into an unreasonably short time period. However, the SDE was an integral part of the SCV project and the loss of so much of this data is truly unfortunate.

The analysis that follows, relies heavily on the C1-2 test to find patterns of conductors for the SCV. A limited number of synthetic studies have indicated results improve significantly when two or more transient tests are used to find the configuration (J. Peterson, pers. comm., 1991). Thus having only one transient test may be a severe liability. However, this exercise was a useful research endeavor with a developing code and a developing methodology. In particular, the

Table 3.4. Compatibility between data sets.

Borehole Interval			Test		
		Flow rate (ml/s) ->	C1-2 5.3	SDE 280	Reliability Rating: 1: both good
		Zone in source ->	H	H,B	2: one good
		Type of test ->	transient	steady	3: incompatible data
name	interval	Zone in interval	% Response	Δs ± error	
N2-1	161-207	B(188-190)	1	45.4±5†	3
N2-2	111-160	K(151-153)	15	75.7±22.5	1
N2-4	2-75.0	M (29-31)		9.2±3†	3
N3-1	101-189	A (162-170), B (133-4)	3	90.9±22	1
N3-2	2-100	M (38-39)		39.3±6†	3
N4-1	142-219	A (153-156)	3	78.2±27	1
N4-2	109-141	B (122-126)		74.2±24	2
N4-3	77-108	M	3	72.1±10†	2
W1-1	92-147	B (130-138), I (108-12)	1	146.7±13	2
W1-3	55-75	Hb (59-60)	[ ]	61.1±20	3
W1-5	2-31.0	H (46-50)	29	95.4±21.5	1
W2-1	110-147	A (124-145), I (116-21)	1	70.6±18	2
W2-2	76-109	B (83-91)	3	53.7±4†	2
W2-3	66-75	Hb (67-71)	4	36.8±42	1
W2-4	48-65	H (50-57)	5	70.8±38	1
C1-2	40-70	H (45-54)	source	no data	2
C1-3	71-105	B (96-100)		no data	3
C1-4	106-150	A (138-148), I (105-9)		no data	3
C2-1	1-70.0	H (63-69)	59	no data	2
C2-2	71-86	B (76-82)	7	no data	2
C2-3	87-124	A (109-113), I (122-4)	1	no data	3
C3-1	1-70.0	H (59-61)	39	no data	2
C4	1-60.0	H (55-59)	61	no data	2
C5-1	83-140	A (118-9)	5	no data	2
C5-2	4-82.0	B (90), H (84-85)	24	no data	2
D2-H	24-27	H (24-26)	82	no data	2
D5-B	28-100	B (90-2), I (94-6)		no data	3

† No steady state estimate available, using instantaneous drawdown. Error when using this data to approximate steady state is much larger than that given.

strong geophysical program at the SCV has allowed us to develop a conceptual model with more confidence and detail than previously possible. Moreover the SCV provides an excellent opportunity for examining the concepts under development.

4.0. MODELING THE PREDICTIONS

The following sections describe how annealing was used to find configurations that match some of the hydraulic data available for the SCV. Once these configurations were found, they were used to make the set of predictions. Through a series of modifications that are described below.

4.1. The SDE Inflow and Drawdown Response

In order to predict the flow into the D-holes, the C1-2 test was used to anneal a configuration. Then the C1-2 node in the model was closed and the equilibrium heads imposed by the boundary conditions were obtained. The head at the D-holes was then lowered by 220 m. Flow into the D-holes was calculated, and the calculated heads were subtracted from the equilibrium heads to obtain drawdowns.

4.2. The Validation Drift Inflow and Drawdown Response and the Inflow to the Remaining D-holes

Calibration to SDE Flow. Before the drift effects were added to the model, the model was first calibrated to the SDE. This was done in one of two ways. Theoretically, the best way is to co-anneal the SDE data along with the C1-2 data. This is done by modeling the SDE as a constant flow test with a flow rate of 0.768 l/min* from the H-zone and 0.942 l /min from the B-zone. Co-annealing was then used to match the drawdown observed at all the intervals during both tests. Co-annealing was used for the two-dimensional model of the H-zone, but there are only two data points, W1 and W2 where a match to both the SDE and with the C1-2 data can be expected. Even for these intervals it may be difficult to match both tests because the response of W1-5 to SDE far exceeded the response of W2-4. However in the C1-2 test the intervals responded almost the same. Consequently annealing was set up to match the smallest acceptable SDE drawdown in W2-4 (32 m). Co-annealing was not attempted for the three-dimensional model.

*The use of "l/min" by all investigators was decided on by the Stripa Project to promote comparisons.

In the three-dimensional case the configuration annealed to C1-2 was used to model the SDE. The SDE was modeled as a steady flow case, with constant flow conditions imposed at the D-holes. A constant flow condition was used because the strength of the source of the SDE was measured, but the drawdown at the D-holes is uncertain. To model the Validation Drift (VD), the head at the D-holes is calculated and decreased by 17 m. This new head is then imposed at the D-holes to model the VD.

Addition of Skin Factor. Given the model calibrated to the SDE flow, it remains to calculate the effect of excavation on inflow. The effect of changing the inner hydraulic boundary conditions from that caused by the six D-holes to that caused by a 2.5 m diameter drift is negligible (Olsson, pers. comm., 1990). However, there might have been other changes due to blasting, degassing, drying, stress changes etc. The physics associated with each of these is poorly understood, but the integrated effect of these phenomena could have been estimated if measurements of head changes near the drift had been made. Given such measurements it might have been possible to match them with annealing, but unfortunately, such measurements could not be made. The only significant physical difference between the SDE inflow conditions and the VD inflow conditions was the change in permeability around the drift. Possible causes of this change are discussed below.

Stress changes around the drift due to excavation will cause some fractures around the drift to open and some to close. For example, there should be an increase in hoop stresses affecting an annulus surrounding the drift; this could account for decreased permeability in fractures which are oriented on planes passing through the axis of the drift. However, fractures sub-parallel to tangents of the drift might tend to open. Net change in inflow could be either up or down depending on how the fractures are interconnected as they enter the drift.

Calculations of the expected stress changes in three-dimensions can be made based on linear elastic theory. One idea is that these changes can then be resolved with respect to the orientation of fractures intersecting the drift and then a laboratory based relationship between stress and permeability can be used to predict the changes in permeability. This stress analysis is

useful, but it may not be the best information for predicting the change in permeability. The problem is that the solution depends on the far field state of stress which is poorly known. More importantly, fractures and fracture zones near the drift may cause significant deviations from the linear elastic solution. In application, there will be an error due to the fact that the actual orientation of the fractures around the drift is not known so the magnitude of stress change and consequent permeability change cannot be resolved. Finally, and most importantly the relationship between stress and permeability will be based on fractures tested in the laboratory and these are small scale, isolated samples that are not likely to be the most important fractures or predict in-situ behavior. The most important fractures from the flow standpoint are in the highly fractured zones and these cannot be recovered for laboratory analysis. In summary, this approach requires that estimates are made based on estimates that are based on estimates and thus has a high probability of introducing significant error.

Beyond the difficulties in using a stress analysis directly, stress is probably not the only cause of permeability change near the drift. Significant changes may occur due to blasting which may both damage the rock and also push gas back through the fractures creating a much lower permeability two-phase flow region. Two-phase flow may also occur due to degassing of the water as it is depressurized near the drift, or due to drying near the drift walls.

None of these phenomena are well understood. The appropriate parameters needed to model the physics in a predictive mode are not available. Therefore, the best approach may be to use the observations of skin made during the Macropermeability Experiment (Wilson et al., 1981) assuming the same phenomena had taken place at both locations. A low-permeability skin can be inferred from the head data recorded in the boreholes emanating from the Macropermeability Drift just to the West of the SCV block. The head measurements made over 5 m packer spacings in these boreholes are shown in Figure 4.1 where it is evident that, for any of the 10 boreholes, the head measurements do not intersect the y-axis at the drift wall. This means that there must be a much steeper hydraulic gradient between the drift wall and the first data points at 5 m depth in the boreholes. Using the line representing the weighted average of all the points, the average per-

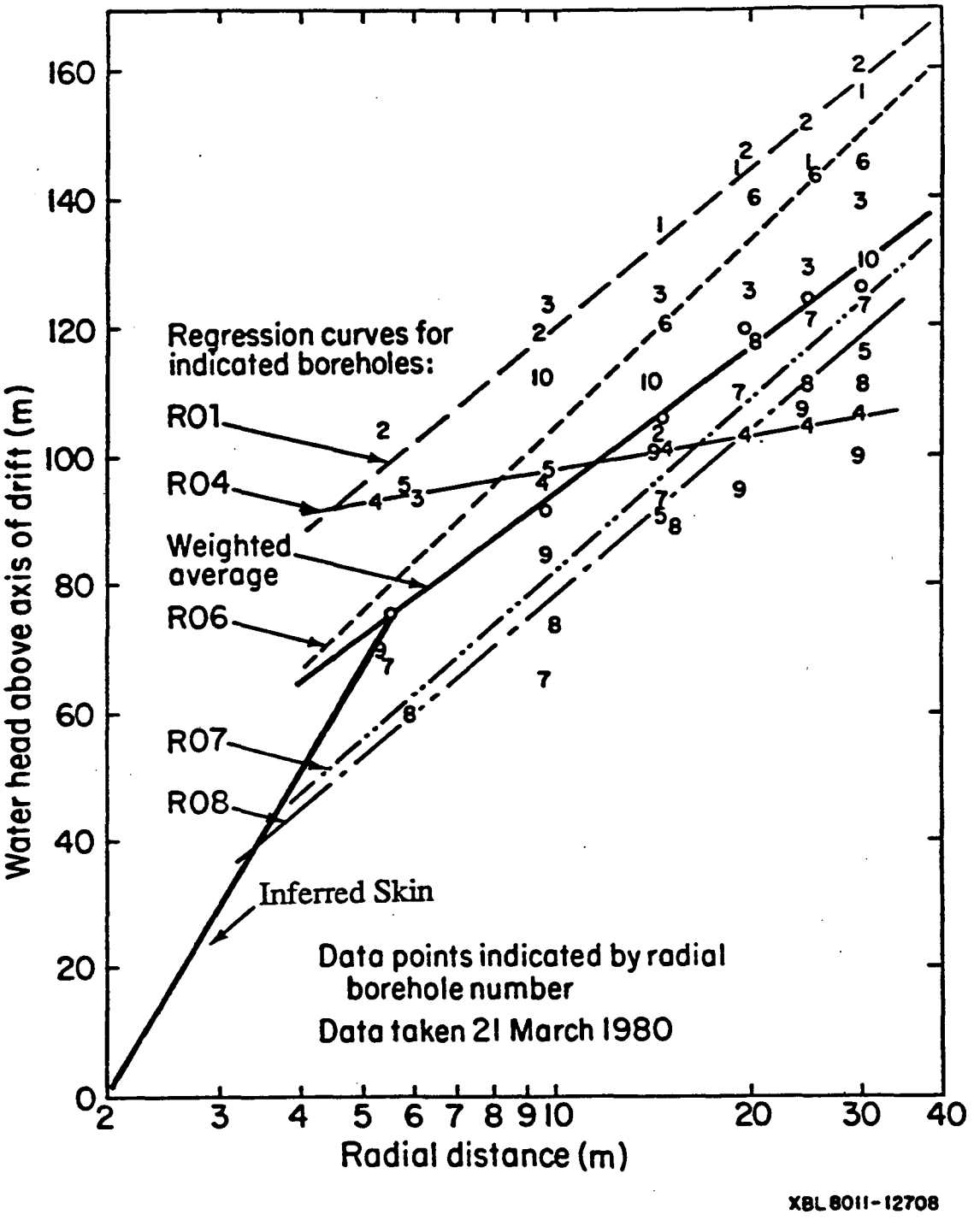

Figure 4.1. Head data from the Macropermeability Test.

meability K_s, that was calculated in the first 5 meters, should be 0.25 the average permeability, elsewhere, K. That is $K_s/K = 0.25$. Using the data from RO4 gives a minimum ratio of $K_s/K = 0.05$. RO6 gives a maximum of $K_s/K = 0.41$.

To get a an average high and low prediction, these three different skin factors (K_s/K) were applied to the permeability of the elements within 5 m of the drift wall (i.e., in the H-zone only). After applying this skin, a drawdown of 237 m (220 m from the SDE minus 17 m for going to atmospheric pressure) was applied to the D-holes and the drawdown response, the flow into the D-holes (B-zone) and the flow into the drift (H-zone) was calculated.

4.3. The Inflow and Drawdown Response Due to Opening T1

To calculate the response to opening T1 the model is first calibrated to the VD conditions. The value of skin around the drift that obtains the measured flow rates into the drift was identified and, in the three-dimensional model, a skin was applied around the remaining D-holes to obtain the measured inflow into the D-holes. This skin around the D-holes was evidently generated after the excavation of the Validation Drift causing the flow in the remaining D-holes to decrease by approximately a factor of two from the SDE measurement to remeasurement after the excavation. (This phenomenon is discussed in detail in Section 7.) With the addition of both skins, the model has then been derived from the SDE and C1-2 tests and then calibrated to the Validation Drift data. It then remains to open T1 in the model using the applied drawdown and calculate the response. To obtain a second estimate of the behavior due to opening T1, a skin factor required to reduce the flow by a factor of two was applied. This reflects the fact that the flow rate into the D-holes dropped by a factor of two when the pressure dropped from 17 m at the end of the SDE to atmospheric after the excavation. As the T1 hole was kept at atmospheric, it was also expected to develop a similar skin.

5.0. TWO-DIMENSIONAL MODELS

The most important fracture zone for the calculation of flow into the SCV drift is the H-zone. The H-zone is the only major zone to intersect the drift. Consequently, much of the analysis can be reduced to two dimensions by only considering the flow in the H-zone. Based on the geologic analysis summarized in Chapter 2, the H-zone is expected to be relatively isotropic. Consequently, a series of two-dimensional models has been constructed which is based on a square grid in the plane of the H-zone.

A major advantage of developing the two-dimensional models is that they are very appropriate for predicting tracer transport in the H-zone. The three-dimensional models described later do not provide as much resolution in the vicinity of the drift where the tracer tests were performed. The great majority of the elements in the three-dimensional models were not involved in the tracer transport. A portion of the three-dimensional models in the H-zone and in the vicinity of the drift could have been "cutout" and boundary conditions obtained from the full model applied to the edges of the cutout. This might have provided a better idea of the boundary conditions, but much worse resolution than the two-dimensional models. Thus, major scientific purpose of the annealed two-dimensional models will be the prediction of tracer transport.

First, the two-dimensional model was annealed to the C1-2 test and this model was then used to predict the SDE. Originally, a two-dimensional model annealed to the steady-state SDE data alone was planned to be used for prediction flow into the Validation Drift. However, there were only two corrected data points for the SDE data in the H-zone (W1-5 and W2-4). Consequently steady state annealing for the H-zone was relatively uninteresting. Second, a model was co-annealed with both C1-2 and the SDE data and this model was used to predict the effects of excavating the Validation Drift (VD). Finally, a model which incorporates data from the C1-2, SDE and the VD was produced and used to predict the effects of opening T1.

5.1. The Two-Dimensional Template

A two-dimensional template was chosen for this example based on three major considerations. The template should include as much detail as possible in the vicinity of the D-holes. Secondly, the mesh should be large enough to prevent the pressure transients from reaching the boundary too soon. Thirdly, the number of elements and bandwidth should be kept as small as possible to keep the annealing time as small as possible. The variable density mesh that was chosen is in keeping with all of these considerations (Figures 5.1a, b, and c). There were 5 nested grid regions, each having twice the grid spacing of its inner neighbor. In addition, 200 m long elements connected each of the nodes lying on the outer edge of the outer grid region to the applied boundaries. This allowed a 1.5 m spacing grid in the vicinity of the D-holes, put the boundaries approximately 400 m from the pumping wells and kept the total number of elements down to 4687.

The element conductance and storativity are scaled in such a way that the whole region has the same average transmissivity and average storage. Table 5.1 gives the mesh specifications.

Table 5.1. Mesh specifications for the two-dimensional model.

Region Number	Outer Dimensions (m X m)	Grid spacing (m)	Conductance relative to region 1	Storativity relative to region 1
1	50 × 50	1.5	1	1
2	75 × 75	3	2	2
3	125 × 125	6	4	4
4	175 × 175	12	8	8
5	400 × 400	24	16	16
fins	800 × 800	24	16	16

Each of the well intervals is included as a node in the mesh. If a well node lay close to an existing node, then the well was simply assigned to the existing node. If it was not close enough, then it was "snapped" into the mesh with three elements connecting it to the three closest nodes. Because a square mesh was used, snapping in all six D-holes would result in a strange geometry for the SDE. To avoid this the mesh was arranged such that D1 was assigned to a node in the

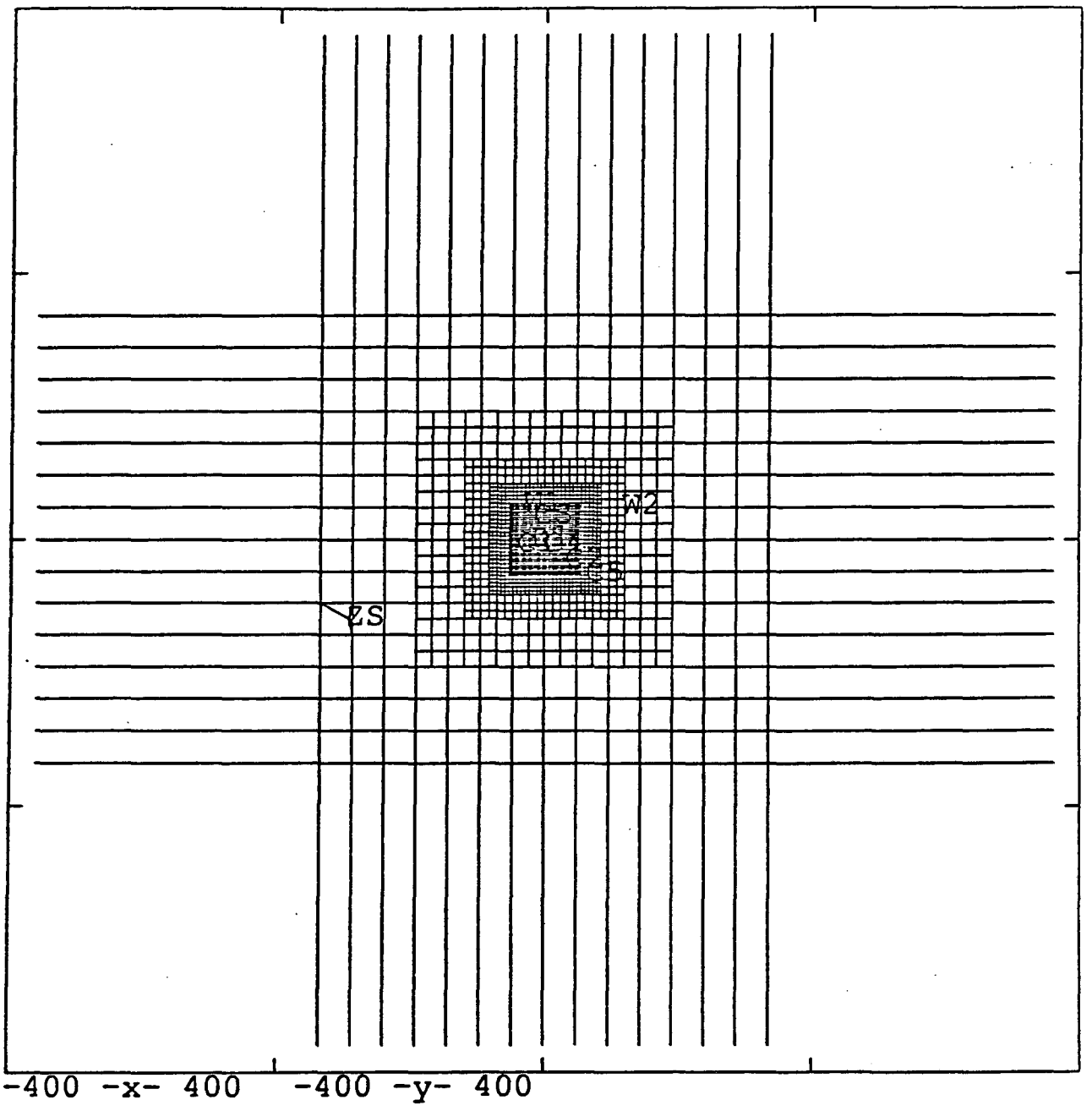

XBL 921-5537

Figure 5.1a. The full mesh used for annealing the two-dimensional model including the five nested grid regions and fins connecting the grids to the boundary.

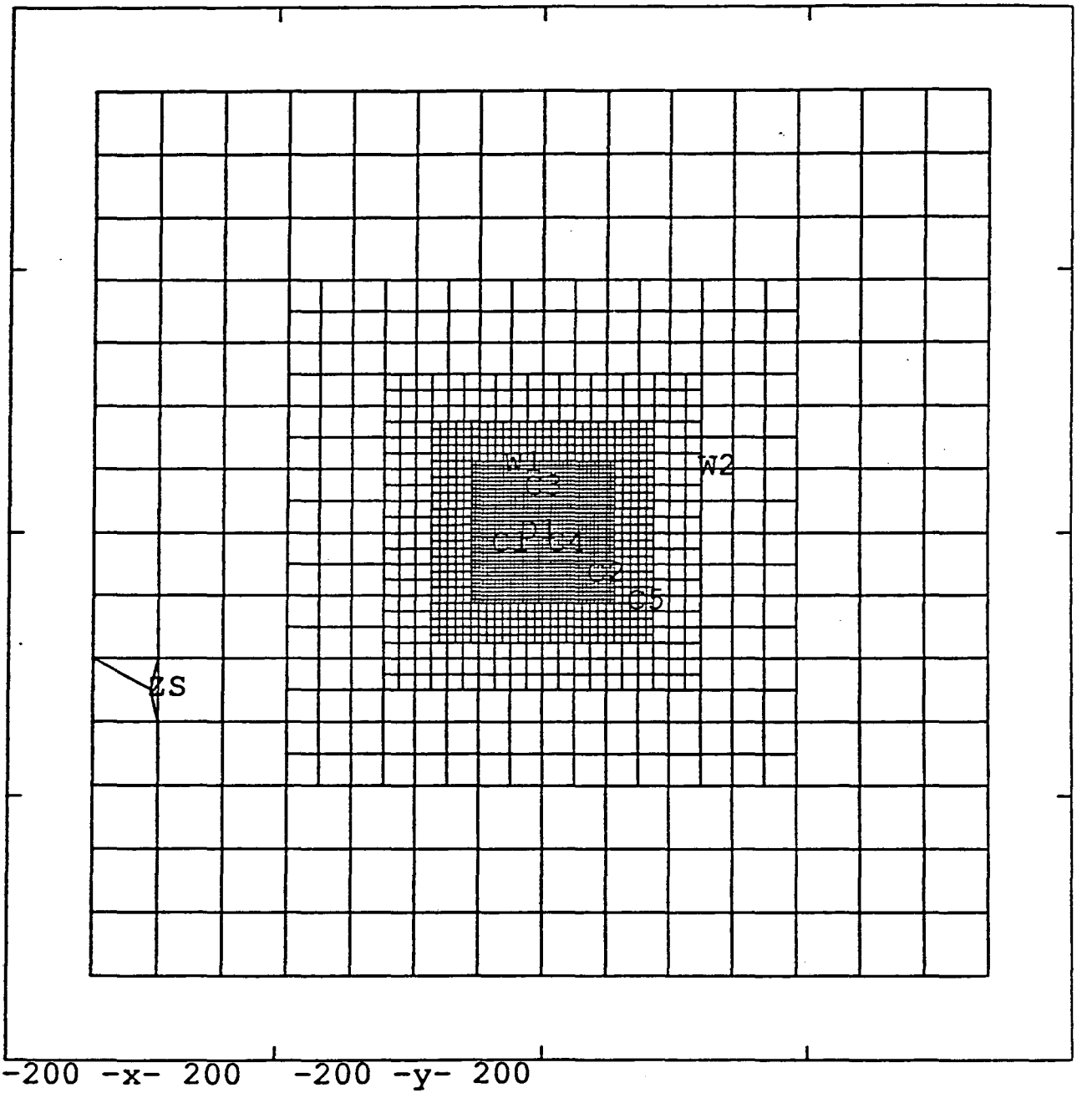

XBL 921-5538

Figure 5.1b. The five nested grid regions showing the location of the intersections between the borehole intervals and the grid plane as well as the intersection with the z-shaft.

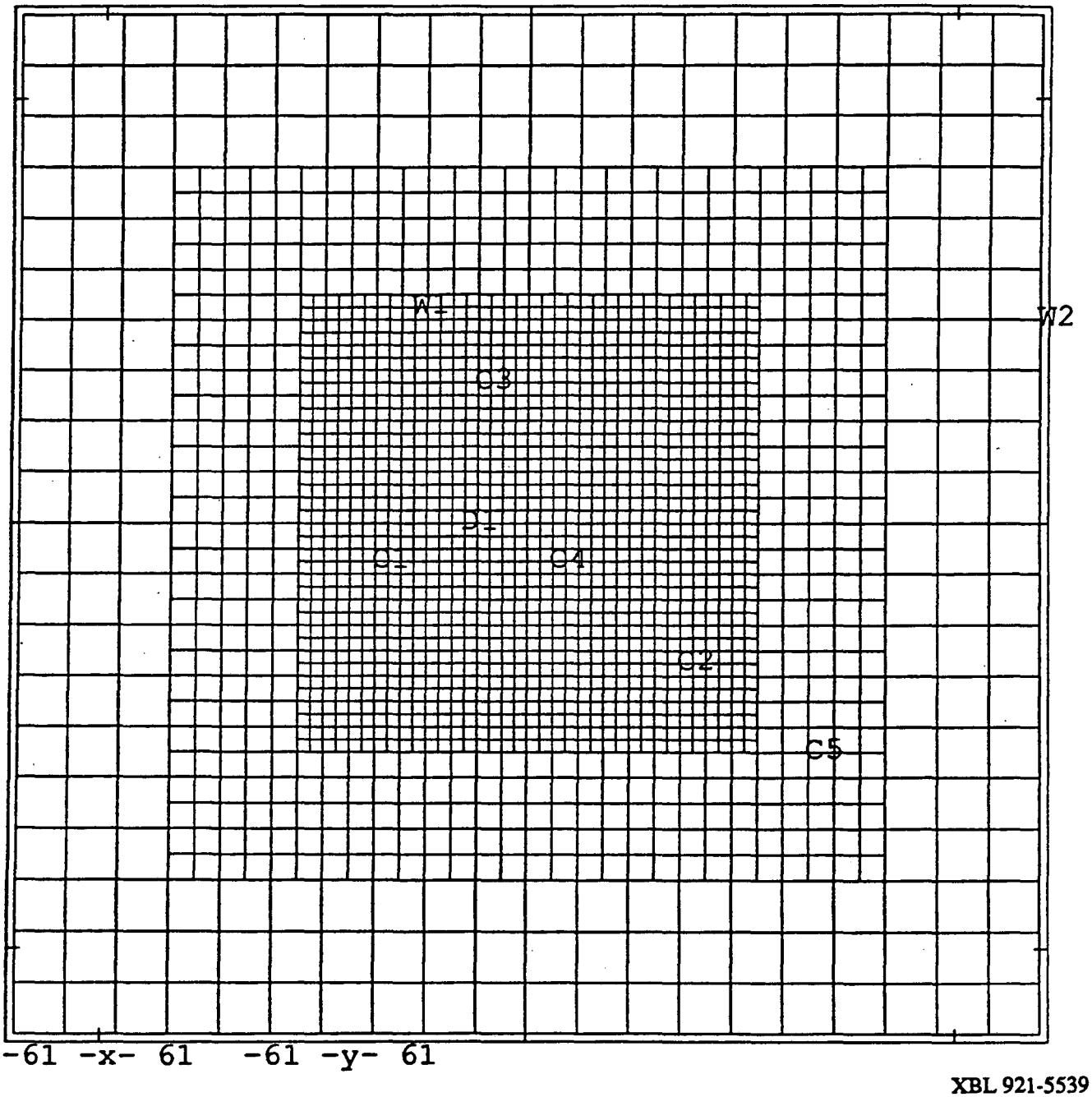

Figure 5.1c. The inner three grid regions showing the location of all the well intervals used in annealing.

middle of four other D-hole nodes (Figure 5.1d). The sixth hole was neglected. This ensures that D1 was completely sheltered by the other D-nodes. The outer four nodes do not exactly correspond to the D-holes. Only D1 is labeled on the large scale figures.

The behavior of the full mesh was checked by running the C1-2 test and examining the drawdown curves. These were smooth, showing no evidence of transition from one grid region to the next.

5.2. Boundary Conditions

The boundary conditions in the model were chosen to get a reasonable match to the estimated equilibrium head values given in Table 3.1. In the H-zone, there are only two values of equilibrium head in the data set: W1-5 and W2-4. These are 212.5 and 226 m respectively. Initial boundary conditions were chosen based on closing all the well intervals in the initial model with 30% of the elements randomly removed. Outer boundary conditions were chosen that gave reasonable values of head at W1-5 and W2-4 while allowing drainage into the Z-shaft which intersects the H-zone, below the D-holes, about 150 m away. A node fixed at -75 m total head is added at the location of the Z-shaft to provide this sink. The value of -75 m reflects the elevation of the water in the Z-shaft relative to the 360 m level.

The boundaries were chosen as shown in Figure 5.2. All of the boundaries were given a constant head except the North edge (right side). After trying many combinations, this one seemed to allow the heads at W1-5 and W2-4 to be relatively close to each other. Otherwise, W2-4 which is much closer to the boundary than W1-5 has a much higher head. As it is not obvious whether constant head or no-flow boundaries are more appropriate, the choice is arbitrary and further, it turns out that the drawdowns, are insensitive to the change in boundary conditions.

The initial boundary conditions were not picked to exactly match the observed heads in W1-5 and W2-4 because annealing would change the permeability of the region and this in turn would change the heads at W1-5 and W2-4. So, at the end of annealing, the boundary conditions were checked again, and readjusted and then the C1-2 test was rerun to see if it was necessary to

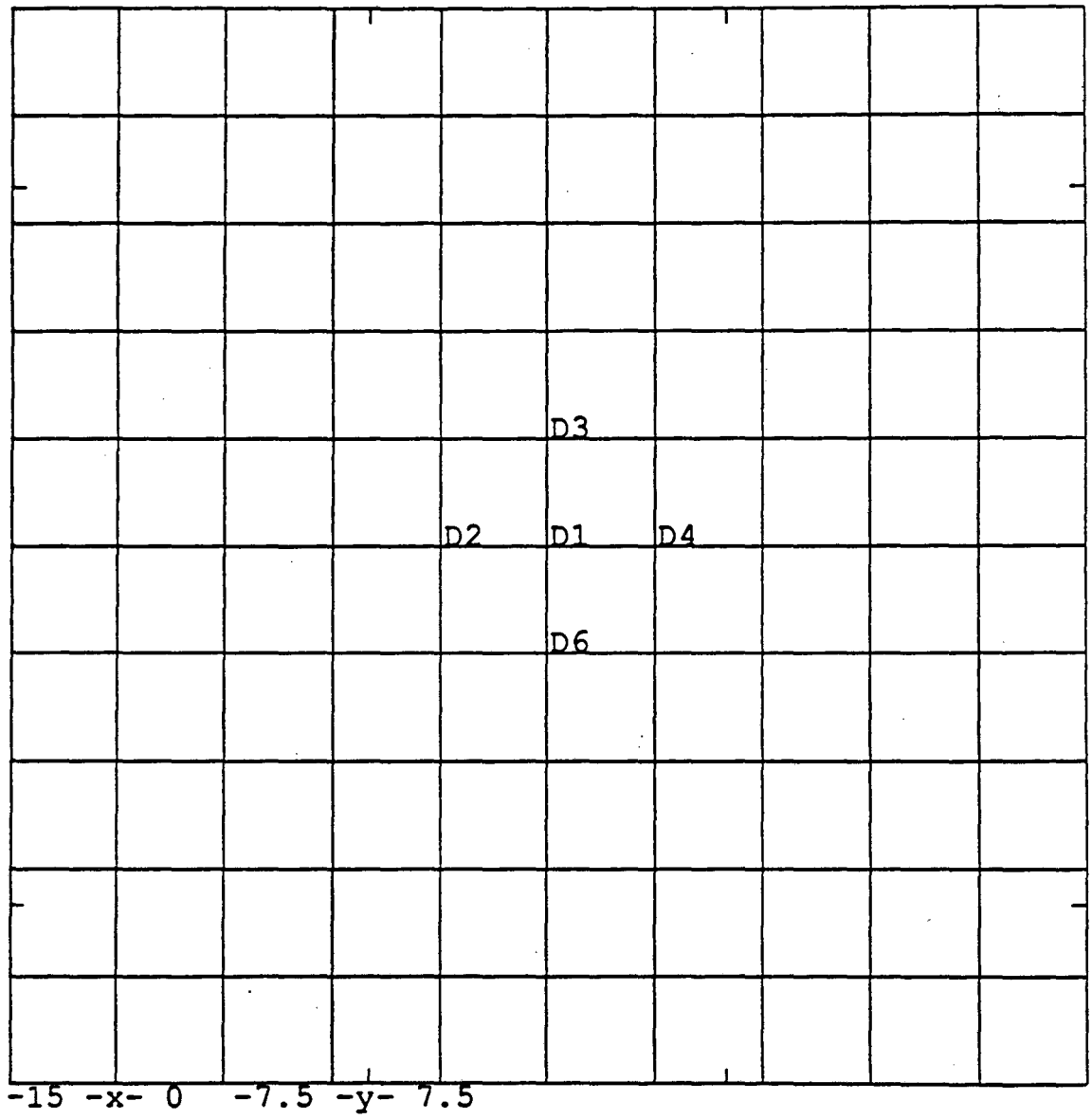

XBL 921-5540

Figure 5.1d. Assignment of the D-holes to nodes in the two-dimensional model.

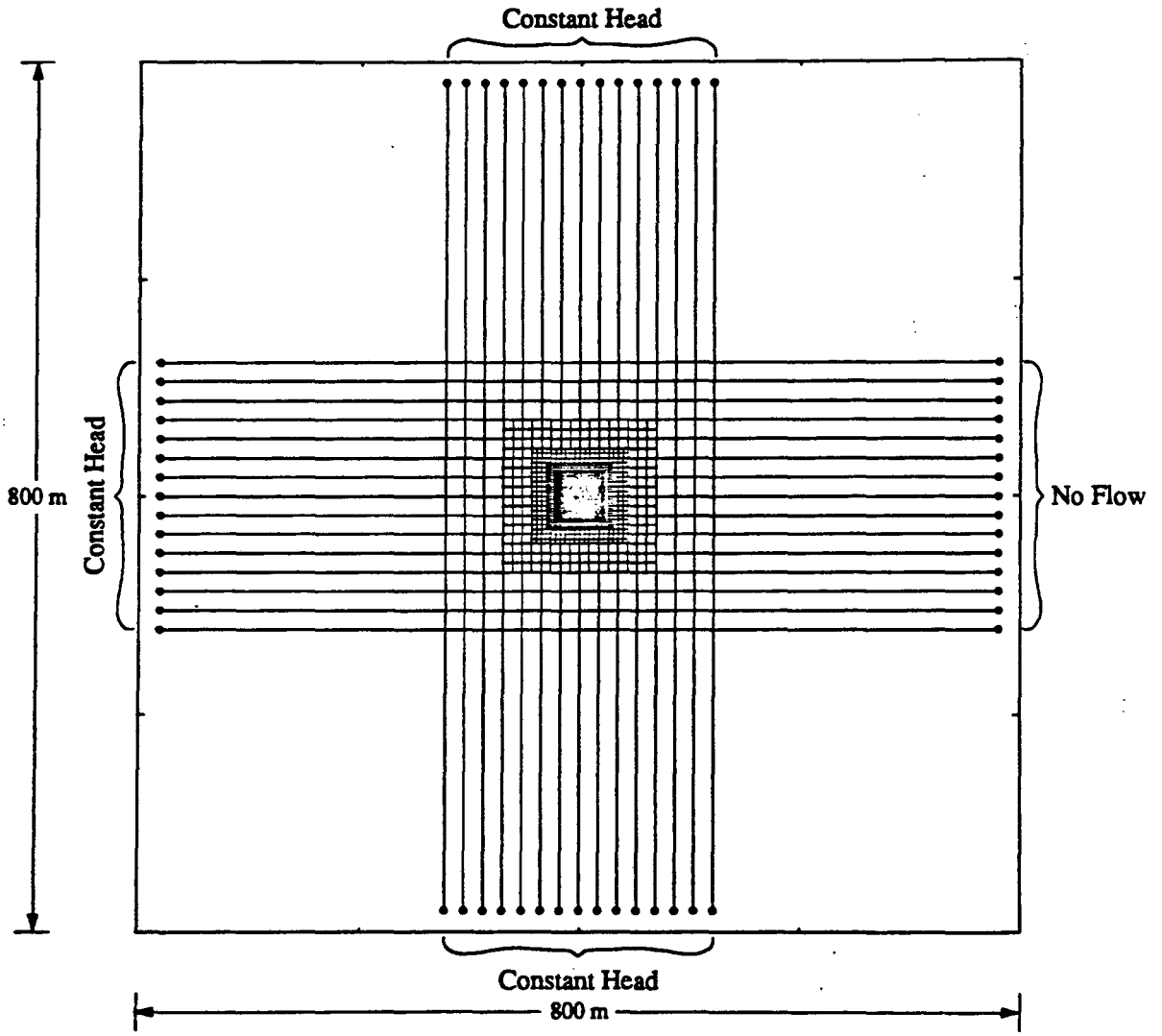

Figure 5.2. Boundary conditions used for the two-dimensional model.

re-anneal the configuration to match C1-2. The annealed configuration had 59% of the original elements present, and because of the reduction in elements the boundary conditions had to be changed. Significantly, the energy of the configuration with respect to the C1-2 test was insensitive to the choice of boundary conditions. The most important effect of the change in boundary conditions was that the annealing code identified a larger x-shift corresponding to an increase in element storativity. This means that the choice of boundary conditions may not play an important role in determining configurations based on transient data. Table 5.2 shows the initial and final values of head at W1-5 and W2-4 versus the applied boundary heads.

Table 5.2. Heads observed under boundary heads (H) applied to the top, bottom and south edges of the two-dimensional model.

Well Interval	Measured head (m)	Calculated heads		
		Initial H=325 m 70% present	Annealed H=230 m 59% present	Co-annealed H = 230 54% present
W1-5	212.5±6	226	217	223
W2-4	226±13	245	213	220
D-H (av)	212± 15	-	207	225

5.3. Prediction of the Simulated Drift Experiment

A prediction of the SDE was made by annealing to C1-2 without using prior information from the D-holes. To then model the SDE a constant head boundary should be applied at the D-holes such that the drawdown imposed at the D-holes was the same as that imposed during the third step of the SDE; not by imposing the head (-8m relative to 360 m) that was imposed in the field. Black (personal communication) estimates the drawdown at 220 m. The error of this estimate may be as much as 35 m so the comparison between these calculations and the measurements of flow and drawdown include a significant error due to lack of knowledge regarding the test conditions.

5.3.1. Annealing to C1-2

As discussed above, the C1-2 test was clearly the best transient well test for this method. Consequently, the two-dimensional model was first annealed to the C1-2 test alone. The resulting configuration is shown in Figure 5.3. The energy versus iteration and temperature schedule for this model is shown in Figure 5.4. Figure 5.5 shows the match between the observed well responses and the model responses.

Running this problem took several days of real time. Recall that the higher the temperature, the more likely it is that the algorithm will accept an unfavorable change. Finding the right temperature schedule is, at this point, more of an art than a science. If the algorithm accepts every change, the temperature is probably too high and should be adjusted. Such adjustments account for the break in temperature schedules seen on Figure 5.4

5.3.2. Results

The configuration was then adjusted to calculate the effects of the SDE. Unfortunately, none of the transient responses to the SDE were available. The transient behavior of the SDE could be calculated, but there were no data to compare with the prediction. Therefore, the SDE was only run as a steady-state problem. The C1-2 interval was closed and the heads at the D2, D3, D4 and D6 (D5 is not modeled) nodes were set to -13 m such a drawdown of 220 m was obtained. Tables 5.3 and 5.4 compare the measured flow and drawdowns with the predicted values respectively. In the last column of Table 5.4 shows the drawdowns at W1-5 and W2-4 when the boundary condition at the D-holes was equal to the observed flow rate, 0.768 l/min.

Annealing to C1-2 has provided enough information to predict the SDE flow rate and one of the observed drawdowns. The other drawdown was too small by at least 17 m. To some extent, this is not surprising because the SDE drawdowns at the W1-5 and W2-4 are very close to each other, but the C1-2 responses were very divergent with W1-5 responding much more than W2-4. Thus a model matching C1-2 would automatically not match the SDE drawdowns at both intervals. It might have been very helpful to have SDE data from the C-holes to compare with these

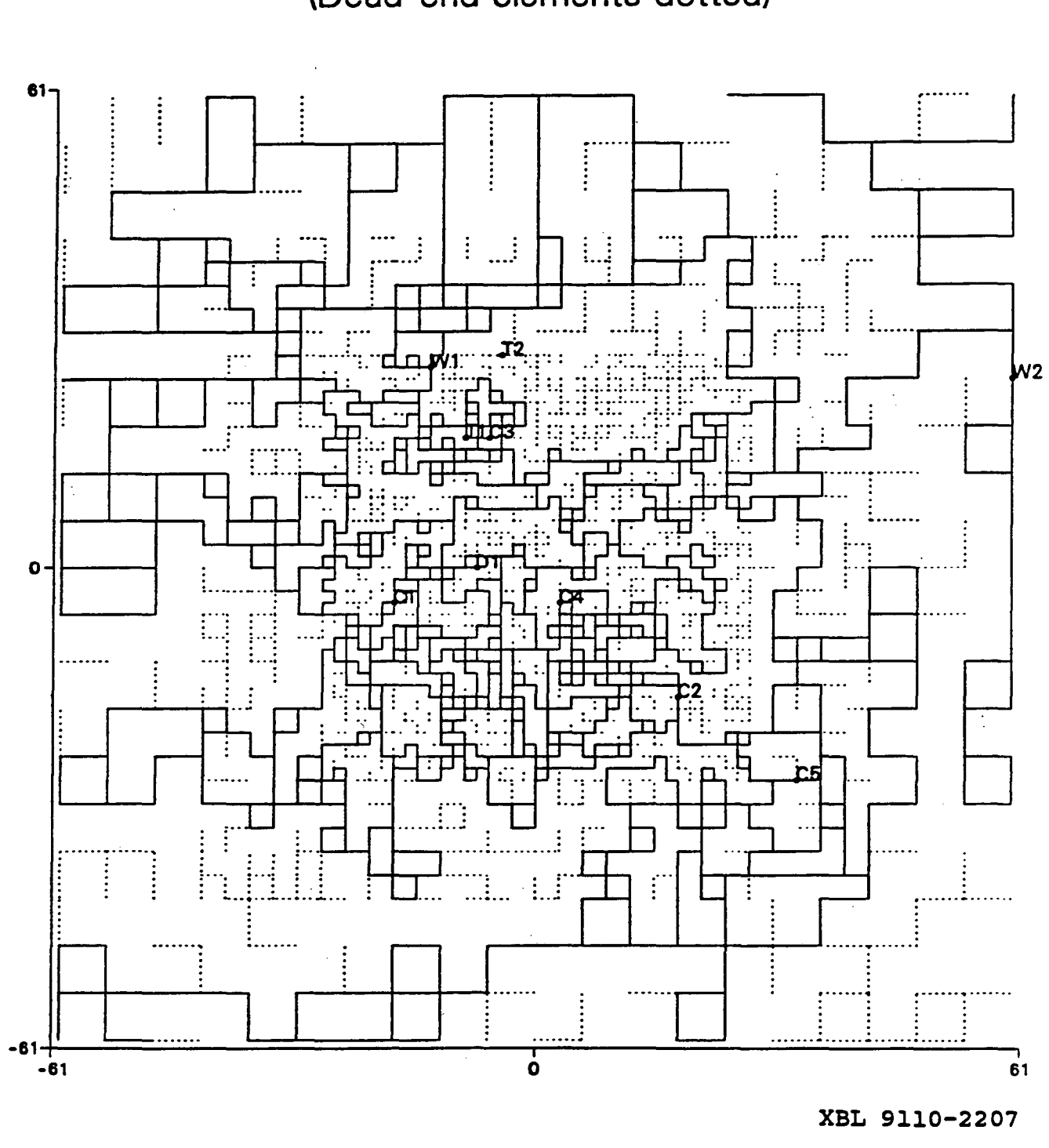

Figure 5.3. The two-dimensional model annealed to C1-2.

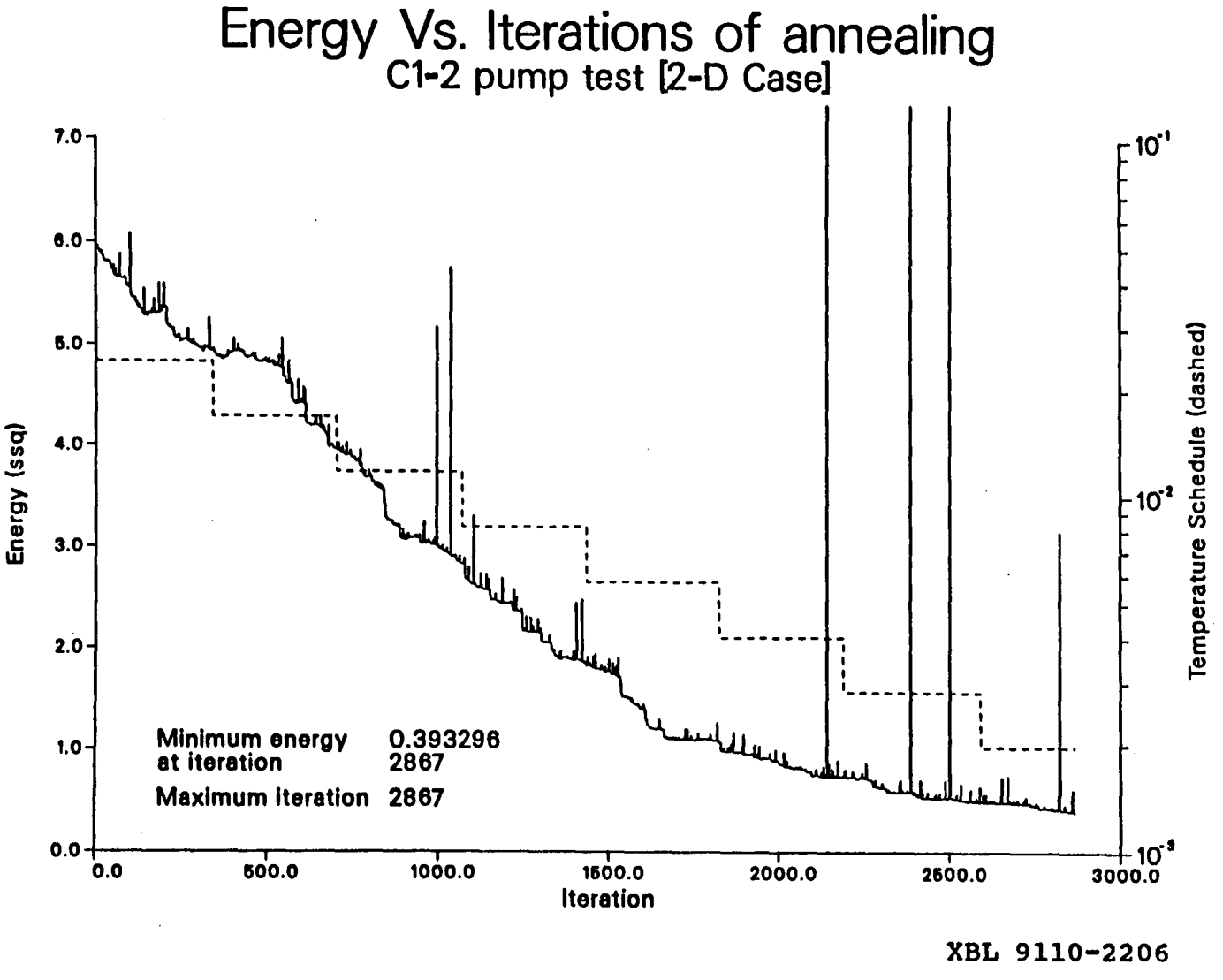

Figure 5.4. The energy vs iteration curve and temperature schedule for the two-dimensional model annealed to the C1-2 test.

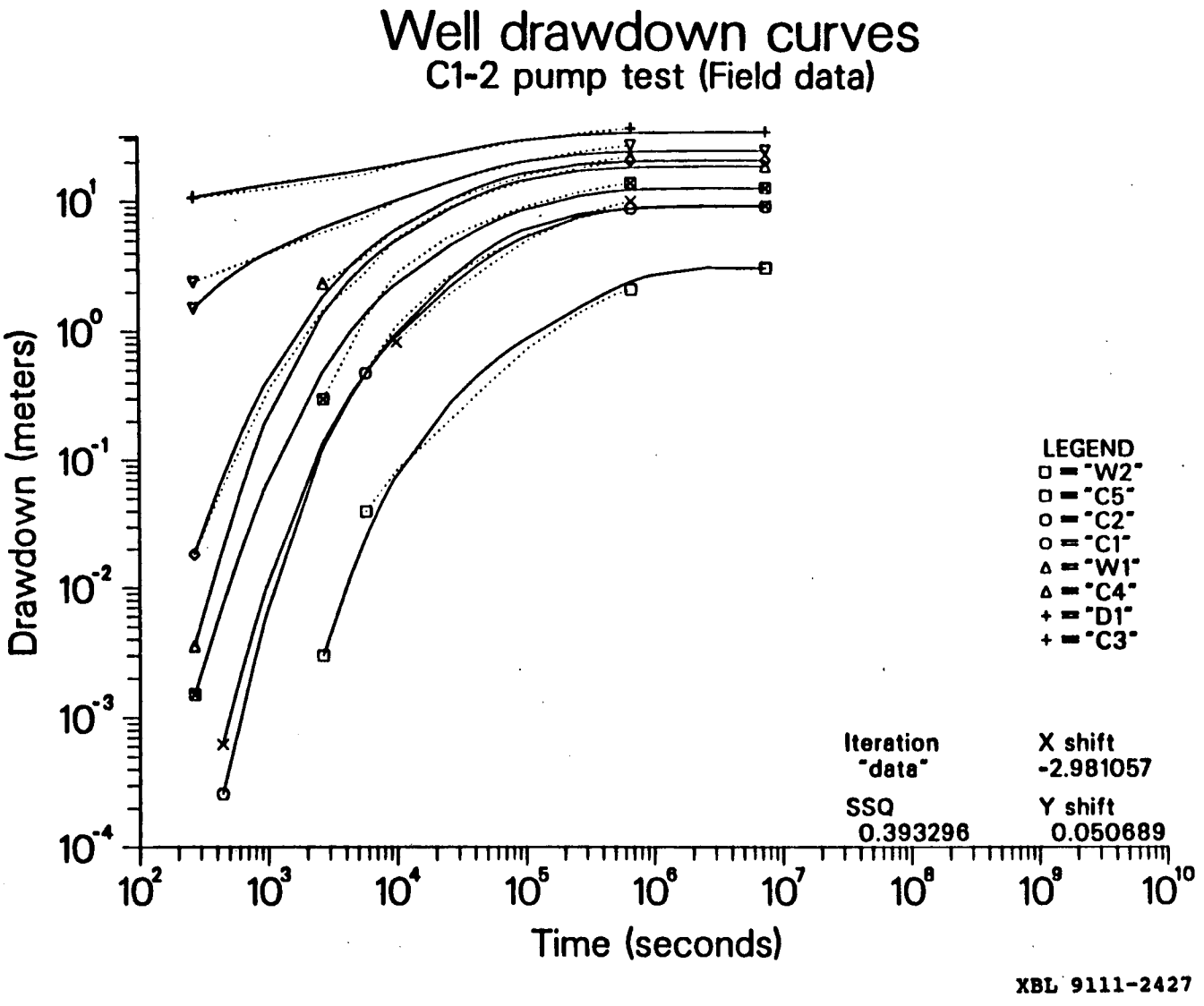

Figure 5.5. Comparison of C1-2 well test response data to model results.

model predictions or have the C1-2 data for a longer period of time. However, this example shows some very encouraging success at being able to predict the steady state SDE results from a short-term transient cross-hole test.

Table 5.3. Prediction of flow into to the SDE using two-dimensional model annealed to C1-2.

B/H Interval Name	Interval	Conceptual Zone in Interval	Measured Flow (l/min) Drawdown =220	Calculated Flow (l/min) Drawdown = 220 m
D-H	24-27	H (24-26)	0.768±0.2	0.77

Table 5.4. Prediction of drawdown due the SDE using two-dimensional model annealed to C1-2.

B/H Interval Name	Interval	Conceptual Zone in Interval	Measured Drawdown (m)	Calculated Drawdown	
				(m) Drawdown = 220 m	(m) Flow = .768
W1-5	2-31.0	H (46-50)	95.4±21.5	88	88
W2-4	48-65	H (50-57)	70.8±38	15	15

5.4. Prediction of the Validation Drift Effects

In order to predict the effects of excavating the Validation Drift (VD), it was first necessary to have a model which behaves like the SDE and hopefully also behaves like the C1-2. To achieve this goal, the configuration was co-annealed to both the C1-2 and the SDE. Once a model that predicts the SDE was obtained, a low permeability skin was applied as described in Section 4, and the inflow and drawdown due to excavation were calculated.

5.4.1. Co-Annealing to C1-2 and SDE

A co-annealing case was set up by treating the SDE as a constant flow well in a pseudo-steady-state calculation. The strength of the sink represented by the SDE was fixed and the model was annealed to the drawdowns observed in the SDE, including the drawdown at the D-holes

(equal to -8 m, i.e., 17 m presure head). In this case the center D-hole (D1) was used as the sink assigned a flow rate of 0.768 l/min. The calculation was set up as a transient problem, but the model was only annealed to the drawdowns at very large values of time (10^6 to 10^7 sec) because the model results reach steady state by 10^6 sec. In addition, annealing was used to match the lower bound of drawdown at W2-4 because the C1-2 response at W2-4 was much lower than the C1-2 response at W1-5. The C1-2 test was run as before. Co-annealing was started from the configuration obtained by annealing to C1-2.

After 2588 iterations, co-annealing was halted. At this point both C2 and C3 had been disconnected from the network. On closer examination a "bug" was found in the annealing code which counts the energy of a disconnected well as zero. Consequently these intervals were manually reconnected and the resulting energy increased by a very small amount indicating that the match to the reconnected C2 and C3 heads was good. This adjusted network was used thereafter. The resulting configuration is shown in Figure 5.6. This network is markedly different than the network derived for C1-2 annealing alone because it is sparser and consequently closer to the percolation limit of 50% (52% for co-annealing as opposed to 54% for C1-2). Small differences in percentages are significant near the percolation limit. The energy versus iteration and temperature schedule for this model is shown in Figure 5.7. Figure 5.8 shows the match between the observed C1-2 well responses and the model responses. Table 5.5 compares the annealed SDE drawdowns to the observed SDE drawdowns.

Co-annealing has been able to match all of the data extremely well with the exception of SDE drawdown in W2-4. It is not clear why the configuration did not match this drawdown. However, annealing to the transients for SDE, or running the case for more than the 2588 iterations might have produced better results.

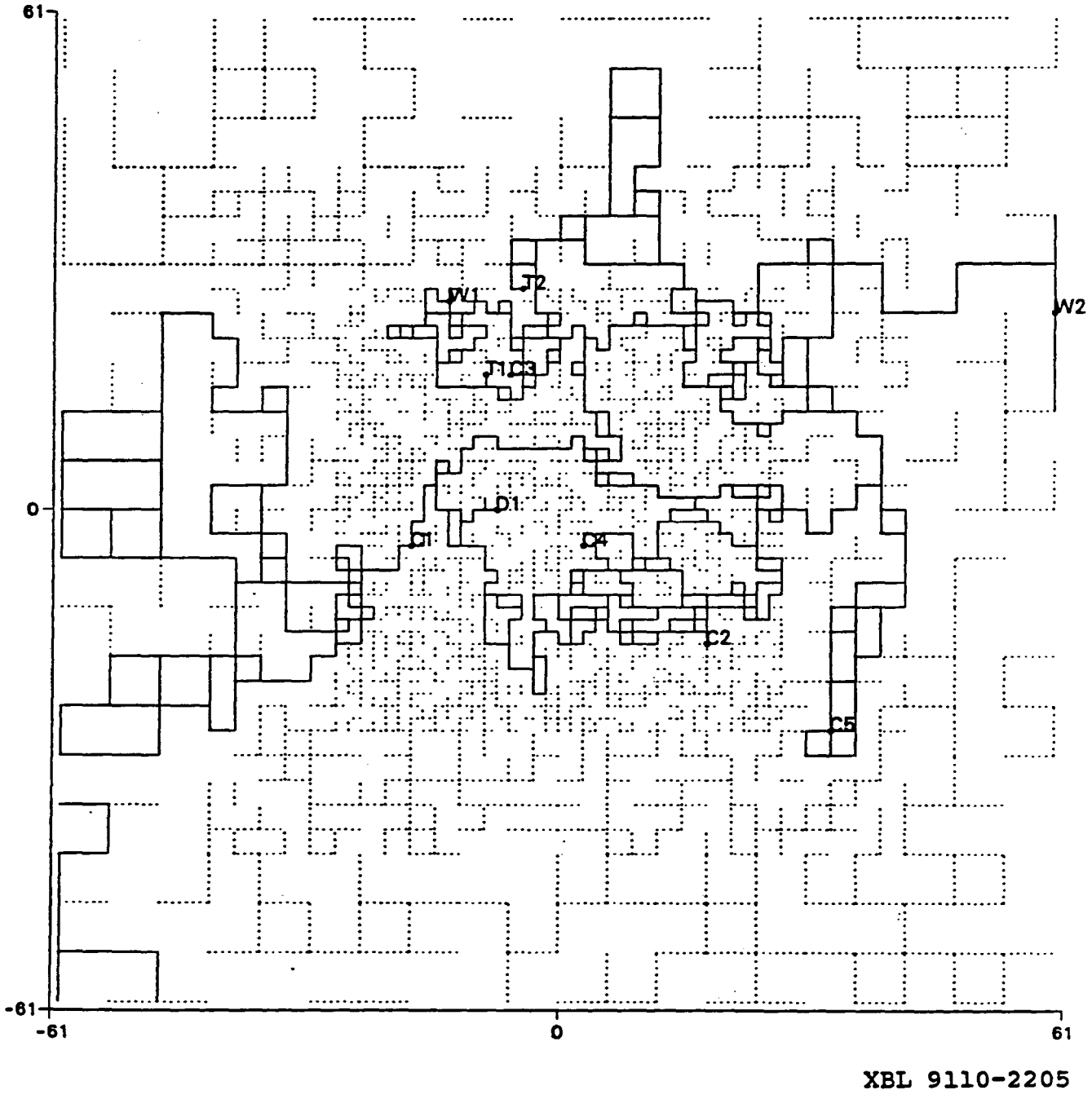

Figure 5.6. The two-dimensional model co-annealed to C1-2 and SDE.

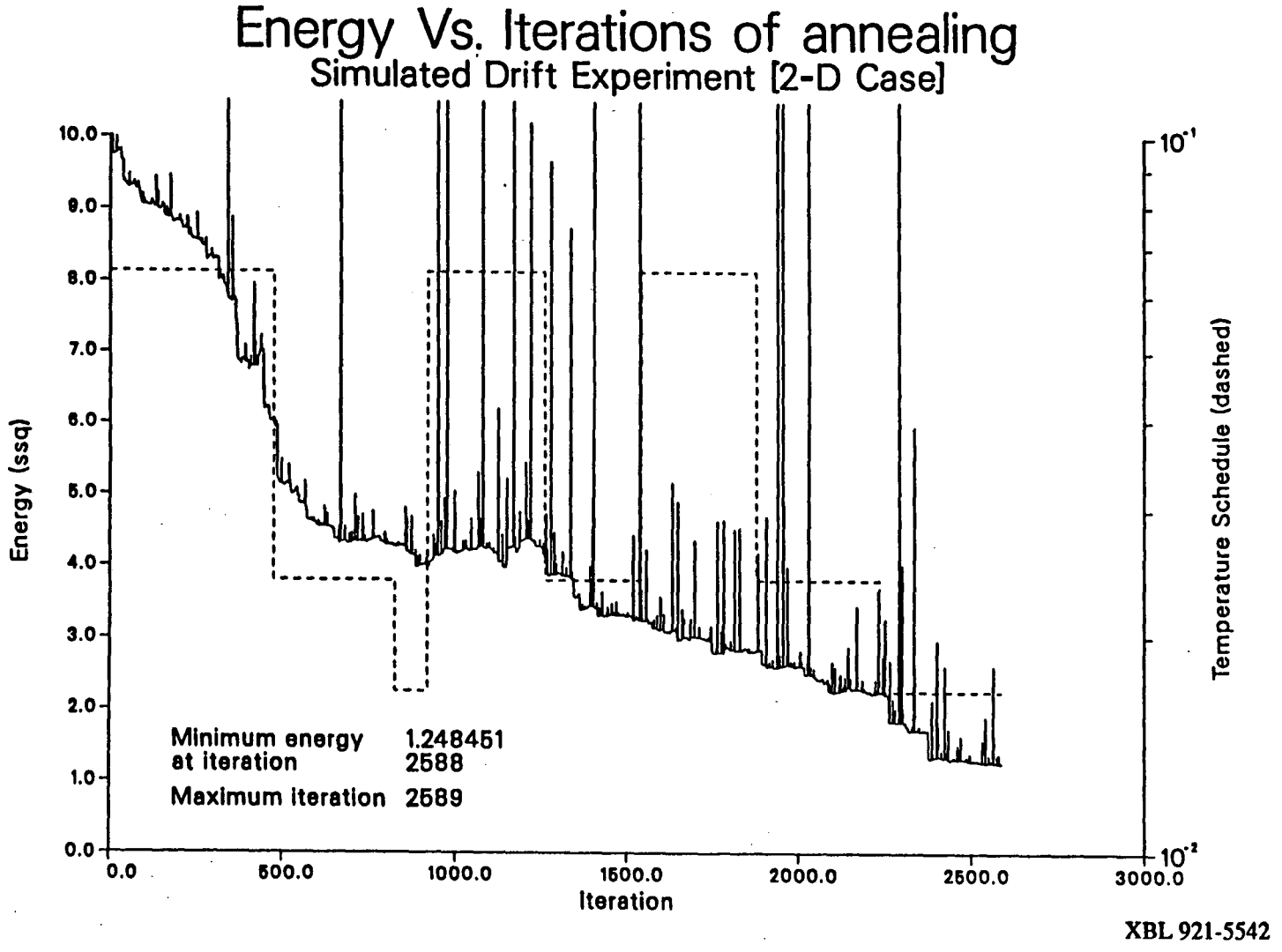

Figure 5.7. The energy vs iteration curve and temperature schedule for the two-dimensional model co-annealed to the C1-2 test and the SDE.

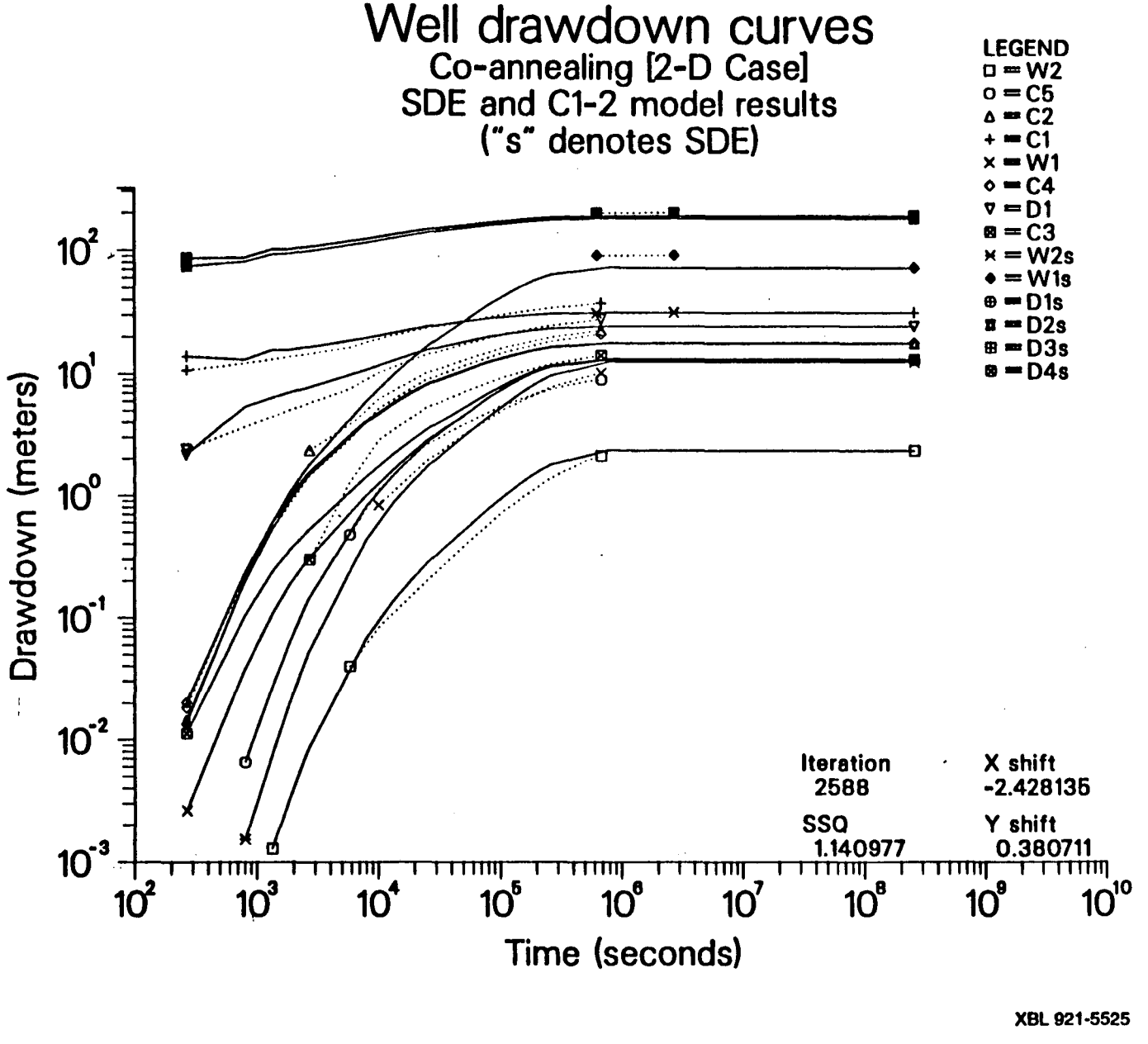

Figure 5.8. Comparison of C1 and SDE well test response data to model results.

Table 5.5. Match with SDE drawdown data for the configuration annealed to both the SDE and C1-2.

B/H Interval Name	Interval	Conceptual Zone in Interval	Measured Drawdown (m)	Calculated Drawdown (m)
W1-5	2-31.0	H (46-50)	95.4±21.5	88
W2-4	48-65	H (50-57)	70.8±38*	15
D1-H		H	220 ±30	230
D2-H	24-27	H(24-26)	220±30	220
D3-H		H	220±30	220
D4-H		H	220±30	230
D6-H**		H	220±30	—

*annealed to a drawdown of 32 m to try to minimize the discrepancy between the C1-2 response and the SDE response.
**disconnected by annealing.

5.4.2. Calibration to SDE

To calibrate the mesh to the SDE, the inner boundary condition at the D-holes was set to constant flow equal to 0.768 l/min. The resulting head at the D-holes is calculated. An average head for D1, D2, D3, D4 and D6 was calculated, eliminating any D-hole that is not connected. Then, heads were assigned to D1, D2, D3, D4 and D6 that were equal to the average head minus 17 m (i.e., -16.7) using a constant head boundary in order to simulate the drift. Table 5.6 gives the heads at the D-holes when the flow at D1 is set to 0.768 l/min.

Table 5.6. Heads in the D-holes calculated when the flow is set to 0.768 l/min.

Borehole	Head (m)
D1	-4.6
D2	5.2
D3	5.2
D4	-4.6
D6	0*
Average	.3

* disconnected by annealing

5.4.3. Addition of Skin Factor

Once the model was calibrated to the SDE flow, it remained to calculate the effect of excavation on inflow. Using the aforementioned estimates of the ratio of skin permeability to average permeability (K_s/K), the permeability of the elements was decreased within 5 meters of the drift wall by a factors of 0.05, 0.25 and 0.41. The resulting flow and drawdowns into the drift are given in Table 5.7 and 5.8.

Table 5.7. Prediction of flow into to the VD drift using two-dimensional model calibrated to the SDE.

B/H Interval Name	Interval	Conceptual Zone in Interval	Measured Flow (l/min) K_s/K =.025*	Calculated Flow (l/min) ±0.2			
				K_s/K =1	K_s/K =.41	K_s/K =.25	K_s/K =.05
D-H	24-27	H (24-26)	0.1 ±?	.84	0.66	0.54	0.18

*Skin required to make the flow equal to 0.1 l/min

Table 5.8. Prediction of drawdown due the VD drift using two-dimensional model calibrated to the SDE.

B/H	Zone	Measured Drawdown (m)	Calculated Drawdown (m)				
			K_s/K=1	K_s/K=.41	K_s/K=.25	K_s/K=.05	K_s/K = .025
W1-5	H	60.0±6	96.5	75	61	21	12
W2-4	H	32.0±13.5	16.6	12.5	10	3	2

*Skin required to make the flow equal to 0.1 l/min

The "average" prediction (i.e., K_s/K = 0.25) of flow into the H-zone (i.e., into the Validation Drift) is .54 l/min, about a factor of 5 too high. Even the lowest prediction is almost two times as large as the measurement. However, the drawdown at W1-5 is predicted quite well with the "average" estimate, and as before the drawdown at W2-4 is not well estimated.

A value of K_s/K = 0.025, was required to make the flow equal to 0.1 l/min and was the best model for flow into the Validation Drift. However, the "average" estimate of skin K_s/K = 0.25, gave better drawdown estimates so this model was used to make the remaining predictions of the effect of opening T1.

5.5. Prediction of T1 Inflow and Drawdown

During the T1 test, the pressure head in the T1 hole was lowered to atmospheric. T1 was drilled after the excavation, and the total equilibrium head in this hole when it was closed was 173 m at an elevation of -13.8 m (i.e., pressure head of 186.8 m). The head in T1 was calculated with T1 closed and the drift and remaining D-holes open and then the head in the T1 hole was set to 186.8 meters lower than the value calculated with T1 closed, (24.9 m).

The prediction of inflow into T1 is given below. Two different values are given. The first prediction assumes no skin around the T1-hole. The second prediction assumes that flow was approximately half what was we predicted without skin. This reduction in flow was based on knowing that the flow into the remaining D-holes (i.e., the last 50 m which intersect zone B) at atmospheric pressure was half that measured during the SDE.

Both of these inflow predictions are high by several orders of magnitude. Therefore, the low inflow rate probably cannot be explained by a low permeability skin. One possibility is that the values predicted by the model reflect a better estimate of inflow to a SDE type experiment located at T1. Of the six holes in the SDE, two are much lower permeability than the other four. Consequently, a number of realizations would have helped significantly in this case.

Two predictions of drawdown were made for each of the skin values. The first prediction is for total drawdown measured against the equilibrium heads before excavation (Table 5.10). Thus the background head for this case was calculated with the co-annealed model with the Z-shaft open and all other holes closed and no skin around the D-hole nodes. The second prediction, which is expected to be more accurate, is based on incremental drawdowns against the equilibrium heads measured after the excavation (Table 5.11). In this case, the background head was calculated with the co-annealed model, with the D-holes at the constant heads indicated in Tables 5.7 and 5.8, and skin $K_s/K = 0.25$ around the D-holes. No data is currently available to compare with these predictions.

Table 5.9. Prediction of flow into to the T1 hole using two-dimensional model based on LSC, SDE and VD results.

B/H Interval Name	Interval	Conceptual Zone in Interval	Measured Flow (l/min)	Calculated Flow (l/min)	
				$K_s/K = 1$	$K_s/K = 0.10$*
T1-H	31-38	H	0.0017	0.64	0.33

*skin required to reduce flow by a factor of 2 (see section 4.3)

Table 5.10. Prediction of total drawdown due the opening of T1 using two-dimensional model based on LSC, SDE and VD results.

B/H Interval Name	Interval	Conceptual Zone in Interval	Measured Drawdown (m)	Calculated Total Drawdown (m)	
				$K_s/K = 1$	$K_s/K = 0.10$*
W1-5	2-31.0	H (46-50)	not avail.	199.3	148.1
W2-4	48-65	H (50-57)	not avail	26.0	18.7

*skin required to reduce flow by a factor of 2 (see section 4..3).ls 2

Table 5.11. Prediction of incremental drawdown due the opening of T1 using two-dimensional model based on LSC, SDE and VD results.

B/H Interval Name	Interval	Conceptual Zone in Interval	Measured Drawdown (m)	Calculated Total Drawdown (m)	
				$K_s/K = 1$	$K_s/K = 0.10$*
W1-5	2-31.0	H (46-50)	not avail	138.5	87.3
W2-4	48-65	H (50-57)	not avail	15.5	8.2
C2-1	71-86	H(63-9)	not avail	66.1	34.8
C3-1	1-70	H(59-61)	not avail	150.7	79.1
C4	1-60.0	H(55-59)	not avail	65.8	34.6

*skin required to reduce flow by a factor of 2 (see section 4..3)

6.0. THREE-DIMENSIONAL MODELS

The three-dimensional model, called the zone model, used the conceptual model of fracture zones developed by Black et al. (1991) without modification. The zone model includes only the fracture zones. Each zone was modeled as a portion of a plane with extent and location as determined by the geophysical investigations. Within the block, each zone is discretized by a square grid of one-dimensional conductors which are then annealed to the well test data. This model reflects what can be learned from a combination of geophysical data and hydraulic data.

6.1. The Template

The template for the three-dimensional models is shown in Figure 6.1. As described in Section 2, the template contained the seven fracture zones identified in Black et al. (1991). These were the major zones: the H-zone (the only zone to intersect the SCV drift), the Hb zone (spur to the H-zone), the B- and I-zones (the only zones to intersect the D-holes which remain after excavation of the SCV), the A-zone (sub-parallel to B); and the minor zones: the M-zone (between A and I) and the K-zone (connecting H to N4). Zones H, and A extend beyond the boundaries of the block. Zones Hb, I, M and K terminate completely within the block. The H-zone in Figure 6.1 stands out in the figure because it was more finely discretized than the other zones. Each zone was represented by a disc, but conductive channels were assigned to the discs only within the block as shown on the figure. Table 6.1 gives the template specifications for each fracture zone. Figure 6.1 does not show the 200 m long "fin" elements that connect nodes on the boundary of the block to the constant head hydraulic boundaries. The north side of the block is a "no flow" boundary as in the two-dimensional case..

In order to connect the well intervals to the fracture zones, a procedure was followed similar to that used for the two-dimensional case. If the center of the well interval was close enough to an existing node in the grid, the well interval is assigned to the node. If it is not close enough, the

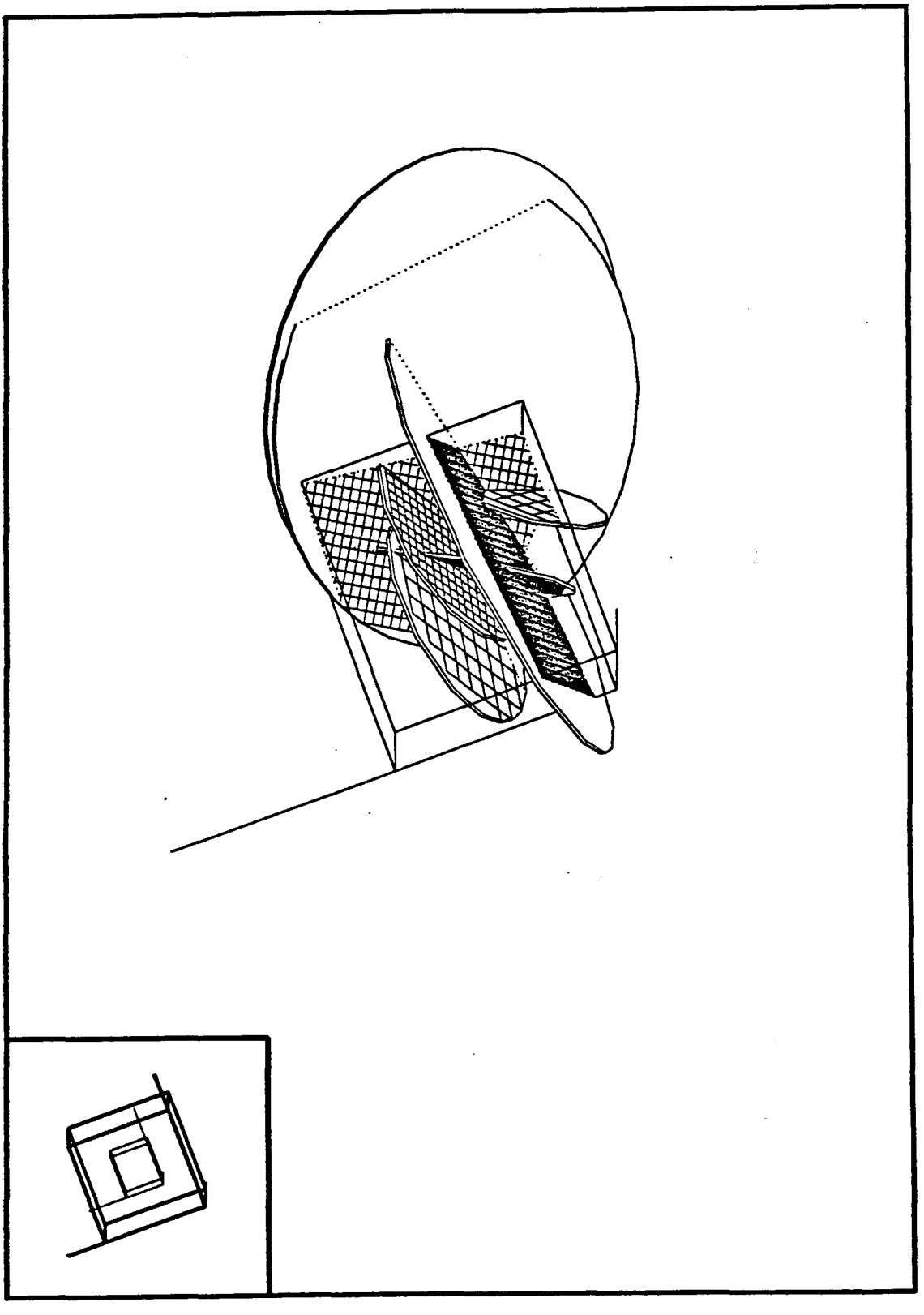

XBL 921-5543

Figure 6.1. The three-dimensional zone template.

well interval was "snapped" into the grid by connecting it to the three closest nodes with new grid elements. In some cases, the interval should have been snapped to more than one fracture zone. However, the center point of the well interval might have been much closer to one of the zones and in this case the "snap" would only connect the interval to one zone. To prevent this, two well nodes were created, one for each end of the interval and connected these by a high permeability element so that both interval nodes have essentially the same behavior. Then each of the well nodes were snapped into the fracture zone grid.

The discretization of the H-zone in the three-dimensional model was on a 6 m spacing. Thus, the D-holes were all snapped to one node. The two intervals D-H and D-B refer to the intersection of the D-holes with the H-zone and the B-zone respectively.

Table 6.1. Template specifications for the three-dimensional zone model.

Attribute		Zone						
		A	B	H	Hb	I	M	K
Center (m): (mine coordinates)	x	598	567	450	470	408	444	478
	y	1100	1100	1097	1063	1043	1056	1140
	z	360	360	360	375	388	404	404
Radius (m)		100	100	100	50	50	50	30
Orientation* (degrees)	ϕ	137	130	85	83	86	30	35
	θ	48	43	76	60	63	87	65
Grid Spacing (m)		10	10	6	12.5	20	12.5	12
Channel conductance ($10^{-6}m^3/s$)		7.59	7.59	4.48	9.89	1.65	9.89	9.89
Channel storativity (10^{-5})		1	1	1	1	1	1	1

* ϕ is azimuth of dip
θ is dip

6.2. Boundary Conditions

The boundary conditions in the model were chosen to get a reasonable match to the estimated equilibrium head values given in Table 6.2. There are 15 values of head that could theoretically be used to set the boundary conditions. As in the two-dimensional model, initial boundary conditions were chosen based on closing all the well intervals in the initial model with

35% of the elements randomly removed. The outer boundary conditions gave heads that were within reason with respect to measured heads while allowing drainage into the Z-shaft which intersects the H-zone below the D-holes about 150 m away. A node fixed at -75 m head (relative to the 360m level) was added at the location of the Z-shaft to provide this sink. The value of -75m reflects the elevation of the water in the Z-shaft.

Table 6.2. Equilibrium heads due to the applied boundary conditions in the three-dimensional model.

Well Interval	Estimated head (m)	1 SDE Annealed H=220 m	2 C1-2 Annealed H=220 m
N2-1	216±5	220	220
N2-2	210.4±4	220	220
N2-4	68.0±3	220	187
N3-1	212.7±7	220	220
N3-2	193.7±6	220	220
N4-1	208.4±6	220	220
N4-2	209.2±8	220	220
N4-3	253.8±10	220	220
W1-1	210.1±5.0	220	220
W1-3	216.9±4	220	220
W1-5	212.5±2.5	220	220
W2-1	212.2±6.0	220	220
W2-2	225.1±4.0	220	220
W2-3	218.1±7.0	220	220
W2-4	226.0±13	220	220
D-H	237 ±10	220	220
D-B	237 ±10	220	220
T1		220	220
T2		220	220

*Disconnected by annealing

At the end of annealing, the boundary conditions were checked again. Table 6.2 gives the long term equilibrium heads compared to the heads calculated using the applied boundary conditions after annealing as described below. The calculated equilibrium heads were subsequently used as the reference to calculate the drawdowns due to the SDE, VD and opening T1. Clearly the Z-shaft had very little effect on the head distribution in three-dimensions. For the C1-2 case, the N2-4 interval evidently became disconnected from the rest of the network because the head

remains 187 m at this point no matter what was done to the other intervals. W1-3 was completely disconnected.

6.3. Steady-State Zone Model

The SDE provides estimates of steady-state head and drawdown at 15 points throughout the SCV block (Table 3.1). None of these points are near the D-holes because the C-holes were either not yet drilled or not packed-off into intervals during this test. However, annealing to the steady state values of head due to the SDE was the most straight forward way to obtain a model that behaves like the SDE.

6.3.1. Modeling

The data used to anneal this model of the SCV site were taken from the estimated steady-state heads at the end of the third stage of the SDE as given in Table 3.1. A constant flow condition was applied at the D-holes (0.768 l/min at D-H and .942 l/min at D-B). Then steady-state annealing was used to match the pattern of estimated steady-state heads. Figure 6.2 shows the annealed configuration for the three-dimensional H- and B-zones of the steady-state model. Table 6.3 gives the calculated versus measured drawdowns for the SDE after annealing to the SDE. The drawdowns are calculated by subtracting the heads predicted by the annealed model with the flow at D-H equal to 0.768 l/min and D-B equal to 0.942 l/min from 220 m (the head calculated with the D-intervals closed).

Figure 6.3 shows the energy versus iteration curve and the temperature schedule used to control the annealing process for this case. In this cases the minimum energy was not zero because the measurement error is significant. Annealing could be considered to obtain minimum energy if the head values fell within the error bounds. Using only the steady state head entries in Table 3.1 without a dagger, the mean squared error for the data is about 400 m^2. For 15 sampling points this is a lower bound total squared error of about 6,000 m^2. Annealing started with an energy of about 100,000 m^2 and dropped to about 4,000 m^2, which is far below experimental error. It is also clear from the energy curve that 10,000 iterations were sufficient.

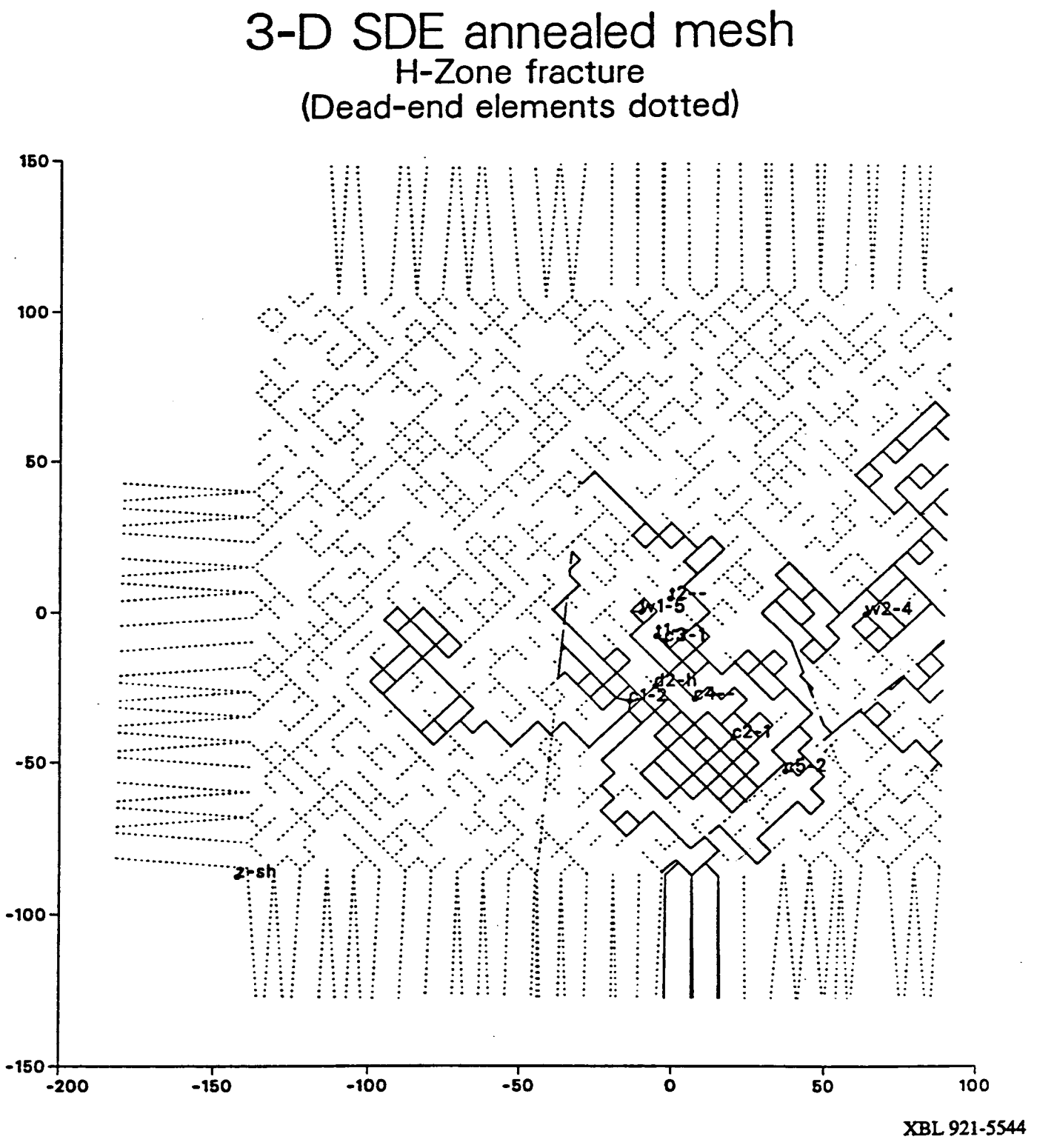

Figure 6.2a. The H-zone in the annealed configuration for the three-dimensional steady-state model.

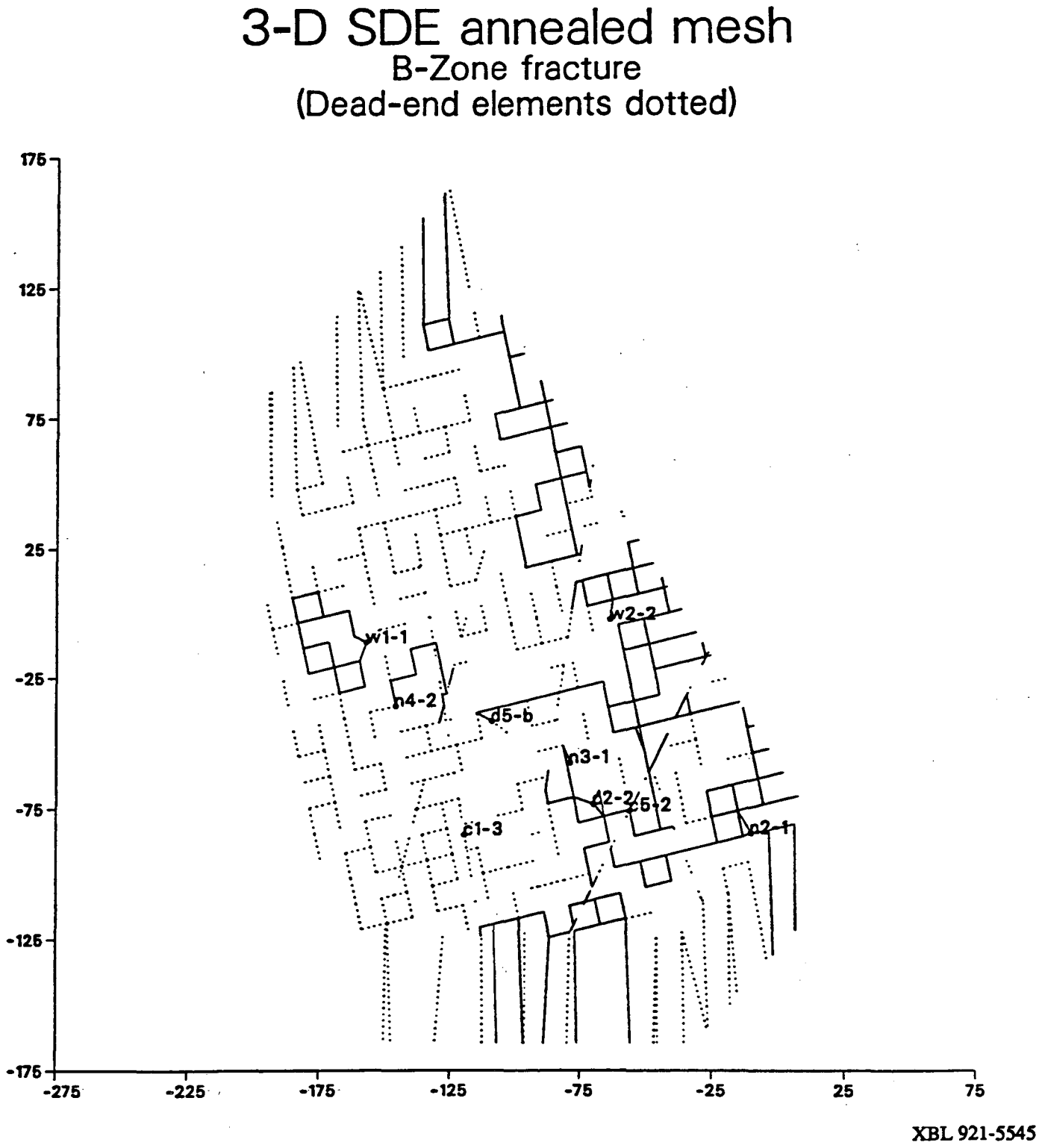

Figure 6.2b. The B-zone in the annealed configuration for the three-dimensional steady-state model.

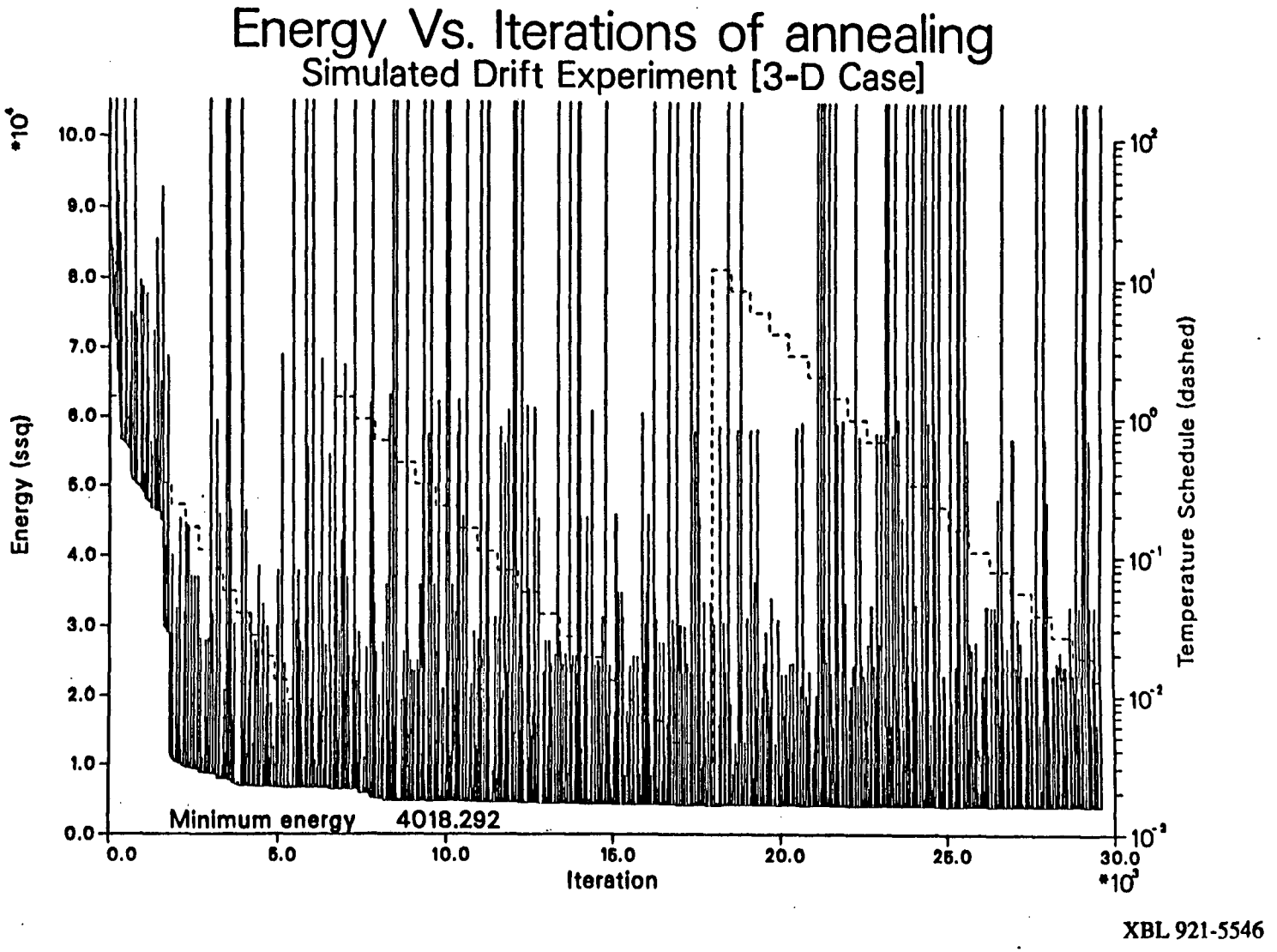

Figure 6.3. The energy versus iteration curve and temperature schedule for the three-dimensional steady-state model.

Table 6.3. Predicted versus measured drawdowns for the SDE after annealing to the SDE.

B/H Interval Name	B/H Interval Interval	Conceptual Zone in Interval	Estimated Drawdown (m)	Calculated* Drawdown (m)
N2-1	161-207	B(188-190)	45.4±5†	34
N2-2	111-160	K(151-153)	75.7±22.5	94
N2-4	2-75.0	M (29-31)	9.2±3†	68
N3-1	101-189	A (162-170), B (133-4)	90.9±22	94
N3-2	2-100	M (38-39)	39.3±6†	63
N4-1	142-219	A (153-156)	78.2±27	94
N4-2	109-141	B (122-126)	74.2±24	94
N4-3	77-108	M (102)	72.1±10†	94
W1-1	92-147	B (130-138), I (108-12)	63.4±18	94
W1-3	55-75	Hb (59-60)	61.1±20	75.9
W1-5	2-31.0	H (46-50)	95.4±21.5	78.3
W2-1	110-147	A (124-145), I (116-21)	70.6±18	94
W2-2	76-109	B (83-91)	53.7±4†	87
W2-3	66-75	Hb (67-71)	36.8±42	104
W2-4	48-65	H (50-57)	70.8±38	103
D2-H	24-27	H (24-26)	220±30	107
D5-B	28-100	B (90-2), I (94-6)	220±30	226

†using instantaneous drawdown as a substitute for equilibrium drawdown.
(Error given in the table is much lower than the true error)
*Table 6.2, col. 1 minus heads calculated by modeling the SDE as a constant flow case.

6.3.2. Prediction of the Validation Drift Effects

To predict the drift effects, the drawdown at D-H and D-B was increased by 17 meters and a skin of low permeability was added to the elements around the drift. With the boundary conditions at the D-H and D-B set to constant flow equal to 0.768 and 0.942 l/min respectively, the resulting head at the D-holes was calculated. Then, constant heads were assigned to D-H and D-B equal to the calculated heads minus 17 m in order to simulate the drift and the remaining open D-holes. Table 6.4 gives the calculated heads at D-H and D-B for the SDE and the D-H and D-B heads used to model the VD. The unreasonably high head at D-H probably reflects the effect of insufficient data near the D-holes.

Using the estimates of the ratio of skin permeability to average permeability (K_s/K)

described in section 3.1, the permeability of the elements within 5 meters of the drift wall were decreased by a factor of 0.25, 0.5 and 0.41. The resulting flow due to the drift is given in Table 6.5. As explained in Section 4, the "average" prediction of inflow was for $K_s/K = 0.25$ and the low and high predictions are for $K_s/K = .05$ and .41 respectively.

Table 6.4. Heads in the D-holes calculated when the D-H and D-B flow is set to 0.768 and 0.942 l/min respectively.

Borehole	SDE Head (m)	VD Head (m)
D-H	113	96
D-B	-6	-23

Table 6.5. Prediction of flow into the Validation Drift using three-dimensional model annealed to steady state SDE data.

B/H Interval Name	Interval	Conceptual Measured in Interval	Flow (l/min) Zone	Calculated Flow (l/min) ±0.2				
				H:K_s/H:K=1	K_s/H:K=.41	H:K_s/K=.25	K_s/K=.05	H:K_s/K*=.025 B:K_s/K*=0.25
D-H	24-27	H (24-26)	0.1±?	0.81	0.63	0.51	0.18	0.09
D5-B	28-100	B (90-2), I (94-6)	0.56±?	0.80	0.81	0.81	0.83	0.60

*H:K_s/K required to make the D- H flow equal to 0.1 l/min.
B:K_s/K required to make the D-B flow equal to 0.56 l/min.

Table 6.6 gives the total drawdown caused by the drift. To calculate the drawdowns, the heads calculated with the drift in place were subtracted from the heads in Table 6.2 calculated for the conditions before excavation, i.e., with the D-holes closed. The drawdowns in Table 6.6 can be compared to the drawdowns in Table 6.3 to see how the heads *increased* after excavation.

6.3.3. Prediction of the Effect of Opening T1

To model the effects of opening T1, the value of K_s/K around the drift was chosen such that the best match to the Validation Drift data was obtained. A skin was also applied around the D-B zone until a match was found for the measured D-B inflow. The values of K_s/K used are given in

Table 6.6. Then, the well interval, T1 was "snapped" into the H-zone and the head in T1 was calculated with T1 closed and the drift and remaining D-holes open. Then the head in the T1 interval was set 186.8 m lower than the value calculated with T1 closed. Table 6.7 gives the prediction of flow into the T1 hole, Table 6.8 gives the predictions of drawdown relative to the pre-excavation estimated equilibrium heads, Table 6.9 gives the prediction of incremental drawdown relative to the post excavation heads (see Table 3.1).

Table 6.6. Prediction of total drawdown due the Validation Drift using three-dimensional model annealed to the steady-state SDE.

B/H Interval Name	Interval	Conceptual Zone	Estimated Drawdown (m)	Calculated Drawdown (m)				
				K_z/K =1	K_z/K =.05	K_z/K =.25	K_z/K =.41	H:K_z/K=.025 B:K_z/K=0.25
N2-1	161-207	B(188-190)	23.4±5.6	60.3	23	44	50.3	14
N2-2	111-160	K(151-153)	24.8±4.2	103.1	97	101	102	70
N2-4	2-75.0	M (29-31)	2.5±3.1	90	28	58	70	16
N3-1	101-189	A(162-170),B(133-4)	41.7±7.5	102.8	97	100	101	70
N3-2	2-100	M (38-39)	43.2±6.5	86.9	29	59	70	17
N4-1	142-219	A (153-156)	28.4±6.5	102.8	97	100	102	70
N4-2	109-141	B (122-126)	29.2±8.5	102.8	97	100	101	70
N4-3	77-108	M (102)	71.4±11.5	102.8	97	100	101	70
W1-1	92-147	B(130-138),I(108-12)	no data	102.8	97	100	101	70
W1-3	55-75	Hb (59-60)	59.0±6	102.5	39	75	87	23
W1-5	2-31.0	H (46-50)	60.0±6	102.5	39	75	87	23
W2-1	110-147	A(124-145),I(116-21)	20.2±7	102.8	97	100	101	70
W2-2	76-109	B (83-91)	31.1±5.0	96.5	92	95	95	67
W2-3	66-75	Hb (67-71)	24.1±8	111.2	106	109	110	77
W2-4	48-65	H (50-57)	32.0±13.5	110.7	106	108	109	76
D2-H	24-27	H (24-26)	no data	124	124	124	124	124
D5-B	28-100	B (90-2), I (94-6)	no data	243	243	243	243	243

*H:K_z/K required to make the D- H flow equal to 0.1 l/min
B:K_z/K required to make the D-B flow equal to 0.56 l/min.

6.4. Three-Dimensional Models Based on Transient Data

A two-stage prediction was done with this model. The zone model is first annealed using only the C1-2 data leaving out all information from the D-holes to see if the SDE experiment

could be predicted. Then the SDE information was used to update the model and predict the effect of excavation of the Validation Drift. The information from the Validation Drift was used to update the model again and predict the response to opening T1.

Table 6.7. Prediction of flow into the T1 hole using three-dimensional model based on steady-state annealing of SDE and calibrated to VD results.

B/H Interval Name	Interval	Conceptual Zone in Interval	Measured Flow (l/min)	Calculated Flow (l/min)	
				$T:K_z/K = 1$	$T:K_z/K = 0.10$*
T1-H	31-38	H	0.0017	1.2	0.7

*$T:K_z/K$ required to reduce flow by a factor of 2 (see section 4.3)

6.4.1. Annealing to the C1-2 Data

The drawdown curves shown in Figure 3.4 were used to anneal the three-dimensional zone model. These curves represent the intervals that did respond to the C1-2 test as shown in Table 3.3. Intervals that did not respond were not specified as annealing targets. Neither negative nor positive response was sought at these locations because the reason the interval did not respond is unknown. The borehole could simply have missed intersecting a hydrologically active fracture by a small distance or the interval could be connected to hydrologically active fractures that are not connected to C1-2. Experience with annealing (Davey et al., 1989) has shown that annealing may find unreasonable ways to disconnect a well if asked to find a negative response. It may be better to either disconnect the intervals that do not respond a priori or simply not specify a target response. In this case, a target response was not specified because the C1-2 test was relatively short and many of the zones which did not respond to the C1-2 test did respond to the SDE (see Table 3.4). The three-dimensional zone model was annealed to the C1-2 test with the resulting H- and B-zone configurations shown in Figure 6.4.

Figure 6.5 shows the energy versus iteration curve and temperature schedule for this annealing process. During annealing, the computational process was halted several times either by computer failures or by the operator. At each of these times, the process was restarted and the

Table 6.8. Prediction of total drawdown due the openning of T1 using three-dimensional model based on SDE and VD results.

B/H Interval Name	Interval	Conceptual Zone in Interval	Measured Drawdown (m)	Calculated Total Drawdown (m)	
				$T:K_z/K=1$	$T:K_z/K=$ *
N2-1	161-207	B(188-190)		84	58
N2-2	111-160	K(151-153)		84	104
N2-4	2-75.0	M (29-31)		105	73
N3-1	101-189	A (162-170), B (133-4)		85	96
N3-2	2-100	M (38-39)		124	84
N4-1	142-219	A (153-156)		84	103
N4-2	109-141	B (122-126)		84	103
N4-3	77-108	M (102)		84	103
W1-1	92-147	B (130-138), I (108-12)		85	103
W1-3	55-75	Hb (59-60)		172	115
W1-5	2-31.0	H (46-50)		172	115
W2-1	110-147	A (124-145), I (116-21)	not available	85	103
W2-2	76-109	B (83-91)		78	97
W2-3	66-75	Hb (67-71)		90	112
W2-4	48-65	H (50-57)		89	111
C1-2	40-70	H (45-54)		104	72
C1-3	71-105	B (96-100)		blank	blank
C1-4	106-150	A (138-148), I (105-9)		blank	blank
C2-1	1-70.0	H (63-69)		134	92
C2-2	71-86	B (76-82)		83	89
C2-3	87-124	A (109-113), I (122-4)		85	103
C3-1	1-70.0	H (59-61)		203	167
C4	1-60.0	H (55-59)		159	107
C5-1	83-140	A (118-9)		0	0
C5-2	4-82.0	B (90), H (84-85)		80	88
D5-B	28-100	B (90-2), I (94-6)		0	0
T2-H		H			

*$T:K_z/K$ required to reduce flow by a factor of 2 (see section 4.3)

Table 6.9. Prediction of incremental drawdown due the openning of T1 using three-dimensional model based on SDE and VD results.

B/H Interval Name	Interval	Conceptual Zone in Interval	Measured Drawdown (m)	Calculated Incremental Drawdown (m)	
				$T:K_z/K=1$	$T:K_z/K=$ *
N2-1	161-207	B(188-190)		70	44
N2-2	111-160	K(151-153)		14	34
N2-4	2-75.0	M (29-31)		89	57
N3-1	101-189	A (162-170), B (133-4)		23	34
N3-2	2-100	M (38-39)		107	67
N4-1	142-219	A (153-156)		14	33
N4-2	109-141	B (122-126)		14	33
N4-3	77-108	M (102)		14	33
W1-1	92-147	B (130-138), I (108-12)		15	33
W1-3	55-75	Hb (59-60)		149	92
W1-5	2-31.0	H (46-50)		149	92
W2-1	110-147	A (124-145), I (116-21)	not available	15	33
W2-2	76-109	B (83-91)		11	30
W2-3	66-75	Hb (67-71)		13	35
W2-4	48-65	H (50-57)		13	35
C1-2	40-70	H (45-54)		88	56
C1-3	71-105	B (96-100)		blank	blank
C1-4	106-150	A (138-148), I (105-9)		blank	blank
C2-1	1-70.0	H (63-69)		113	71
C2-2	71-86	B (76-82)		30	36
C2-3	87-124	A (109-113), I (122-4)		15	33
C3-1	1-70.0	H (59-61)		180	144
C4	1-60.0	H (55-59)		136	84
C5-1	83-140	A (118-9)		0	0
C5-2	4-82.0	B (90), H (84-85)		26	34
D5-B	28-100	B (90-2), I (94-6)		0	0
T2-H		H			

*$T:K_z/K$ required to reduce flow by a factor of 2 (see section 4.3)

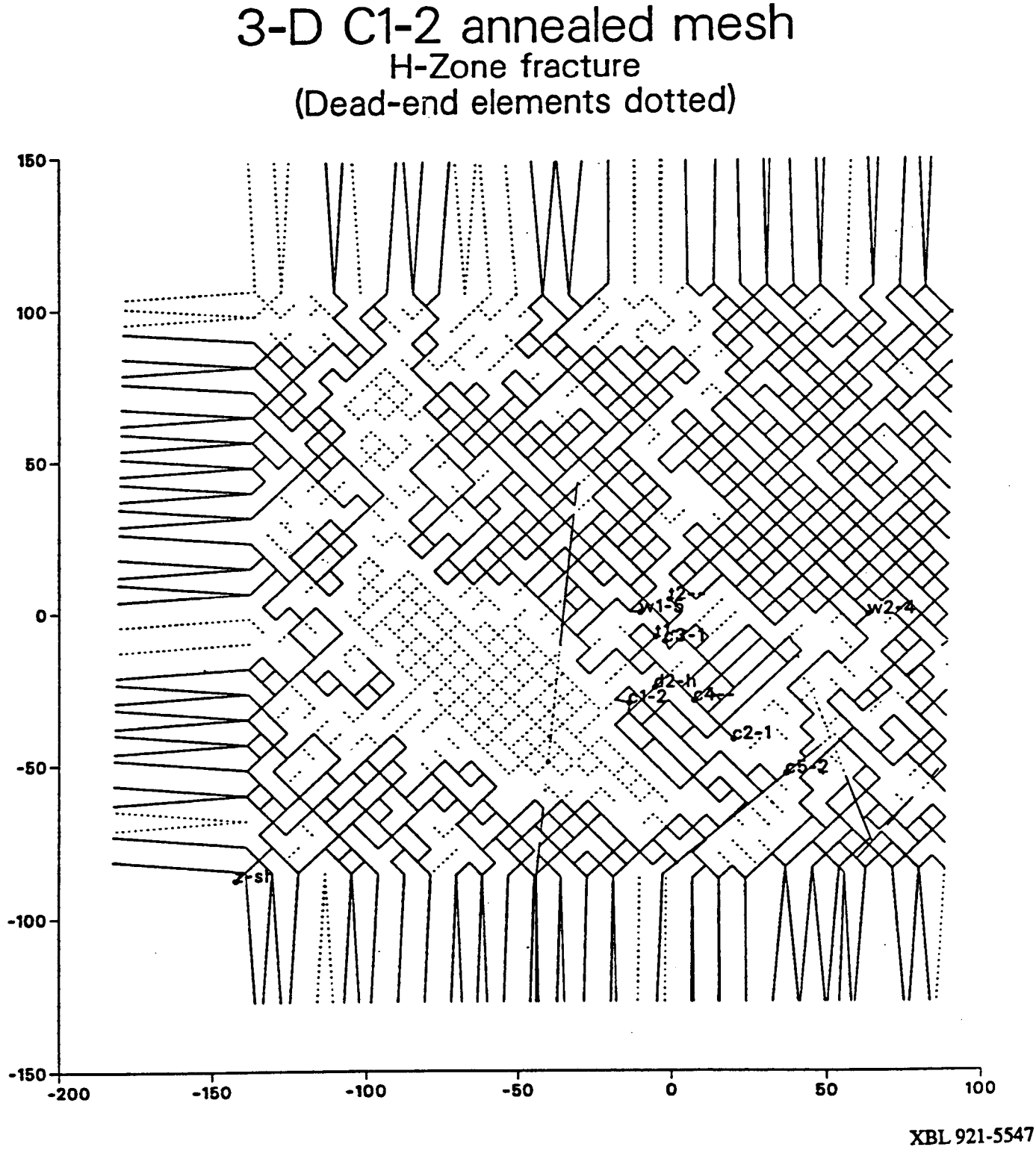

Figure 6.4a. The H-zone from the three-dimensional zone template annealed to C1-2 test.

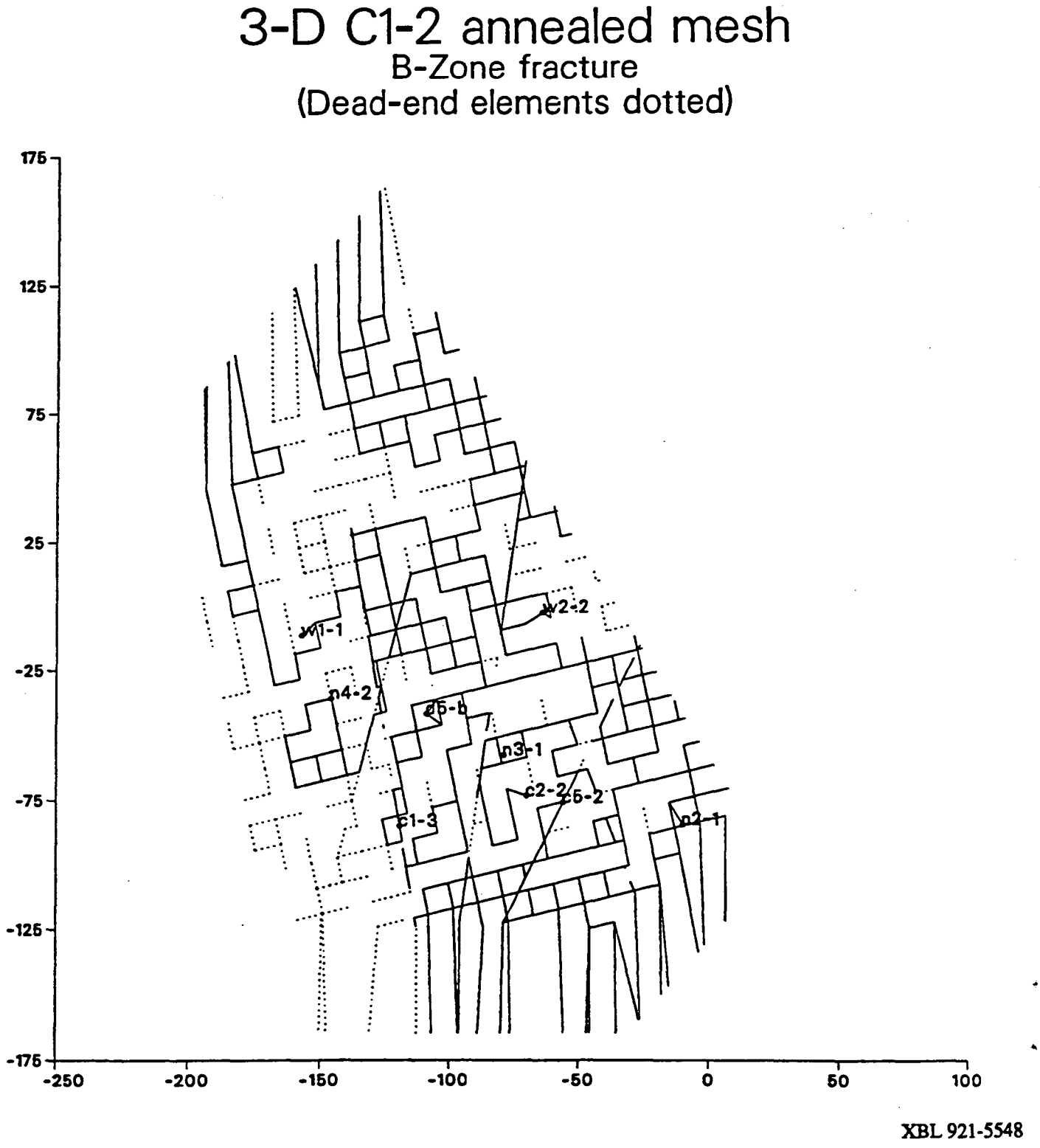

Figure 6.4b. The B-zone from the three-dimensional zone template annealed to C1-2 test.

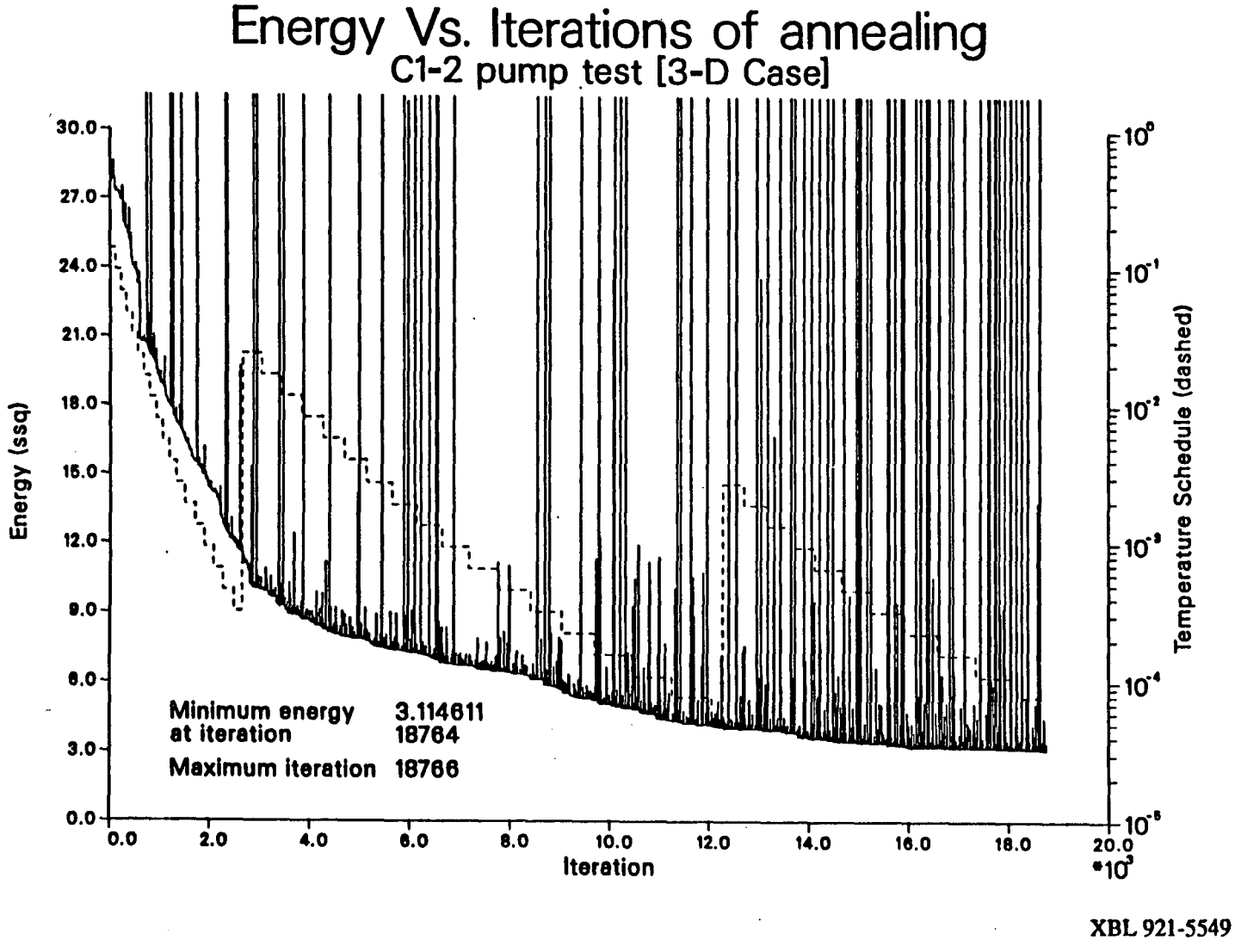

XBL 921-5549

Figure 6.5. The energy versus iteration curve and temperature schedule for the three-dimensional transient model.

temperature schedule was specified to start where it left off, or was changed. The points where the temperature schedule is changed are easily seen on Figure 6.5. Finding the best temperature schedule is at this point an art rather than a science. However, there is some indication on Figure 6.5 that the slope of the energy curve is related to the temperature schedule. Clearly, this is an area that requires research because a good choice of temperature schedules could probably find low energy solutions in a fraction of the time required with a bad temperature schedule.

Figure 6.6 shows the well test data and model responses for the C1-2 test. Overall these show excellent agreement.

6.4.2. Prediction of the SDE

The annealing of this large three-dimensional problem took several weeks. It was not possible to do co-annealing with both the C1-2 and the SDE in the time available. Consequently, configurations were periodically removed as the C1-2 annealing progressed and used to predict the SDE drawdowns. This was a way to determine if the C1-2 annealing was converging on a solution that would also do well predicting the SDE. The subset of the intervals responding to C1-2 which also responded to the SDE and which had reliable data for both tests were selected for this purpose. These are the intervals ranked "1" in Table 3.4. There are only six such intervals. Then, for each configuration, the SDE was modeled as a steady-state flow case with a constant flow rate from D-B and D-H as described in Section 6.3.1. An SDE energy was computed by comparing the estimated drawdowns for the last step of the SDE (given in Table 3.1) with the drawdowns calculated with the configuration. The contribution to the energy was counted as zero if the computed drawdown lies within the error bounds given in the table. To calculate drawdown, the equilibrium heads for each configuration were assumed to all be 220 m. Figure 6.7 shows the energy with respect to the SDE for the selected configurations as a function of the iteration number. One can see from this plot that the SDE energy is decreasing as a function of iteration. In other words, C1-2 annealing is slowly converging on a good prediction of the SDE drawdowns.

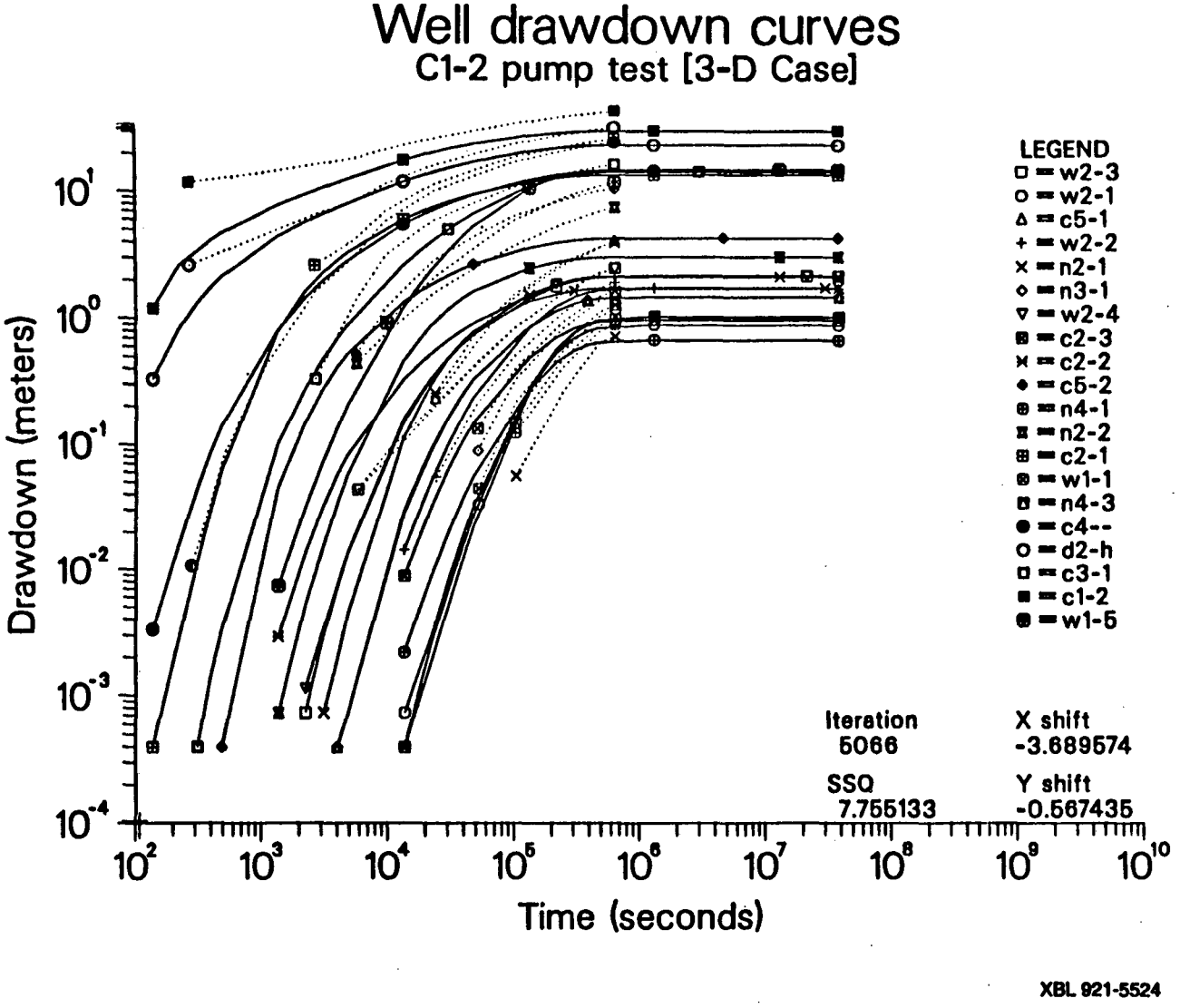

Figure 6.6. Comparison of C1-2 well test response data with model results.

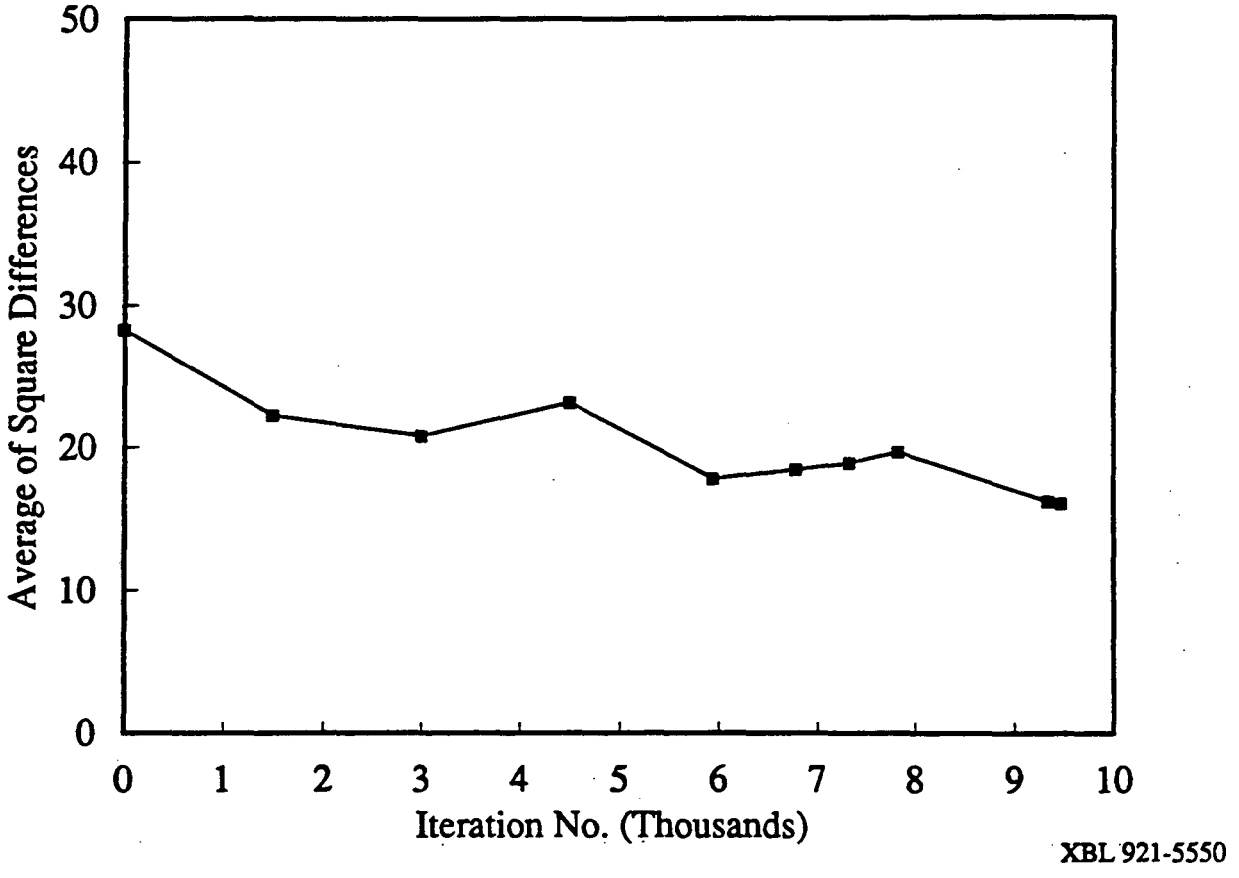

Figure 6.7. The energy with respect to the SDE data for the six well intervals that have compatible responses for both SDE and C1-2 calculated at different iterations of C1-2 annealing.

If one looks in more detail at the SDE energy in the later iterations, most of the energy is coming from intervals W2-4 and N2-2 and the N intervals. For the W2-4 case, it may have been difficult for annealing to find a solution that matches both the SDE and C1-2 because W2-4 responded strongly to the SDE but gave a negligble response to the C1-2. This behavior might have been matched if co-annealing with transient SDE data had been possible. Also, the SDE energy may be reflecting the limitations of using a quasi-two-dimensional conceptual model. Annealing may perform better if three-dimensional slabs are used to model the fracture zones. The C1-2 test was primarily a test of the H-zone, and the N-holes do not intersect the H-zone. Therefore, it is not too surprising that annealing to C1-2 does not help predict drawdowns outside of the H-zone as well as in the H-zone.

Another point of interest is that the annealing process disconnected some of the intervals that did not respond to the C1-2 test, notably W1-3 in the H-zone. This is particularly interesting because no match was sought at these points. Table 6.10 gives the head differences between the modeled SDE and an estimated equilibrium head of 220 m for each interval as a function of selected iterations of annealing to C1-2.

Table 6.10. Differences between observed and calculated SDE heads for different configurations during C1-2 annealing.

Iteration	Well Interval						Energy: Averaged squared difference in drawdown
	W2-3	N3-1	W2-4	N4-1	N2-2	W1-5	
	Measured drawdown						
	36.8±42.0	90.0±22	70.8±38.0	78.2±27	75.7±22.5	95.4±21.5	
0	27.4	20.6	17.8	16.2	21.5	99.8	28.2
1497	42.4	41.0	32.7	19.2	21.6	60.6	22.3
2995	39.0	36.6	35.8	26.4	22.5	88.2	20.8
4498	36.0	33.4	13.5	23.3	24.8	95.2	23.1
5941	47.7	45.4	16.7	29.6	28.2	110.7	17.8
6778	46.5	44.4	17.5	27.8	27.4	106.4	18.5
7322	47.9	43.9	19.1	26.0	16.8	100.8	18.9
7820	41.0	40.0	18.6	28.5	25.5	94.4	19.7
9343	40.7	72.8	17.9	28.4	24.4	84.9	16.2
9469	40.4	72.5	17.7	28.9	24.4	84.7	16.1

One of the final configurations described above was chosen to predict the steady-state effects of the third step of the SDE experiment. In this case we model the SDE as a constant head test with the heads at D-H and D-B equal to 0m relative to the 360m level. In this way a drawdown of 220 m is produced at the D-holes and flow can then be predicted into the D-holes. Tables 6.11 and 6.12 give comparisons between the measured and predicted flow and drawdown data respectively.

6.4.3. Calibration of the C1-2 Model to the SDE Data

The above tables show that the model annealed to C1-2 estimates the flow into D-H within the experimental error of ± .2 l/min. However it overestimates the flow into D-B by about a factor of two. The predicted drawdowns in Table 6.11 are on average about right. The best choice of action for obtaining a model which behaves like both the C1-2 and SDE would have been to use co-annealing to both C1-2 and the SDE as was done in the two-dimensional case. However, the size of this problems and the time available precluded this choice. Alternatively, the annealed model could be calibrated by decreasing the conductance of all the elements by 25%. This improves the model prediction of flow into D-H and D-B does not affect the drawdowns. In essence, these changes reflect the fact that there was confidence in the information from the C1-2 test with respect to the pattern of conductances, but more confidence in the SDE as a good measure of average permeability of the rock. This new model was used as a basis for all the remaining calculations.

Table 6.11. Comparison of measured and predicted flow for the SDE using the three-dimensional zone model annealed to C1-2.

B/H Interval Name	Interval	Conceptual Zone	Estimated Flow (l/min)	Calculated Flow (l/min)	Calculated Flow with 75% conductances l/min
D-H	24-27	H (24-26)	0.768±.2	0.95	0.716
D-B	28-100	B (90-2), I (94-6)	0.942±.2	1.82	1.36

Table 6.12. Comparison of measured and predicted drawdowns for the SDE using the three-dimensional zone model annealed to C1-2 and constant head boundaries at the D-holes.

B/H Interval Name	Interval	Zone	Estimated Conceptual (m)	Calculated Drawdown (m)
N2-1	B(188-190)	161-207	45.4±5†	13
N2-2	111-160	K(151-153)	75.7±22.5‡	26
N2-4	2-75.0	M (29-31)	9.2±3†	0
N3-1	101-189	A (162-170), B (133-4)	90.9±22‡	156
N3-2	2-100	M (38-39)	39.3±6†	74
N4-1	142-219	A (153-156)	78.2±27‡	72
N4-2	109-141	B (122-126)	74.2±24	147
N4-3	77-108	M (102)	72.1±10†	53
W1-1	92-147	B (130-138), I (108-12)	63.4±18	95
W1-3	55-75	Hb (59-60)	61.1±20	0*
W1-5	2-31.0	H (46-50)	95.4±21.5‡	99
W2-1	110-147	A (124-145), I (116-21)	70.6±18	88
W2-2	76-109	B (83-91)	53.7±4†	79
W2-3	66-75	Hb (67-71)	36.8±42‡	77
W2-4	48-65	H (50-57)	70±38‡	24

†Drawdowns are instantaneous drawdowns. These are underestimates of extrapolated drawdowns and have a very large error.
*Disconnected by annealing
‡Data for both SDE and C-12 are compatible

6.4.4. Prediction of the Validation Drift Effects

To predict the drift effects, heads were calculated for D-H and D-B as follows and then a skin of low permeability was added around the drift. Having reduced the model conductance by 25% and with the boundary condition at the D-H and D-B set to constant flow equal to 0.768 and 0.942 l/min respectively, the resulting head at the D-holes was calculated. Table 6.13 gives the drawdowns at D-H and D-B calculated using this model. Then, constant heads were assigned to D-H and D-B equal to the calculated heads minus 17 m in order to simulate the drift and the remaining open D-holes. Table 6.14 gives the calculated heads at D-H and D-B for the SDE and the D-H and D-B heads used to model the Validation Drift. The fact that the calculated SDE head at D-B is unreasonable is a reflection of the fact that the SDE data were not used in annealing.

Table 6.13. Comparison of measured and predicted drawdowns for the SDE using the three dimensional model annealed to C1-2, calibrated to SDE and constant flow boundaries at the D-holes.

B/H Interval Name	B/H Interval Interval	Zone	Estimated Conceptual (m)	Calculated Drawdown (m)
N2-1	B(188-190)	161-207	45.4±5†	12
N2-2	111-160	K(151-153)	75.7±22.5‡	25
N2-4	2-75.0	M (29-31)	9.2±3†	0
N3-1	101-189	A (162-170), B (133-4)	90.9±22‡	112
N3-2	2-100	M (38-39)	39.3±6†	65
N4-1	142-219	A (153-156)	78.2±27‡	52
N4-2	109-141	B (122-126)	74.2±24	106
N4-3	77-108	M (102)	72.1±10†	56
W1-1	92-147	B (130-138), I (108-12)	63.4±18	73
W1-3	55-75	Hb (59-60)	61.1±20	0*
W1-5	2-31.0	H (46-50)	95.4±21.5‡	96
W2-1	110-147	A (124-145), I (116-21)	70.6±18	63
W2-2	76-109	B (83-91)	53.7±4†	59
W2-3	66-75	Hb (67-71)	36.8±42‡	59
W2-4	48-65	H (50-57)	70±38‡	21
DB		H		156
DH		H		226
T1		H		176
T2		H		113

†Drawdowns are instantaneous drawdowns. These are underestimates of extrapolated drawdowns and have a very large error.
*Disconnected by annealing
‡Data for both SDE and C12G are good and compatible

Table 6.14. Heads in the D-holes calculated when the D-H and D-B flow is set to 0.768 and 0.942 l/min respectively for the three-dimensional model annealed to C1-2 and heads 17 m lower to be used at the D-holes for the VD.

Borehole	SDE Head (m)	VD Head (m)
D-H	-9	-26
D-B	64	47

Using the estimates of the ratio of skin permeability to average permeability (K_s/K) described in section 3.1, the permeability of the elements within 5 meters of the drift wall was

decreased by a factor of 0.41, 0.25 and 0.05. The resulting flows due to the drift (using the heads for the VD given in Table 6.14) are given in Table 6.15. As explained in Section 4, the best prediction of inflow is for K_e/K=0.25 and the low and high predictions are for K_e/K=0.05 and 0.41 respectively. To actually match the observed flows the permeability around the H-zone must be reduced by a factor of 67 and in the B-zone by a factor of 11. The best estimate of drift inflow is high by a factor of five and inflow to the B-zone is by high a factor of 2. Possible reasons for this are discussed in Chapter 7.

Table 6.15. Prediction of flow into the Validation Drift using three-dimensional model annealed to C1-2.

B/H Interval Name	Interval	Conceptual Zone in Interval	Measured Flow (l/min)	Calculated Flow (l/min) ±0.2				
				H:K_e/K =1	H:K_e/K =.41	H:K_e/K =.25	H:K_e/K =.05	H:K_e/K * = .024 B:K_e/K* = .11
D2-H	24-27	H (24-26)	0.1 ±?	.82	.65	.53	.19	0.10
D5-B	28-100	B (90-2), I (94-6)	0.563	1.05	1.06	1.07	1.1	0.57

* H:K_e/K required to make the D- H flow equal to 0.1 l/min
B:K_e/K required to make the D-B flow equal to 0.56 l/min.

Table 6.16 gives the total drawdown caused by the drift. To calculate the drawdowns, the heads calculated with the drift in place are subtracted from the heads in Table 6.2 calculated for the conditions before excavation, and with the D-holes closed. The heads increased after excavation and this predicted "drawup" is compared to measurements in Table 6.17. In this case the models that predicted flow well underpredicted drawdown.

6.4.5. Prediction of the Effect of Opening T1

The effects of opening T1, are modeled by choosing the value of H:K_e/K = 0.024 around the drift and B:K_e/K = 0.11 around the D-B interval that gives the best match to the Validation Drift flow data. Then the well interval, T1 was snapped into the H-zone and calculate the head in T1 with T1 closed and the drift and remaining D-holes open. Finally the head in the T1 interval was set to 186.8 m lower than the value calculated with T1 closed. Table 6.17 gives the prediction of

flow into the T1 hole, Table 6.19 gives the predictions of drawdown relative to the pre-excavation estimated equilibrium heads, Table 6.20 gives the prediction of incremental drawdown relative to the post excavation heads (see Table 3.1). Flow into T1 is again high by two orders of magnitude.

Table 6.16. Prediction of total drawdown due to the Validation Drift using three-dimensional model annealed to C1-2.

B/H Interval Name	B/H Interval Interval	Conceptual Zone	Estimated Drawdown (m)	Calculated Drawdown (m)				
				H:K_v/K=1	K_v/K=.41	K_v/K=.25	K_v/K=.05	H:K_v/K=.024 B:K_v/K=0.11
N2-1	161-207	B(188-190)	23.4±5.6	13	11	10	7	4
N2-2	111-160	K(151-153)	24.8±4.2	27	23	20	10	6
N2-4	2-75.0	M (29-31)	2.5±3.1	0	0	0	0	0
N3-1	101-189	A(162-170),B(133-4)	41.7±7.5	124	123	123	121	84
N3-2	2-100	M (38-39)	43.2±6.5	71	63	57	41	21
N4-1	142-219	A (153-156)	28.4±6.5	57	57	56	55	24
N4-2	109-141	B (122-126)	29.2±8.5	118	116	116	113	48
N4-3	77-108	M (102)	71.4±11.5	62	59	51	51	26
W1-1	92-147	B(130-138),I(108-12)	no data	70	76	75	66	32
W1-3	55-75	Hb (59-60)	59.0±6	0**	0**	0**	0**	0**
W1-5	2-31.0	H (46-50)	60.0±6	103	88	76	43	22
W2-1	110-147	A(124-145),I(116-21)	20.2±7	70	68	68	65	21
W2-2	76-109	B (83-91)	31.1±5.0	65	63	62	57	24
W2-3	66-75	Hb (67-71)	24.1±8	64	62	60	55	25
W2-4	48-65	H (50-57)	32.0±13.5	23	20	19	4	8
D2-H	24-27	H (24-26)	no data	189	155	131	58	31
D5-B	28-100	B (90-2), I (94-6)	no data	121	101	87	44	24

* H:K_v/K required to make the D- H flow equal to 0.1 l/min
B:K_v/K required to make the D-B flow equal to 0.56 l/min.

**Disconnected by annealing

Table 6.17. Prediction of incremental "drawup" due to VD excavation using the three-dimensional model based on C1-2.

B/H Interval Name	Interval	Conceptual Zone in Interval	Estimated "Drawup" (m)	Calculated Total Drawdown (m)	
				K_z/K=1	H:K_z/K=0.24 B:K_z/K = 0.11
N2-1	161-207	B(188-190)	22	3	9
N2-2	111-160	K(151-153)	53	6	20
N2-4	2-75.0	M (29-31)	6.7	0	0
N3-1	101-189	A (162-170), B (133-4)	49	33	72
N3-2	2-100	M (38-39)	-3.9	17	53
N4-1	142-219	A (153-156)	50	16	48
N4-2	109-141	B (122-126)	45	31	99
N4-3	77-108	M (102)	.7	2	27
W1-1	92-147	B (130-138), I (108-12)	no data	20	63
W1-3	55-75	Hb (59-60)	1.9	0*	0*
W1-5	2-31.0	H (46-50)	35	23	77
W2-1	110-147	A (124-145), I (116-21)	50	20	67
W2-2	76-109	B (83-91)	23	17	55
W2-3	66-75	Hb (67-71)	13	17	52
W2-4	48-65	H (50-57)	39	5	16

*disconnected by annealing

Table 6.18. Prediction of flow into the T1 hole VD and remaining D-holes (D-B) using three-dimensional model based on annealing to C1-2, SDE data and calibrated to VD results.

B/H Interval Name	Interval	Conceptual Zone in Interval	Measured Flow (l/min)	Calculated Flow (l/min)	
				T:K_z/K= 1	T:K_z/K = .09*
T1-H	31-38	H	0.0017	0.37	0.18
D-H				.068	.085
D-B				.56	0.57

*T:K_z/K required to reduce flow by a factor of 2 (see section 4.3)

Table 6.19. Prediction of total drawdown due to the opening of T1 using three-dimensional model based on C1-2, SDE and VD results.

B/H Interval Name	Interval	Conceptual Zone in Interval	Estimated Drawdown (m)	Calculated Total Drawdown (m)	
				$T:K_v/K=1$	$T:K_v/K=.09$*
N2-1	161-207	B(188-190)		7	6
N2-2	111-160	K(151-153)		15	10
N2-4	2-75.0	M (29-31)		0	0
N3-1	101-189	A (162-170), B (133-4)	Not	86	85
N3-2	2-100	M (38-39)	available	47	33
N4-1	142-219	A (153-156)		26	25
N4-2	109-141	B (122-126)		54	51
N4-3	77-108	M (102)		35	30
W1-1	92-147	B (130-138), I (108-12)		46	38
W1-3	55-75	Hb (59-60)		0	0
W1-5	2-31.0	H (46-50)		76	45
W2-1	110-147	A (124-145), I (116-21)		36	33
W2-2	76-109	B (83-91)		40	37
W2-3	66-75	Hb (67-71)		41	37
W2-4	48-65	H (50-57)		12	10
C1-2	40-70	H (45-54)		58	43
C1-3	71-105	B (96-100)		110	109
C1-4	106-150	A (138-148), I (105-9)		109	108
C2-1	1-70.0	H (63-69)		85	56
C2-2	71-86	B (76-82)		34	26
C2-3	87-124	A (109-113), I (122-4)		30	28
C3-1	1-70.0	H (59-61)		88	57
C4	1-60.0	H (55-59)		106	68
C5-1	83-140	A (118-9)		25	21
C5-2	4-82.0	B (90), H (84-85)		17	13
T2-H		H		84	46

*$T:K_v/K$ required to reduce flow by a factor of 2 (see section 4..3).ls 2

Table 6.20. Prediction of incremental drawdown due to the opening of T1 using three-dimensional model based on C1-2, SDE and VD results.

B/H Interval Name	Interval	Conceptual Zone in Interval	Estimated Drawdown (m)	Calculated Incremental Drawdown (m)	
				T:K_v/K=1	T:K_v/K=.09*
N2-1	161-207	B(188-190)		3	2
N2-2	111-160	K(151-153)		9	4
N2-4	2-75.0	M (29-31)		0	0
N3-1	101-189	A (162-170), B (133-4)	Not	2	1
N3-2	2-100	M (38-39)	available	26	12
N4-1	142-219	A (153-156)		2	1
N4-2	109-141	B (122-126)		6	3
N4-3	77-108	M (102)		9	4
W1-1	92-147	B (130-138), I (108-12)		12	6
W1-3	55-75	Hb (59-60)		0	0
W1-5	2-31.0	H (46-50)		54	23
W2-1	110-147	A (124-145), I (116-21)		5	2
W2-2	76-109	B (83-91)		6	3
W2-3	66-75	Hb (67-71)		6	2
W2-4	48-65	H (50-57)		4	2
C1-2	40-70	H (45-54)		31	16
C1-3	71-105	B (96-100)		1	0
C1-4	106-150	A (138-148), I (105-9)		1	0
C2-1	1-70.0	H (63-69)		60	31
C2-2	71-86	B (76-82)		15	7
C2-3	87-124	A (109-113), I (122-4)		3	1
C3-1	1-70.0	H (59-61)		61	33
C4	1-60.0	H (55-59)		79	39
C5-1	83-140	A (118-9)		8	4
C5-2	4-82.0	B (90), H (84-85)		8	4
T2-H		H		60	1

*K_v/K required to reduce flow by a factor of 2 (see section 4..3)

7.0. PRELIMINARY CONCLUSIONS

A comparison of the model predictions with the SDE measurements provides some insight into the way annealing works to find predictive models. Very little can be learned about annealing from the prediction of the Validation Drift effects. However, by comparing the measurements before and after excavation in light of the model results, it is possible to gain some insight with respect to the physics of the excavation effects. These two topics are discussed below.

7.1. Comparison of Model Predictions of SDE

Two predictions of the SDE were made based on the C1-2 data. The first was based on the two-dimensional H-zone model and the other was based on the three dimensional zone model. Table 7.1 summarizes the inflow predictions. The drawdown predictions are given in Tables 5.4 and 6.12. In both the two-dimensional and three-dimensional cases, the C1-2 data alone was used to predict the SDE inflow to the H-zone within the experimental error. The prediction of B-zone inflow is not as good because C1-2 is not a test of the B-zone. Drawdowns are matched in both cases in about one half of the intervals. This leads us to conjecture that additional cross-hole data in the B-zone might have improved this prediction. In summary, both the two- and three-dimensional annealing models were very successful at predicting inflow to the SDE.

Table 7.1. Comparison of model predictions for inflow to the SDE.

Case	Flow to the H-zone (l/min)	Flow to the B-zone (l/min)
Measured	0.768+_0.2	0.942+_0.2
2D annealed to C1-2	0.77	NA
3D annealed to C1-2	0.95	1.82

7.2. Comparison of Model Predictions of Validation Drift Inflow

Three different predictions of inflow to the Validation Drift were made and these are summarized in Table 7.2.

Table 7.2. Comparison of model predictions for inflow to the Validation Drift.

Case Measured	Flow to the H-zone (l/min) 0.1			Flow to the B-zone (l/min) 0.0.56		
	K_s/K=.05	K_s/K=.25	K_s/K=.41	K_s/K=.05	K_s/K=.25	K_s/K=.41
2D co-annealed to C1-2 and SDE	0.18	0.54	0.66	NA	NA	NA
3D annealed to SDE	0.18	0.51	0.63	0.80	0.81	0.81
3D annealed to C1-2	0.3	0.86	1.05	1.24	1.2	1.18

All the predictions of inflow to the Validation Drift based on the average estimate of skin (K_s/K=.25) are high by a factor ranging between five and eight. Recall that the difference in hydraulic boundary conditions due to six D-holes compared to one two-meter diameter tunnel is negligible. Since predictions of the Validation Drift inflow incorporate knowledge of the SDE inflow, the fact that predictions are all too high means that either (1) the skin around the Validation Drift experiences a larger decrease in permeability than the average decrease observed during the Macropermeability Experiment or (2) other sinks in the vicinity of the Validation Drift become relatively more important after the Validation Drift skin forms. Other possible reasons for the difference, such as radical changes in boundary conditions between the SDE and the Validation Drift are unlikely.

Additional sinks are not likely to explain these results. In the first place, the Z-shaft was accidentally disconnected from the 3D zone model during annealing. When the Z-shaft was reconnected, the effect on the model was negligible. Other drifts are not likely candidates as sinks. For example, holes drilled from the 3D-drift obtain ambient heads (~200m) very close to the drift walls. Thus, this tunnel apparently has a very low permeability skin as well and was consequently not a very effective hydraulic sink. Although the strengths of all the possible sinks were

not well known, it seems likely that they would not decrease the flow into the Validation Drift by much more than a factor of two. It seems that the most likely explanation for the low flow is that the average skin at the Validation Drift was of lower conductivity than the minimum skin observed at the Macropermeability Drift. This idea is analyzed below.

7.3. Analysis of Skin Effects

Some of the possible reasons can be examined why the Validation Drift skin might be much lower permeability than expected. The simplest scenario is that, whatever is causing the skin, only the low end of the skin distribution that was observed in the Macropermeability Drift was sampled. Below some of the possible physics effecting permeability change near the drift are examined. Based on the aforementioned model results, the decrease in flow could be explained by a decrease in the average permeability by a factor of about 40 in a 5 m zone around the drift.

7.3.1. Elastic Stress Effects due to Excavation

Drifts can significantly perturb the stress field and hence the fracture conductivity within a few diameters of a drift. The effects are strongest at the drift walls and depend on the orientation of the drift, the far-field principal stresses, and on the orientation of the fractures near the drift. In most cases, the excavation of a drift at depth promotes the opening of pre-existing fractures that parallel the perimeter of the drift, whereas pre-existing fractures radiating from the drift will tend to close. The effect on fractures that are approximately perpendicular to the drift axis would be minor. Because the radial and drift-perpendicular fractures would carry water into the drift, the stress effects on these fractures are particularly important. The perturbing effects would be greatest for drifts oriented perpendicular to the most compressive far-field principal stress (σ_1) and least for drifts that trend parallel to σ_1. For a drift oriented obliquely to the principal stress axes, perturbation effects will vary significantly along the drift. For the case at hand, the drift is nearly parallel to σ_1.

The stress perturbation caused by the excavation of the Validation Drift was analyzed to examine the possible effect of inflow to it along the H-zone. The Validation Drift at Stripa trends

at 287°, and is inclined down to the west-northwest at 3°. The orientations of the drift and the most compressive far-field horizontal stress differ by only 4°. The H-zone intersects the 2 m diameter drift approximately 30 meters from its east end. The stress state and the relevant geometries thus indicate that a 2-D plane strain analysis is useful for analyzing the stress effects on the H-zone due to excavation. Using the most recent stress measurements for the Validation Drift area, the compressive normal stress tangential to the drift wall should increase between 50% (at the drift walls) and 133% (at the roof and floor of the drift); these effects decay to less than 10% within a few meters from the drift (Figure 7.1).

At the levels of normal stress near the Validation Drift, experimental work suggests that the ratio of the change in fracture hydraulic conductivity to the change in normal stress varies as $\sigma_N^{\alpha-1}$ (Black et al., 1991). Accordingly, the hydraulic conductivity along fractures oriented radially to the drift should decrease by no more than 55% at the drift perimeter and by no more than 17% as averaged over a 5-meter distance from the drift (Figure 7.2). The absolute magnitude of the normal stress changes parallel to the drift are small (<15%) and average to zero around the perimeter of the drift. There should be little direct effect on the inflow along drift-perpendicular fractures (i.e. the longest H-zone fractures). The excavation of the drift causes the compressive stress normal to the drift walls to be reduced to atmospheric pressure, and pre-existing fractures that ring the drift should open. Although this should cause the hydraulic conductivity to increase, these fractures would not be oriented to conduct water into the tunnel. If air can invade these fractures, then two-phase flow conditions could contribute to a decrease in the hydraulic conductivity near the drift. Elastic stress perturbations due to drift excavation seem unlikely to decrease the permeability around the drift by even a factor of 2, but it is extremely difficult to see how stress changes could decrease the permeability by a factor of 20.

7.3.2. Ventilation Effects

Two-phase flow caused by differential drying during ventilation has been suggested as a possible reasons for a decrease in flow (K. Pruess, pers. comm., 1991). Drying could occur due to the ventilation procedure. Figure 7.3 shows a cartoon of expected ventilation effects. As the

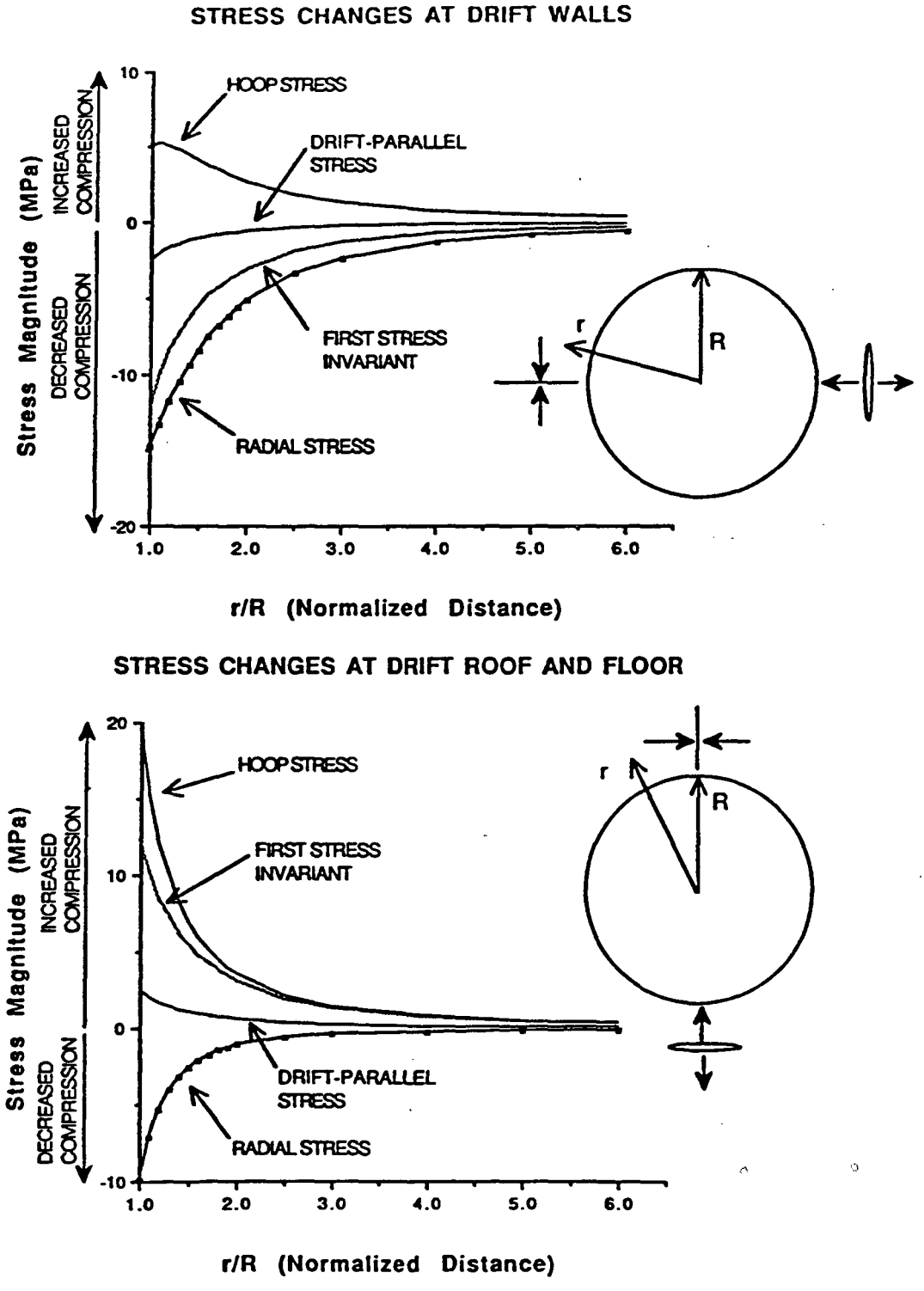

Figure 7.1. Stress changes near the Validation Drift.

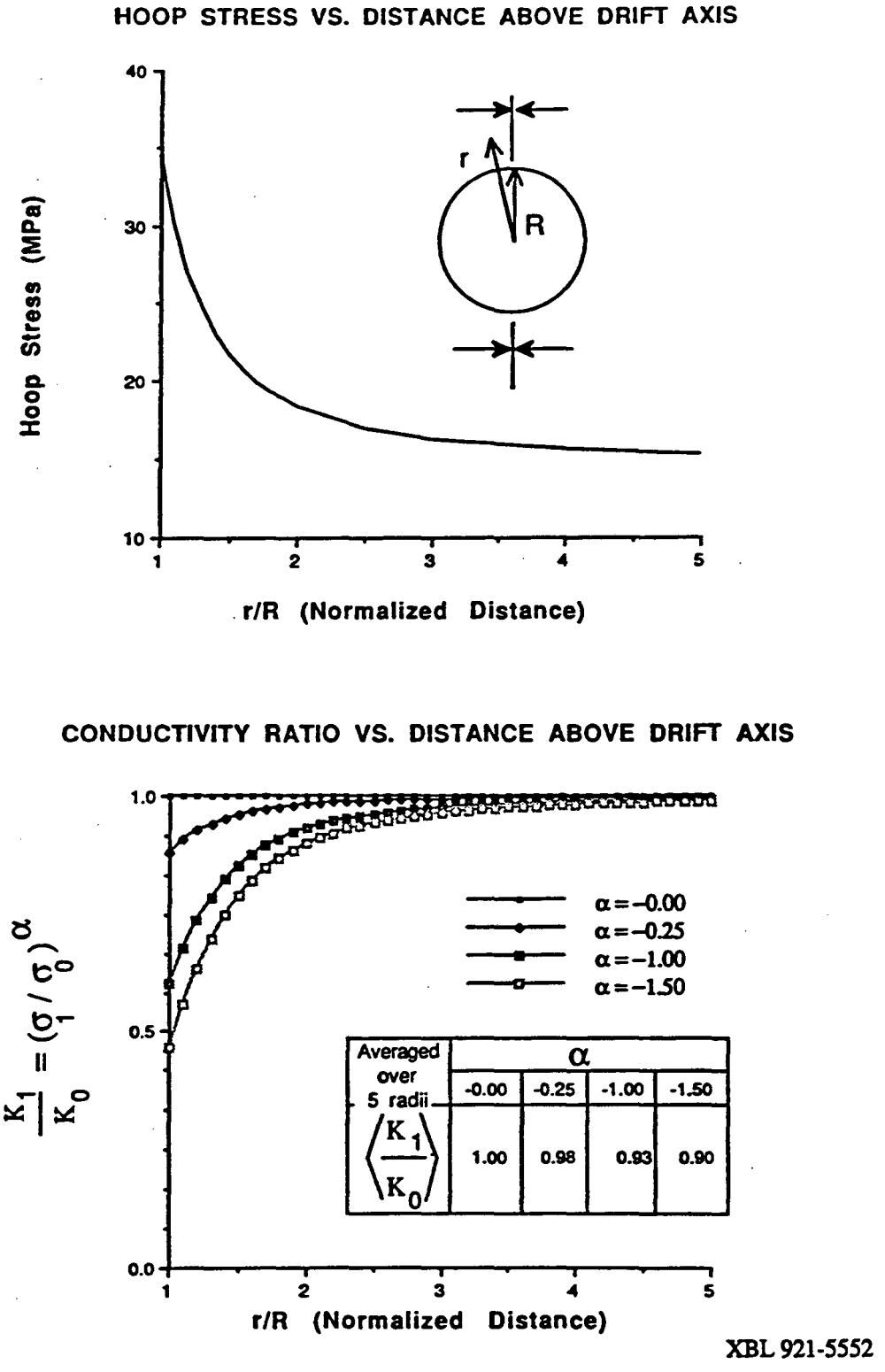

Figure 7.2. Conductivity changes near the Validation Drift due to hoop stresses.

ventilation rate is increased, either by raising the temperature in the drift or increasing the air flow rate, the measured inflow of water will change. At first, an increased rate will increase the measured flow as more water is essentially sucked out of the rock. Then, the rock will start to dry out and air invasion could decrease the effective conductivity of the rock near the wall. One piece of evidence points toward the Validation Drift being on the early part of this curve: When the plastic sheets were removed, the measured flow rate increased. Thus, it seems that the rock ventilation was not producting significant two-phase flow effect. In conclusion, it does not seem that interface effects are likely to be important.

7.3.3. Blasting Effects

Blasting can damage the rock and reduce the permeability near the drift or blasting can open the fractures near the drift wall. The Macropermeability Drift and the Validation Drift were excavated by different blasting methods. Relative to the Macropermeability Drift, the Validation Drift was excavated much more carefully. The estimated skin around the Validation Drift is of lower permeability relative to the estimated skin for the Macropermeability Drift, so it is reasonable to assume that in the Validation Drift careful blasting simply did not increase the permeability near the drift as much as blasting the Macropermeability Drift did. This scenario is also supported by examination of the 3D Drift which was intermediately carefully blasted (O. Olsson, pers. comm., 1991). Based on head profiles, the 3D Drift apparently has a skin intermediate between the Validation Drift and the Macropermeability Drift.

Another factor may be that the carefully blasted in the Validation Drift pushed air back into the rock in a more uniform layer than at the Macropermeability Drift. This air would then uniformly block pore throats and significantly and uniformly decrease the permeability. One argument against this effect is that the gaseous products of the blast are probably mostly CO_2 (N. G. W. Cook, pers. comm., 1991) which is very soluble in water. Thus the blast would have to push ambient air back into the rock and it is not clear whether this is a reasonable possibility.

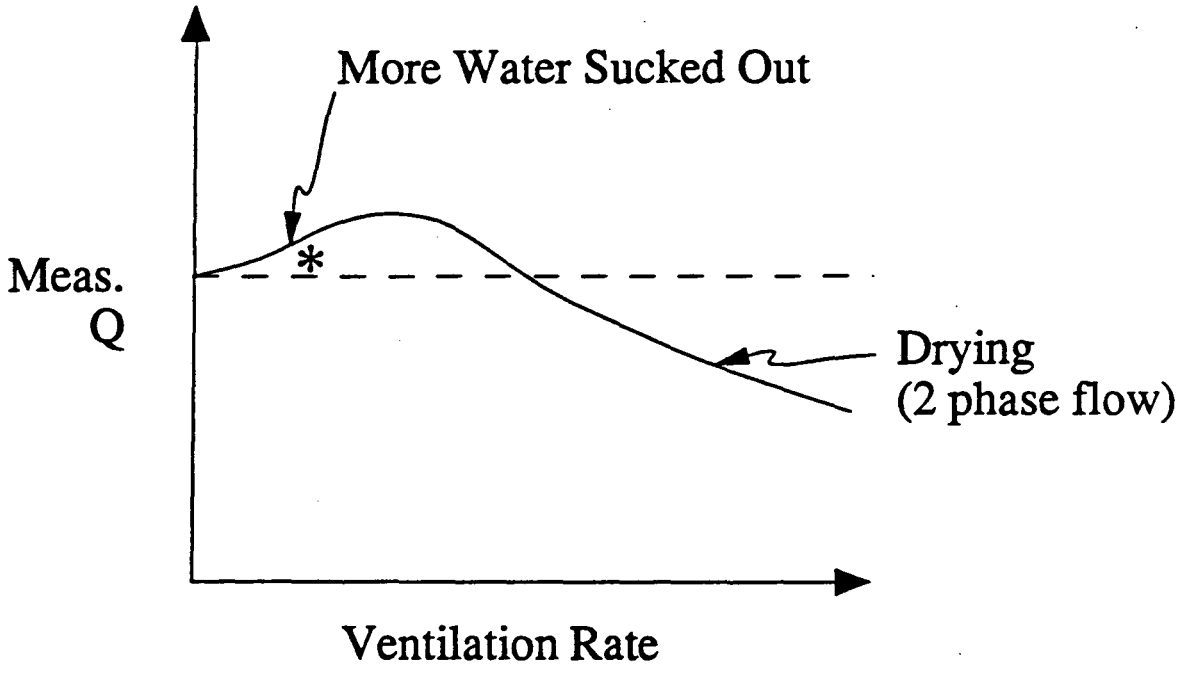

Sheets Off → More Flow *

XBL 921-5553

Figure 7.3. Effect of ventilation on measured flow.

7.3.4. Degassing

During the last step of the SDE, gas bubbles were observed in the outflow tubing. Gas bubbles that are constantly released as water approaches atmospheric pressure could have a very significant effect by causing two-phase flow and a significant decrease in relative permeability. However, in order to explain the observed skin effect the amount of gas coming out of solution would have to be significantly greater for the conditions imposed by the Validation Drift than for the conditions imposed by the SDE. For the Validation Drift, water entered the Drift at atmospheric pressure. For the SDE, water entered the D-holes at a pressure head of 17m. So, if a significant increase in degassing takes place between 17 m and atmospheric pressure, then degassing could explain a significant decrease in flow. To address this question, a water sample was taken at ambient pressure (≈200 m head above 360 m level) and the volume and type of gas released at atmosphere was measured. Table 7.4 gives these results for the most significant gases (Laaksoharju, 1991).

Table 7.3. The results from 3 gas sample analyses from the V2 borehole in the Stripa Mine.

Sample no	Depth m	Flow mL/min	O_2 ppm	N_2 ppm	CO ppm	CO_2 ppm	CH_4 ppm	C_2H_6 ppm	C_2H_4 ppm	C_2H_2 ppm	Vol. % gas
V2:3	799-807	32.6	<1000	27000	<1	42	270	0.4	<0.1	<0.1	2.8
V2:2	812-820	66.3	<1000	40000	<1	11	200	0.5	<0.1	<0.1	4.4
V2:1	970-1240	12.4	<1000	25000	<1	10	280	2.8	<0.1	<0.1	2.9
D1-6	350-450	470	<1000	30000		640	190	0.5			3.1

For the purpose of determining the possible significance of these results, assume that the gas coming out of solution is entirely N_2 and that about 3% by volume comes out of solution at atmospheric pressure. Now assume that the flow enters the rock through a single fracture perpendicular to the axis of the two-meter-diameter drift with an aperture of 0.1 cm. This means that flow into the drift takes place through a cross-sectional flow area at the drift wall of about 600 cm^2. Further, assume that no gas released from solution escapes the rock. Then, ignoring

radial effects the fracture will fill with gas at approximately 0.05 cm/min. In other words, if no gas escapes, nearly 4 cm of fracture could be filled with gas in an hour. This is clearly a significant amount of gas.

Using Henry's Law, and N_2 as the reference gas the amount of gas that would come out of solution at 17 m head based on knowing that 3% comes out at atmospheric pressure can be calculated. This is about 0.5%. Therefore, there is a significant increase in the amount of gas that comes out of solution between 17 m and atmospheric, i.e., between the SDE and the Validation Drift. One simple way to check this effect would be to measure flow rate from a borehole as a function of pressure all the way down to atmospheric. If this analysis is correct, there should be a significant decrease in expected flow between 17 m and 0 m head. This experiment was carried out by Olsson (pers. comm., 1991) in the D-holes with the expected results.

Clearly there was a very large amount of gas continuously coming out of solution under the Validation Drift conditions. It is quite possible that this gas was responsible for creating a significant decrease in the permeability of the skin. A forty-fold permeability decrease due to two-phase flow effects is well within reason. However, degassing does not explain the difference between the Validation Drift and the Macropermeability Drift. If the water contains gas at the Validation Drift, it should contain gas at the Macropermeability Drift. Here again, the blasting effects in the Macropermeability Drift could be offsetting the two-phase flow effects. In other words, a reasonable scenario is that two-phase flow is decreasing the permeability roughly by the same amount in the two drifts, but the more irregular blasting used to excavate the Macropermeability Drift increases the permeability more than the careful blasting of the Validation Drift.

In conclusion, the most plausible cause for a significant decrease in the permeability of the skin surrounding the Validation Drift is degassing as the pressure of the water is dropped to atmospheric on inflow. Excavation method seems to have had significant role. Stress effects are probably only marginally responsible. Other causes seem to be unimportant.

7.4. Prediction of the Effects of Opening T1

Three different predictions of the effects of opening T1. A comparison of the inflow predictions is given below in Table 7.4. These estimates indicate that the T1 hole could capture much of the flow otherwise going to the drift. However, the measured value of flow into T1 is very much smaller than that predicted. For the purpose of comparing these predictions to the measurement the actual inflow to T1 is negligible and T1 could be considered as "unconnected." There are two possible ways to look at this problem. One is to repeat an SDE type experiment at T1. This provides an inflow value which is averaged over a larger volume and thus easier to predict as seen above. Another is to produce more solutions using the annealing process noting how often T1 is disconnected from the network.

Table 7.4. Comparison of model predictions for inflow to the T1.

Case	Flow to T1 (l/min)	
	$K_s/K=1$	$K_s/K=XXX$
Measured	Not Avail.	Not Avail.
2D co-annealed to C1-2 and SDE	0.64	0.33
3D annealed to SDE	1.2	0.6
3D annealed to C1-2	0.37	0.18

7.5 Comments on Research Progress

The annealing technique is a new approach to developing discontinuum models for fracture flow based on inversion of well test data. Some of the results are quite encouraging, particularly the prediction of the SDE results using a single cross-hole test. In other cases questions have arisen. Many of these could not be explored under the time and budget constraints of this project. In particular, arbitrary assumptions were made about boundary conditions and methods to use for calibrating models beyond annealing. Very high conductances were assigned to the elements that lie along fracture intersections. These elements can be removed by annealing, but a very different solution might have been found with different conductance intersections. The way these

decisions affect the results has not been explored. Another issue is that of weighting data in co-annealing. It would be very interesting to try a series of co-annealings with different weighting factors to see how well each made the relevant predictions. An annealing example was conducted with a three-dimensional grid but this analysis was done with uncorrected data and is therefore invalid. This study could be usefully repeated to see if annealing finds fracture zones. Finally, a limited number of realizations were produced. This is nowhere near enough information for any stochastic technique. However, Figures 5.3, 5.6, 6.2a and 6.4a are all realizations of the H-zone and these can be compared. Figures 5.3 and 5.6 are much closer to each other than they appear. The number of elements present differs by only 2% between these figures, which is very encouraging. Because they are close to the percolation limit, 2% removes a significant number of connections. (Recall that the solid lines in the figure are only the connected elements, but the dashed lines are also present.) A steady-state annealing will de-emphasize elements that only provide storage. So it makes sense that Figure 5.6 which uses the steady-state SDE data appears sparser than 5.3. Even though the grid orientations are different for the three-dimensional solutions, similarities can be found in the conductance patterns in the vicinity of the sampling points among all the figures, particularly Figures 5.6, 6.2a and 6.3a.

It is clear that a much better evaluation of this technique would be achieved by conducting a simple series of cross-hole tests and using the first to predict the second, the first and second to predict the third, etc.

Finally, the excavation of the drift did nothing to help us evaluate the modeling approach. On the other hand, the combination of the SDE and the VD measurements along with the modeling provided excellent information for evaluating drift excavation effects.

8.0. REFERENCES

Black, J., O. Olsson, J. Gale, D. Holmes, 1991. Site Characterization and Validation, Stage 4. Preliminary Assessment and Detail Predictions, Stripa Report in preparation.

Carlsten, S., 1985. Hydrogeological and Hydrogeochemical Investigations in Boreholes -- Compilation of Geological Data, Swedish Nuclear Fuel Co., Stripa Project Report 85-04.

Davey, A., K. Karasaki, J. C. S. Long, M. Landsfeld, A. Mensch and S. Martel, 1989. Analysis of the Hydraulic Data of the MI Experiment, Report No. LBL-27864, Lawrence Berkeley Laboratory, Berkeley, CA.

Finsterle, S. and S. Vomvoris, 1991. Inflow to Stripa Validation Drift Under Two-Phase Conditions: Scoping Calculations, Nagra Report 91-40, Baden, Switzerland.

Laaksaharju, M., 1991. in Stripa Project Quarterly Report, Oct.-Dec. 1989. Swedish Nuclear Fuel Co., Stockholm, Sweden.

Long, J., K. Karasaki, A. Davey, J. Peterson, M. Landsfeld, J. Kemeny and S. Martel, 1991. An Inverse Approach to the Construction of Fracture Hydrology Models Conditioned by Geophysical Data—An Example from the Validations Exercises at the Stripa Mine, *Int. J. Rock Mech, Min. Sci and Geomech. Abstr. 28*, (2/3), 121–142.

Martel, S., 1991. Structure of Fracture Zones at the SCV Site, LBL Report (in preparation).

Olsson, O., J. H. Black, J. E. Gale and D. C. Holmes, 1988. Site Characterization and Validation, Stage 2—Preliminary Predictions, Swedish Nuclear Fuel and Waste Management Co., Stockholm, Sweden. Report ID No. TR 89-03.

Wilson, C. R., J. C. S. Long, R. M. Galbraith, K. Karasaki, H. Endo, A. O. Dubois, M. J. McPherson and G. Ramqvist, 1981. Geohydrological Data from the Macropermeability Experiment at Stripa, Sweden, Report No. LBL-12520, Lawrence Berkeley Laboratory, Swedish-American Cooperative Report SAC-37, Berkeley, CA.

Wollenberg, H., S. Flexser and L. Andersson, 1980. Petrology and Radiogeology of the Stripa Pluton, Lawrence Berkeley Laboratory Report LBL-11654.

LAWRENCE BERKELEY LABORATORY
UNIVERSITY OF CALIFORNIA
TECHNICAL INFORMATION DEPARTMENT
BERKELEY, CALIFORNIA 94720